Lawrence Berkeley National Laboratory
Recent Work

Title
Fluorescence Spectroscopy of Excitation Transfer in Photosystem I

Permalink
https://escholarship.org/uc/item/8t5327dk

Author
Mukerji, I.

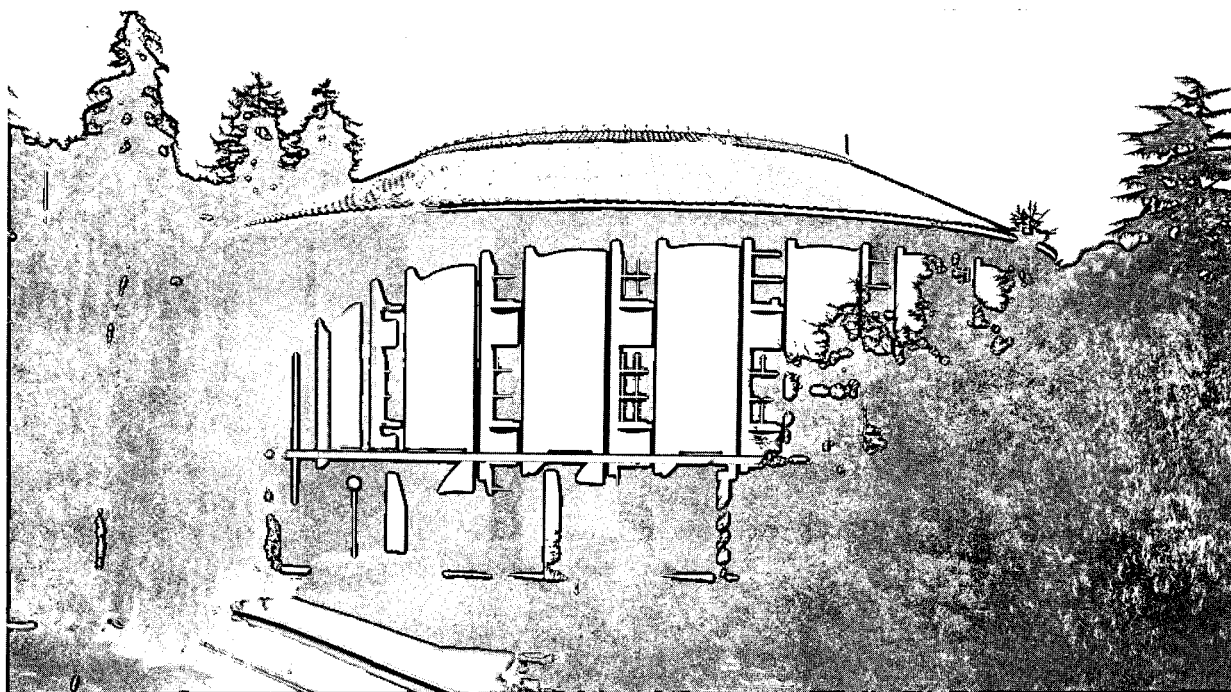**Publication Date**
1990-12-01

Lawrence Berkeley Laboratory
UNIVERSITY OF CALIFORNIA

CHEMICAL BIODYNAMICS DIVISION

Fluorescence Spectroscopy of Excitation
Transfer in Photosystem I

I. Mukerji
(Ph.D. Thesis)

December 1990

DISCLAIMER

Fluorescence Spectroscopy of Excitation Transfer in Photosystem I

by

Ishita Mukerji

Ph.D. Thesis

December, 1990

Chemical Biodynamics Division

Lawrence Berkeley Laboratory

University of California

Berkeley, CA 94720

Fluorescence Spectroscopy of Excitation Transfer in Photosystem I

Ishita Mukerji

Abstract

This thesis centers on the study of excitation transfer in a photosynthetic antenna array. The spectroscopic properties of two pigment-protein complexes were investigated. These complexes, isolated from higher plants, display an unusual temperature dependent fluorescence behavior. We have chosen to study this fluorescence behavior with respect to energy transfer to the reaction center and in an isolated intact antenna preparation.

A Photosytem I complex, PSI-200, was isolated from spinach. This complex contains the reaction center, primary electron acceptors and a 200 Chl antenna complement. We have characterized this system by both steady state and time-resolved fluorescence spectroscopy. At room temperature the main emission peak occurs at 690 nm with a large shoulder extending from 710 to 740 nm. Selective excitation of Chl b enhances fluorescence emission at longer wavelengths (F735). Additionally, the intensity of F735 increases dramatically as the temperature is lowered to 77K, while F690 remains relatively constant. Fluorescence polarization measurements indicate that this emission arises from pigments which absorb in the long wavelength region of the spectrum and comprise a relatively small portion of the antenna population. Comparison of spectral characteristics were made with a PSI complex isolated from the thermophilic cyanobacterium, *Synechococcus*, sp. The thermophilic complex has a smaller antenna complement relative to PSI-200 and is more stable with respect to thermal degradation.

To address the role of Chl b in stimulating long wavelength fluorescence and the temperature dependence of the system, we have studied the energy transfer dynamics in an antenna complex, LHC-I isolated from PSI-200. This intact antenna preparation has an emission maximum at 685 nm (F685) with a large shoulder ranging from 710 to 740 nm. We observe that both emission bands increase as the temperature is lowered; at 77K F735 completely dominates the emission spectrum. Kinetic measurements indicate that initially absorbed excitation is rapidly redistributed to longer wavelength emitting pigments within 40 ps. The temperature dependence of F685 results from increased back transfer from long wavelength emitters to F685. We suggest that changes in excitation transfer between the various emitting species and a non-radiative fluorescence quenching mechanism account for the temperature dependence of the system.

Acknowledgements

Several people have contributed to the completion of this work. Of course, it is difficult to acknowledge everyone. Undoubtedly, I could not have proceeded without the support of my group members. Certain people deserve a special word of thanks; although, everyone's support was greatly appreciated. I am especially grateful to Ann McDermott and Sarah Tabbutt for showing me how to isolate green stuff. I am indebted to Trish Maxson and Hermann Keuper for getting me started and showing me the thrills of the laser system. Vickie DeRose and Vittal Yachandra have been really good friends and colleagues. Holger Dau was really helpful in pulling everything together at the end.

I have many good friends at the round house and I am thankful to them for always "being there" for me. I can honestly say that without the expert assistance of Phil Eggers and Gary Smith it would have taken me a lot longer to get the work for this thesis done. Lois Soule, Beth Klingel, Vangie Peterson and Rosalyn Miles were always very helpful whenever I had a problem.

My graduate adviser, Ken Sauer, has been a great source of encouragement and support. I am thankful for the independence I was given to pursue research ideas. I feel fortunate to have worked with such a nice person.

Lastly, I would like to thank my family and friends for all their love, patience and support.

Table of Contents

Abbreviations

Bchl	Bacteriochlorophyll
CD	Circular dichroism
Chl	Chlorophyll
CFD	Constant Fraction Discriminator
E_A	Activation Energy
F685	Fluorescence at 685 nm
F690	Fluorescence at 690 nm
F720	Fluorescence at 720 nm
F735	Fluorescence at 735 nm
HITC	1,1',3,3,3',3'-Hexamethylindotricarbocyanine
IRF	Instrument Response Function
kDa	kiloDalton
LHC-I	Light harvesting complex of Photosystem I
LHC-II	Light harvesting complex of Photosystem II
MCA	Multi-channel analyzer
MCP-PMT	Microchannel plate-photomultiplier tube
NADP	Nicotinamide adenine dinucleotide phosphate
P700	Reaction center of Photosystem I
PD	Photodiode
PMT	Photomultiplier Tube
PSI	Photosystem I
PSI-200	Isolated Photosystem I with a 200 Chl antenna complement
PSI-100*	Isolated Photosystem I from *Synechococcus*, sp.
PS II	Photosystem II
QRC	Quantum Reference Counter
RC	Reaction center
RT	Room temperature
SDS	Sodium dodecyl sulfate
SDS-PAGE	Sodium dodecyl sulfate-polyacrylamide gel electrophoresis
TAC	Time-amplitude Convertor
T_{KS}	Kennard-Stepanov Temperature
Tris	Tris[hydroxymethyl]aminomethane
Tricine	N-tris[Hydroxymethyl]methylglycine

Chapter I: Introduction

In higher plants, two photosystems acting in concert are essential components in a chain of electron transfer events which drive the oxidation of H_2O and the reduction of NADP, ultimately providing electrons for the Calvin cycle. The primary charge separation within each photosystem is a light driven reaction. Protein complexes containing proportionally large amounts of pigment molecules serve to harvest light energy and transfer it to the reaction center, the site of charge separation. The migration of energy through the antenna to the reaction center is both fast and efficient; however, at this time the mechanism of excitation transfer is poorly understood.

We have used fluorescence spectroscopy to study the energy transfer pathways within isolated antenna complexes. In Photosystem I (PSI) the fluorescence characteristics of the associated antenna are unusual. At room temperature a large portion of the emission occurs at lower energy than the reaction center; additionally, this emission shifts to longer wavelengths as the temperature is lowered. Since the flow of energy is typically from higher energy to lower energy, the fluorescence behavior of PSI suggests an alternate mechanism of energy transfer within the antenna complex. This study centers on the absorption of light energy and subsequent excitation transfer to the reaction center. The efficiency of this process in plants and bacteria is greater than 90%. [1]

Light harvesting systems, pivotal in the photosynthetic process, are vastly different from species to species. These systems, however, do possess some common characteristics:

1) Pigment molecules are specifically associated with polypeptides. This interaction can either be a covalent or non-covalent linkage and results in spectrally distinct pigment-protein complexes. Generally, Bchl and Chl are ligated to histidine residues through the central Mg ion of the chromophore. Chromophores of phycobilisomes are attached covalently to the protein via a thioether linkage.

2) The polypeptides act as a scaffolding for the chromophores. The three dimensional arrangement of the pigments by the protein affects the flow of energy transfer within the system. The interaction of several antenna complexes can be governed by protein-protein interactions.

3) The natural environment of the organism is one of the major influences on the pigment composition and morphology of the antenna system. For example, absorption

maxima of pigments in a light harvesting complex are correlated with the wavelengths of available light. Additionally, the size of the light harvesting system is influenced by the intensity of light. In purple bacteria antenna domain size increases at lower light intensities.

4) Antenna complexes can be either intra or extra-membrane. If an antenna is extra-membrane it is anchored to the membrane through a protein interaction such as the linker polypeptides in phycobilisomes or the protein baseplate in the chlorosomes. Thus, in a discussion of excitation transfer in light harvesting systems it is important to consider the protein matrix. This matrix serves as the framework for the arrangement of chromophores and hence, the flow of energy within the system.

It is of interest to first examine the light harvesting systems of bacteria and algae because they are evolutionary predecessors to higher plants. Also, in most cases these systems have been more extensively studied, leading to specific knowledge of structure-function relationships. A complete discussion of these light harvesting systems is beyond the scope of this work, certain characteristics are highlighted in order to draw parallels with higher plant antenna complexes.

1. *Cyanobacteria*

The primary light harvesting system of cyanobacteria and red algae is an extra-membrane system called the phycobilisome. These pigment-protein complexes form vast arrays of well-defined rods and cores on the surface of the lamellae. The bilin chromophores in these systems are open-chain tetrapyrroles held in a fixed extended conformation by the protein environment. The pigments are covalently attached to the protein through a thioether bond. The protein matrix can affect the absorption and emission maxima of a particular system. For instance, phycocyanin and allophycocyanin contain the same chromophore phycocyanobilin, yet their absorption maxima differ by 30 nm. The flow of energy through the rods to the cores is energetically downhill, because the pigments absorb at increasingly longer wavelengths closer to the core. These pigment-protein complexes exist in well-defined aggregates of monomers. The monomers are composed of one α and one β subunit, weighing approximately 17-22 kDa. [2] Structural information is obtained from the crystal structure of C-phycocyanin isolated from *Mastigocladus laminosus*. [3,4] The α-subunit holds one chromophore, while the β-subunit contains two. The dominant structural feature of the subunits are 8 α-helices. Higher order aggregates consist of trimers and hexamers; each rod is composed of stacked discs of hexamers. Uncolored

"linker" polypeptides mediate assembly of the biliproteins into appropriate aggregates, modify spectroscopic properties and determine the location of the aggregate within the rod structure.

2. *Green Bacteria*

Green bacteria, like the cyanobacteria, contain large light harvesting arrays, referred to as the chlorosomes. The chlorosomes are also an extra-membrane system; although they exist in long rods which lie parallel to the membrane in contrast to the phycobilisomes. Chromophores in this system can be Bchl c, d or e, which have a peripheral double bond in ring II of the tetrapyrrole causing them to resemble Chl more closely than Bchl a or b. [5] It is thought that the rod structures are composed of Bchl c protein complexes. In the rods the Bchl appear to be in a well-ordered array with pigment-pigment interactions occurring through carbonyl and hydroxy-ethyl functional groups of the porphyrin system. [1] Recent data are indicative that the chlorosomes might be somewhat atypical with respect to other light harvesting systems. In isolation procedures a fixed ratio of Bchl c to protein could not be obtained, causing Holzwarth et al. [6] to conclude that protein-free chromophore aggregates are functioning as the light harvesting system. Further evidence stems from the fact that fluorescence spectra of in vitro aggregates resemble those obtained in vivo. This surprising result was observed in *Chloroflexus aurantiacus*; characterization of other green bacteria is needed prior to accepting it as a dominant structural motif. In any case the pigment to protein ratio is quite high in this system, possibly leading to behavior more like that of chromophore aggregates.

The chlorosomes are attached to the cytoplasmic membrane through a protein baseplate. This baseplate contains a Bchl a protein that is thought to serve as an energy transfer intermediate between the chlorosomes and the reaction center. Transfer efficiency from the Bchl c to Bchl a is estimated to be 60-70%. The protein isolated from *Prosthecochloris aestuarii* has been crystallized. It consists of three identical subunits, each containing seven Bchl a molecules. Five of the seven Bchl a molecules are ligated to histidine residues, one to a water molecule and one to a carbonyl oxygen of the polypeptide backbone. [7,8] As in the phycobilisomes the orientation and position of the pigment molecules is determined by their specific interactions with the protein. Although this polypeptide was the first light harvesting chromoprotein to be crystallized, there are few structural similarities with membrane-bound light-harvesting polypeptides. β sheets enclose a core of pigment, in which the hydrophobic

interactions of the phytyl tails are thought to assist in protein folding. Recent data are indicative,however, that α-helical structure is more predominant in intrinsic membrane-bound proteins.

Nevertheless, there are many similarities between green bacteria and PSI. In green bacteria the primary electron acceptor is a monomeric pigment molecule,.and other electron transfer components include iron-sulfur centers. Similar acceptors are observed in the reaction center of PSI of higher plants. Additionally, in the Bchl a protein and in a reaction center pigment protein complex isolated from *Prosthecochloris aestuarii*, it has been reported that lower temperatures induce shifts in fluorescence emission from 817 to 828 nm. In the Bchl a protein the yield at 828 nm increases 5.8 fold from 120K to 4K. Swarthoff et al. [9] attribute the changes in intensity ratios in the emission to a thermal equilibrium between two emitting species with an energy difference of 150 cm^{-1}. In *C. aurantiacus* isolated membranes containing the Bchl 808-866 nm complex also demonstrate a temperature dependent shift in emission maximum In that case as well, it was determined that the two species were in thermal equilibrium. [10] Similarly, in PSI the emission maximum shifts to longer wavelengths at lower temperatures and the fluorescence yield increases. The temperature dependence of PSI fluorescence will be discussed in chapters 3 and 5. In green bacteria the reaction center absorbs at 840 nm and therefore excitation transfer from either of these emission bands is an energetically downhill process, whereas in PSI it appears to be an uphill process.

3. *Purple Bacteria*

Compared with the phycobilisomes and the chlorosomes the antenna size of the purple bacteria is considerably smaller, with approximately 100-150 Bchl/ RC. The number of Bchl/RC is variable depending on the light intensity. In purple bacteria the photosynthetic units are situated in invaginations of differentiated membranes. As in the green bacteria, the pigments are non-covalently bound to polypeptides. In this case the primary chromophores of the system are Bchl a, Bchl b and carotenoids. In most species, although there are notable exceptions, the antenna consists of two light harvesting complexes, B800-850 and B875. Based upon exciton annihilation measurements, electrophoretic mobility and analysis of crystals it appears that the light harvesting system is organized in hexamers of α and β subunits, recalling the structural unit of the phycobilisomes. In Bchl 850 six histidines are conserved in the αβ trimer, postulated to be binding sites for the Bchl. [11] As in the phycobilisomes

α-helices are an important structural component of the trimers.

The purple bacteria, especially in the case of *Rps. viridis*, are interesting with respect to their energy transfer dynamics because they contain pigments which must transfer energy uphill to the RC. In *Rps. viridis* the antenna absorbs at 1040 nm and the reaction center absorbs at 985 nm. The chromophore of the antenna in *Rps. viridis* is Bchl b. It has also been reported for *R. rubrum* and *Rb. sphaeroides* that an integral pigment of the antenna absorbs at 896 nm. [12] In both cases excitation transfer to the RC is significantly uphill. For the B896 pigment it is thought that excitation is concentrated on this pigment prior to transfer to the RC. [13] Recently, it has been shown that the quantum yield of primary photochemistry in *Rps. viridis* for the B1040 antenna is 0.97, implicating an effective uphill energy transfer mechanism in that system. [14]

The absorption bands of the Bchl are considerably red-shifted, maximally 260 nm, as compared with in vitro measurements. The exact mechanism for this red-shift is unknown; although, there are several possibilities. One of which is that dimeric or oligomeric forms of the chromophore exist in vivo and thus the shifts result from excitonic interactions between neighboring transition dipoles. Electrochromic effects caused by charged amino acids located close to the chromophores could also result in the shift in the absorption band. [5] This situation is analogous to that of PSI, where it appears that long wavelength absorbing pigments exist and transfer energy uphill to the reaction center.

It has also been reported for *R. rubrum*, *Rb. sphaeroides* and *C. vinosum* that the emission maximum shifts to longer wavelengths upon cooling. [15] This behavior is reminiscent of the green bacteria and PSI. In *R. rubrum*, which contains only one antenna species, the increase in fluorescence yield is attributed to a decrease in the energy transfer rate constant based upon decreasing overlap of donor and acceptor chromophores. For *Rb. sphaeroides* and *C. vinosum* the fluorescence yield increases and the emission maximum shifts approximately 30 nm to longer wavelength as a function of decreasing temperature. In both of these species the ratio of the shorter wavelength and longer wavelength emission bands remained relatively constant from 80K to 4K, indicating that the two emitting species are not in thermal equilibrium at these temperatures, in contrast to the temperature dependent behavior observed in green bacteria and in *R. rubrum*. It is also possible that the occurence of more than one antenna species precludes a simple relation between temperature and fluorescence yield.

4. *Higher plants*

In higher plants the antenna systems and reaction centers are not so well characterized as their bacterial counterparts. The primary chromophores of higher plants and green algae are Chl a, Chl b and carotenoids. Chl proteins which bind Chl a and not Chl b are most closely associated with the reaction centers. Typically, they are highly hydrophobic and contain only Chl a and β-carotene. Additionally, these proteins are chloroplast encoded, whereas the Chl a/b binding proteins are nuclear encoded and must be transported across the chloroplast.

Photosystem II. The PS II reaction center has two Chl a binding polypeptides associated with it. Fifty percent of the amino acid residues of the proteins, CP 43 and CP 47, are hydrophobic. It is thought that this hydrophobic region contains seven trans-membrane α-helices. The molar Chl to protein ratio is 20-25 in this antenna species. [16]

PS II of higher plants also has an additional intramembrane light harvesting complex, which appears to be the functional replacement for the phycobilisomes found in cyanobacteria and red algae. This antenna complex, LHC-II, contains approximately half the polypeptide and Chl content of plant thylakoids. LHC-II has a 1:1.2 Chl a: Chl b ratio with non-stoichiometric amounts of carotenoid. Approximately 8 Chl a and 7 Chl b are bound per polypeptide. [1] The protein, isolated from plants, consists of at least 3 polypeptides with very similar primary structure. LHC-II polypeptides are the product of a multi-gene family. Currently, the exact polypeptide composition of LHC-II remains in some doubt, because several Chl a/b binding polypeptides have been isolated using the method of non-denaturing SDS-PAGE. Additionally, it appears that the proteins might be a mixture of processing products of several different genes. [16]

Recently, 2-dimensional and 3-dimensional crystals of LHC-II have been obtained and some aspects of structure have been elucidated by electron crystallography. [17-19] From these studies it was determined that LHC-II is composed of 3 polypeptides with 3 fold symmetry. This trimeric arrangement recalls the structure of the phycobilisomes, the Bchl a protein of green bacteria, and the purple bacteria. Each subunit contains 3 transmembrane α-helices and a large portion of the polypeptide chain is located outside the lipid bilayer, possibly assisting in grana stacking and phosphorylation of the polypeptide. From negative staining methods it was determined that the majority of the Chl is contained in the central region of the trimer. CD measurements on the crystal indicated the presence of a Chl b exciton of 3

fold symmetry and a Chl a-Chl b exciton, which did not show this symmetry. [20]

Photosystem I. This study centers on the energy transfer dynamics of photosystem I, thus it will be discussed in some detail in subsequent chapters. At this juncture it is useful to discuss some general properties of the system to make comparisons with the bacterial light harvesting systems. The complex employed for this study, PSI-200, consists of two high molecular weight (MW) polypeptides which bind the initial electron donors and acceptors. (figure 1.1) As in the green bacteria the first electron acceptor is thought to be a monomeric chlorophyll molecule. Three Fe-S centers also function as electron acceptors; the Fe-S centers reduce water soluble ferredoxin, which in turn reduces NADP. The lower MW polypeptides include an Fe-S center binding protein and a light harvesting complex, LHC-I. The two reaction center-containing polypeptides have a high degree of mutual homology, with approximately 45% conserved amino acids. Based upon hydropathy plots it is proposed that each polypeptide has 11 transmembrane α-helical segments. It is thought that these polypeptides bind 100 Chl a molecules through histidine residues, which are highly conserved between the two proteins. Seventy percent of the conserved histidines are found in the putative membrane spanning regions. [21]

The pigment-to-protein ratio is quite large for the PSI core polypeptides; it is possible that the actual pigment interaction is more akin to the chromophore aggregates observed in the chlorosomes. Chl can be removed from the reaction center polypeptides without removing any protein by either linear density gradients or column chromatography, indicating that the pigment-protein interaction is not so strong as in other systems. We speculate that chromophore-chromophore interaction is very significant with respect to the energy transfer dynamics within this system. Additionally, this reaction center complex with an 100 Chl a antenna complement has an emission maximum at 690 nm at RT. The emission at 720 nm increases dramatically with decreasing temperature until it completely dominates the fluorescence spectrum. The entire PSI-200 complex has an emission maximum at 735 nm at 77K. This dramatic increase of longer wavelength emission at lower temperatures is suggestive of the existence of low energy pigments within the antenna system. This situation is analogous to what has been reported for purple bacteria. Interestingly, in PSI approximately 50% of the fluorescence emission at room temperature occurs at lower energy than the absorption maximum of the reaction center, implicating the occurence of uphill energy transfer to the reaction center. This study will address the
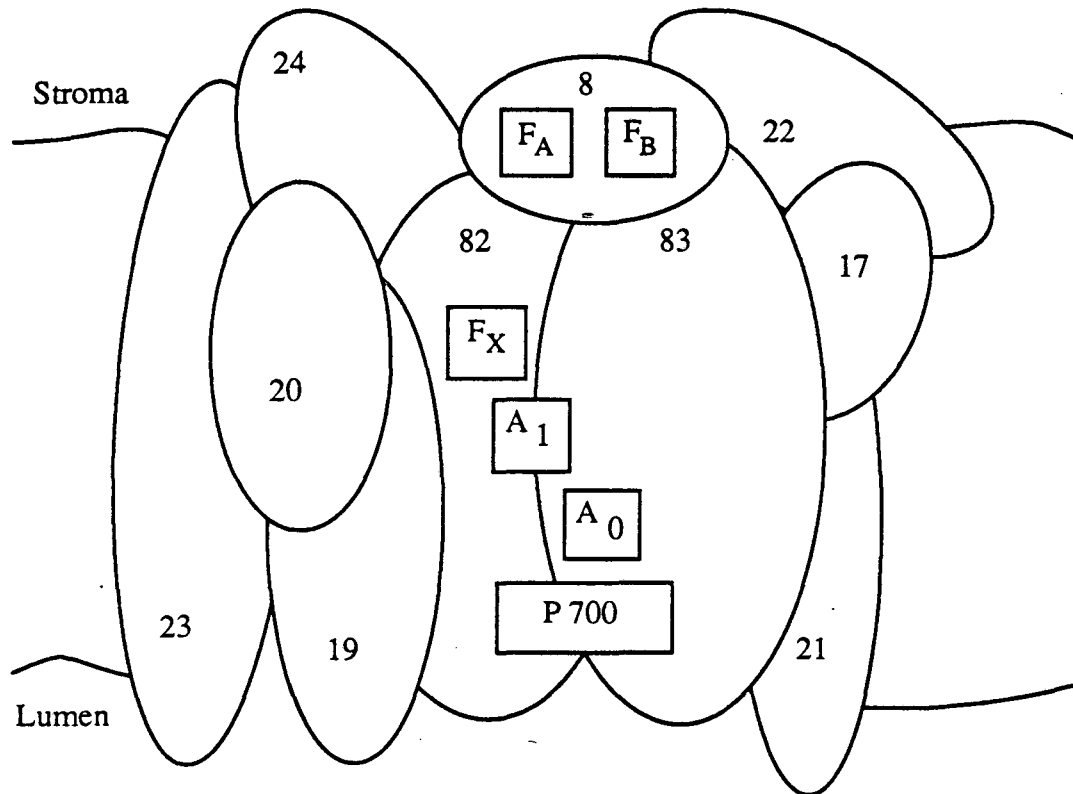
Figure 1.1: Schematic representation of PSI-200. Major polypeptide and electron transfer components are depicted. Numbers indicate approximate weight of polypeptides in kDa. 82 and 83 kDa proteins contain reaction center, P700, primary electron acceptors A_0, A_1 and Fe-S center X. These proteins also hold 100 Chl a molecules. Other Chl-containing polypeptides are 24, 23, 20 and 21 kDa, which comprise LHC-I. 19 and 22 kDa proteins are plastocyanin- and ferredoxin-docking proteins, respectively. The 8 kDa protein binds Fe-S centers A and B.

temperature dependence of the long wavelength fluorescence in two PSI reaction center complexes , one isolated from spinach and one from cyanobacteria. In both cases the energy transfer dynamics as a function of temperature will be discussed.

Spectroscopic studies have also been performed on the isolated light harvesting complex of PSI. Common characteristics of the two light harvesting complexes of higher plants include:

1) The molecular weights of the associated polypeptides generally fall in the 20 to 30 kDa range and the proteins are all nuclear encoded.

2) These complexes are absent in dark grown plants; under illumination LHC-I and LHC-II are synthesized with the same kinetics .

3) Polypeptides of LHC-II and LHC-I are believed to be products of the Chl a/b binding protein multigene family and appear to be immunologically related, although there are some conflicting reports. [22-24] Some sequence homology exists; in a comparison of genes from tomato and petunia it was found that approximately 50 amino acid residues are highly conserved. [16]

At this time it is not clear whether there are single or multiple copies of each polypeptide. In LHC-I it appears that the 20-21 kDa proteins are responsible for the emission at 730 nm (LHCI-730), while emission at 680 nm stems from the 23 kDa protein (LHCI-680). [25] Bassi and Simpson [26] were able to isolate a complex from maize which contains the LHCI-730 proteins and the reaction center polypeptides. This pigment-protein complex has the 730 nm emission characteristic of LHC-I, implicating close contact between the long wavelength emitting species and the reaction center complex.

To address the mechanism of excitation transfer within a light harvesting assembly a detailed knowledge of structure assists in the elucidation of function. The distances between chromophores and their relative orientation influence the energy transfer properties amongst the chromophores. The structures of several different light harvesting complexes have been discussed. At present detailed structural information is available for only a few systems; however, some structural motifs are emerging. The predominance of α-helices even in extra-membrane water soluble chromoproteins indicates they are a dominant structural feature for this class of complexes. Certainly, the association of monomeric subunits into trimers appears to be a primary structural characteristic for light harvesting assemblies. Trimers have been observed in the Bchl a-protein, purple bacteria, LHC-II, PSI-RC and of course, the well-characterized phycobilisomes. We speculate that the 3-fold symmetry of these structures allows the

absorption of light to be independent of the rotational orientation of the complex to the light source. Thus, the harvesting of light energy is more efficient as a result of a rotationally isotropic antenna.

5. *Mechanisms of energy transfer*

One mechanism of energy transfer within photosynthetic systems has been described in terms of donors, D and acceptors, A. In general, transfer from D to A is an energetically downhill process and results in the quenching of fluorescence of D and an enhancement of the emission of A, stimulated by the photons absorbed by D. Thus, the fluorescence yield of the donor, D becomes a measure of the degree of energy transfer to the acceptor, A. The fluorescence yield of D can be expressed as:

$$\Phi_D = \frac{k_F}{k_F + k_{IS} + k_{IC} + k_{DA}}$$

where k_F is the intrinsic radiative rate constant of D and k_{IS} and k_{IC} are the rate constants of intersystem crossing and internal conversion, respectively. k_{DA} represents the net rate constant of transfer from D to A. If all other deactivation processes from the excited state remain constant then the amount of energy transfer from D to A will inversely affect the fluorescence yield of D.

The Coulombic interaction of transition dipoles is the primary mechanism of energy transfer. There are two limiting cases, strong coupling and very weak coupling, which arise from essentially the same interaction. [27] The distinct characteristics of the cases result from the differences in magnitude of the interaction when compared with the electronic bandwidth and individual vibronic bandwidth. In the strong coupling case the electronic excitation is very rapidly delocalized over the components of the system. In a donor-acceptor pair the excitation is delocalized between the pair in a coherent process. After approximately 1 ps the exciton has become more diffuse and is localized on neither the donor nor the acceptor. [28] CD spectra display a characteristic conservative spectrum for excitonically coupled species. Other spectroscopic signatures of excitonic interactions include the shift or splitting of peaks in absorption spectra. For strong coupling the interaction can be described using point dipole approximations for the two transition dipoles,

$$J = \left(\frac{\mu_A \cdot \mu_D}{R_{AD}^3} \right) - \frac{3 (\mu_D \cdot R_{AD})(R_{AD} \cdot \mu_A)}{R_{AD}^5}$$

μ_A, μ_D = transition dipoles of acceptor, donor

R_{AD} = separation between the dipoles

In the case of larger distances or longer times energy transfer can be treated using the Förster formulism for very weak coupling. It should be stressed again that these different cases are the extreme limits of the same dipolar interaction. In weak coupling the excitation is more localized on either the donor or the acceptor resulting in a "hopping" mechanism of energy transfer. [29] For the simple case of a donor-acceptor pair the transfer rate constant,

$$k_{DA} = k_F^D \left(\frac{R_o}{R_{DA}} \right)^6$$

where k_F^D is the rate constant of fluorescence of the donor in the absence of acceptor. R_o, is a characteristic distance defined as:

$$(R_o)^6 = \frac{9 \ln 10 \; \kappa^2 \; k_D^F}{128 \; \pi^5 \; n^4 \; N_A} \int F_D(v) \; \varepsilon_A(v) \; v^{-4} \; dv$$

$F_D(v)$ = the normalized emission spectrum of the donor in the absence of the acceptor.
$\varepsilon_A(v)$ = the molar extinction coefficient of the acceptor at frequency, v.
n = refractive index of the medium
$\kappa = \cos \alpha - 3 \cos \beta_1 \cos \beta_2$, where α is the angle between the two dipoles and β_1, β_2 is the angle of each dipole with R_{AD}.
N_A = Avogadro's number

Thus, the parameter (R_o) is strongly dependent on the overlap between the donor emission and the acceptor absorption spectrum. The inverse sixth dependence of R_o results from the square of the dipole-dipole coupling. Typical values for R_o range from 2.0 to 7.0 nm. When $R = R_o$ then the monomolecular decay rate effectively competes with the transfer rate, when $R < R_o$ then the absorbed photon is more likely to undergo pairwise transfer. [30] For identical molecules in similar environments transfer can occur in either direction. The angle, α can be determined by monitoring the polarized emission of A with respect to a polarized excitation of D. For randomly oriented pigments κ has a value of 2/3. Additionally, linear dichroism measurements yield information regarding the angle of the transition dipoles relative to a given plane of orientation.

At present time-resolved measurements on photosynthetic systems are instrumentally limited to probing localized energy transfer processes. Certainly, spectroscopic studies of the Bchl a protein, C-phycocyanin and LHC-II indicate that excitons are present within these systems. With the advent of sub-picosecond laser pulses, it is becoming possible to address the presence of excitonic interactions within light harvesting arrays. The inherent time constant of these interactions makes them

difficult to assess by more standard time-resolved measurements. In the present work the time scale of the single photon counting measurements performed, as discussed in chapter 2, limits discussion to a more localized mechanism of energy transfer.

6. *References for Chapter I*

1. Zuber, H. (1985) *Photochem. Photobiol.*, **42**, 822-844.
2. Glazer, A.N. (1983) *Ann. Rev. Biochem.*, **52**, 125-57.
3. Schirmer, T., Bode, W., Huber, R., Sidler, W. and Zuber, H. (1985) *J. Mol. Biol.*, **184**, 257-277.
4. Schirmer, T., Bode, W. and Huber, R. (1987) *J. Mol. Biol.*, **196**, 677-695.
5. Amesz, J. and Vasmel, H. (1986) in Light Emission by Plants and Bacteria (Govindjee, J. Amesz and D.C. Fork, eds.) New York: Academic Press, 423-450.
6. Holzwarth, A.R., Griebenow, K. and Schaffner, K. (1990) *Z. Naturforsch.*, **45c**, 203-206.
7. Fenna, R.E., Matthews, B.W., Olson, J.M. and Shaw, E.K. (1974) *J. Mol. Biol.*, **84**, 231-240.
8. Matthews, B.W., Fenna, R.E., Bolognesi, M.C., Schmid, M.F. and Olson, J.M. (1979) *J. Mol. Biol.*, **131**, 259-285.
9. Swarthoff, T., Amesz, J., Kramer, H.J.M. and Rijgersberg, C.P. (1981) *Isr. J. Chem.*, **21**, 332-337.
10. Vasmel, H., van Dorssen, R.J., De Vos, G.J. and Amesz, J. (1986) *Photosynthesis Res.*, **7**, 281-294.
11. Hunter, C.N., van Grondelle, R. and Olsen, J.D. (1989) *Trends in Biochem. Sci.* **14**, 72-76.
12. Hunter, C.N., van Grondelle, R. and van Dorssen, R.J. (1989) *Biochim. Biophys. Acta*, **973**, 383-389.
13. Bergström, H., van Grondelle, R. and Sundström, V. (1989) *FEBS Lett.*, **250**, 503-308.
14. Trissl, H.W., Breton, J., Deprez, J., Dobek, A. and Leibl, W. (1990) *Biochim. Biophys. Acta*, **1015**, 322-333.
15. Rijgersberg, C., van Grondelle, R. and Amesz, J. (1980) *Biochim. Biophys. Acta*, **592**, 53-64.
16. Green, B.R. (1988) *Photosynthesis Res.*, **15**, 3-32.
17. Kühlbrandt, W. (1984) *Nature*, **307**, 478-480.
18. Kühlbrandt, W., Becker, A. and Mäntele, W. (1988) *FEBS Lett.*, **226**, 275-279.

19. Kühlbrandt, W. (1988) in Photosynthetic Light Harvesting Systems (H. Scheer and S. Schneider, eds.) Berlin: W. de Gruyter, 211-215.

20. Ide, J.P., Klug, D.R., Kühlbrandt, W., Giorgi, L.B. and Porter, G. (1987) *Biochim. Biophys. Acta*, **893**, 349-364.

21. Malkin, R. (1987) in The Light Reactions (J. Barber, ed.) Amsterdam: Elsevier Science Publishers, 495-524.

22. Evans, P.K. and Anderson, J.M. (1986) *FEBS Lett.*, **199**, 227-233.

23. Williams, R.S. and Ellis, R.J. (1986) *FEBS Lett.*, **203**, 295-300.

24. White, M.J. and Green, B.R. (1987) *Eur. J. Biochem.*, **163**, 545-551.

25. Lam, E., Ortiz, W. and Malkin, R. (1986) *FEBS Lett.*, **168**, 10-14.

26. Bassi, R. and Simpson, D. (1987) *Eur. J. Biochem.* **163**, 221-230.

27. Förster, T. (1965) in Modern Quantum Chemistry, Part 3 (O. Sinonaglou, ed.) New York: Academic Press, 93-137.

28. Knox, R.S. (1977) in Primary Processes of Photosynthesis (J. Barber, ed.) Amsterdam: Elsevier, 55-97.

29. Pearlstein, R.M. (1982) in Photosynthesis: Energy Conversion by Plants and Bacteria, Vol. I. (Govindjee, ed.) New York: Academic Press.

30. Knox, R.S. (1986) in Encyclopedia of Plant Physiology, New Series, Vol. 19 (L.A. Staehelin and C.J. Arntzen, eds.) New York: Springer-Verlag, 286-298.

Chapter II: Materials and Methods

1. Steady State Measurements

     Absorption spectra were obtained using a Varian 2300 Spectrophotometer in the UV-Vis mode. In general samples were diluted with 0.05M Tricine buffer, pH=7.8 to give a [Chl]=10 μg/ml. Pathlength for measurements was 1.0 cm.

     Protein composition of the preparations was assessed by sodium dodecyl sulfate polyacrylamide gel electrophoresis (SDS-PAGE). The electrophoretic procedure was based on the Laemmli system. [1] Only Bio-Rad electrophoresis-grade reagents were employed and all solutions were filtered and degassed. The running gel consisted of 12.5% acrylamide (w/v), 1.1% bis (w/v), 0.1% SDS (w/v), 0.05% ammonium persulfate (w/v), 0.05% TEMED (w/v) and 0.375M Tris, pH=8.8. Stacking gels contained 6% acrylamide (w/v), 0.5% bis (w/v) and 0.125M Tris, pH=6.8; other constituents were the same concentration as in the running gel. The sample buffer used was 62.5mM Tris, pH=6.8, 2% SDS (w/v), 10% glycerol (v/v) and 5% 2-mercaptoethanol (v/v). The tank buffer contained .25M Tris, pH=8.3, 0.192M glycine and 0.1% SDS. Gels were cast between two 16 x 18 cm glass plates separated by 0.75 mm. Gels were run at 16 mA constant current for approximately 4 h at 295K.

     The amount of Chl/P700 was determined by light-induced absorption changes using an Aminco DW-2 spectrophotometer in the split beam mode. Side illumination was achieved with a tungsten lamp. Two Corning 4-96 color filters were used to select the wavelengths (350-650 nm) of exciting light. The actinic light was introduced into the sample compartment using a fiber optic cable. (figure 2.1) Absorption changes were monitored at 700nm with an EMI GENCOM 9684 (S1 type) photomultiplier tube through a 700 nm narrow bandpass filter. The concentration of P700 was calculated using $\Delta\varepsilon=64$ mM^{-1} cm^{-1}. [2] Samples were suspended at 10 μg Chl/ml in 1 mM ascorbate, 0.05M Tricine, pH=7.8.

     Steady state fluorescence emission spectra were taken with a SPEX Fluorolog 2 model 212 spectrofluorimeter. An interface to an Epson Equity I computer was established through a Fluorimeter Control System (Brown's Software). A cooled RCA 31034A photomultiplier tube (PMT) was used for fluorescence detection. All measurements were made at 90° to the direction of excitation. Monochromator slits were adjusted minimally for signal/noise=1000 and maximally to avoid saturation of the PMT at 150,000 cps. In general this adjustment resulted in a bandpass of 2-4 nm.
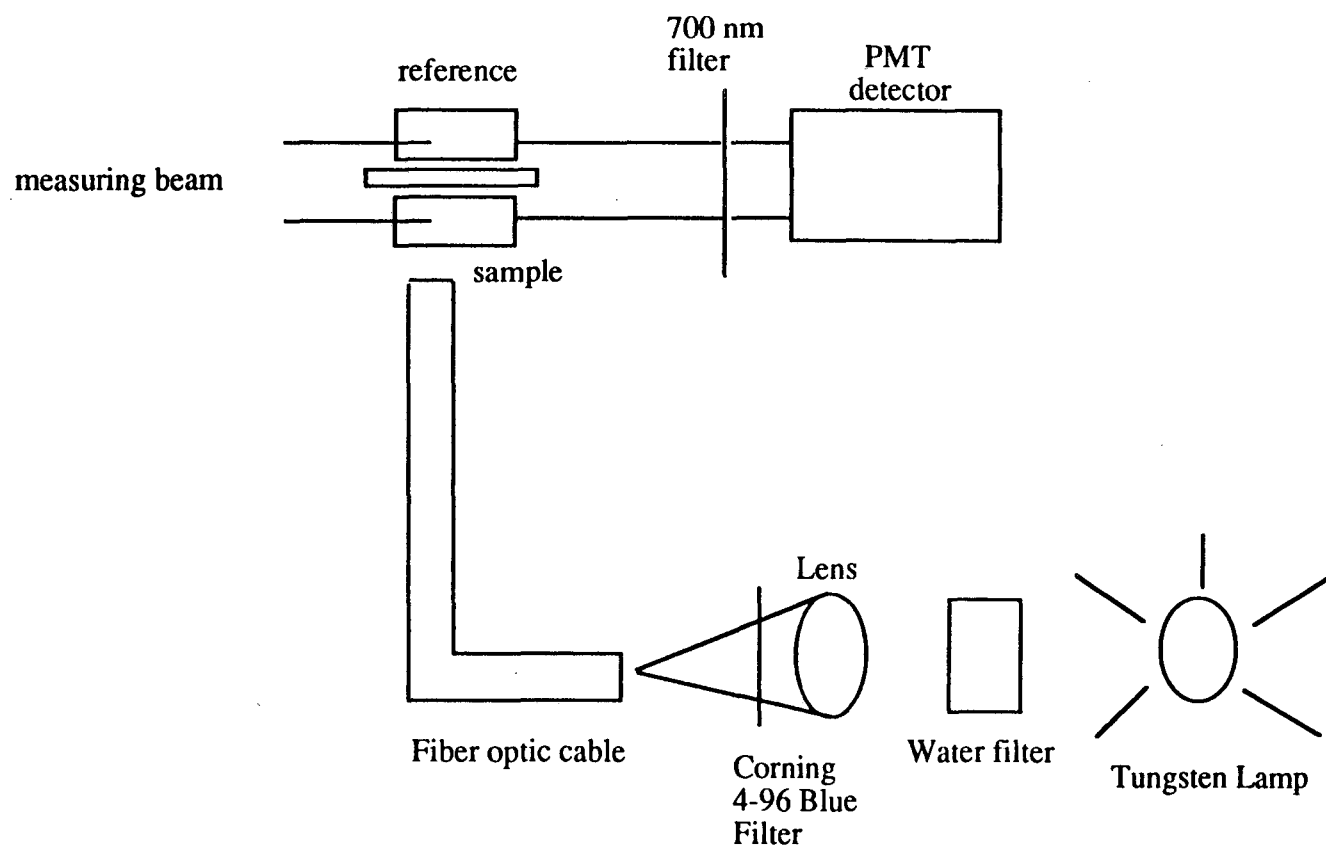
Figure 2.1: Optical Bleaching Assembly. Actinic light is introduced into the sample compartment via a fiber optic cable. The measuring beam is perpendicular to the actinic light.

Measurements on the PSI-200 complex had a bandpass of 4 nm, while measurements on LHC-1 had a bandpass of 2 nm. The wavelength dependence of the emission monochromator and photomultiplier tube was corrected by calibration with a standard lamp (Optronics Laboratories 245C). The wavelength dependence of the lamp and excitation monochromator were corrected using a quantum reference counter (QRC). [3] For the wavelength range 250-600 nm, the dye Rhodamine 610 was placed in front of the QRC. From 550 nm to 800 nm the dye, HITC, was used. [4] In both cases an excitation correction file was generated to compensate for differences in detection between the QRC and emission PMT. These files were created by placing a cuvette containing the appropriate dye in the sample compartment using a mirror assembly for rear angle fluorescence detection similar to the QRC detection system. For room temperature measurements samples were diluted with 0.05M Tricine, pH=7.8, to 0.1 absorbance at 675 nm in a 1.0 cm pathlength cell. Fluorescence studies at 77 K were done using a liquid nitrogen filled cylindrical glass dewar. Samples were diluted to 0.1 absorbance at 675 nm and were frozen to a cracked glass in 60% glycerol, 40% 0.05M Tricine, pH=7.8 in a glass NMR tube. Variable temperature measurements from 77 K to 298 K were done using an Oxford liquid nitrogen cryostat (D1020). For measurements done over a small temperature range, 269 K-303 K, sample temperature was controlled by a temperature regulating recirculating bath (Neslab, RTE-5B). The bath contained a 50% ethylene glycol/50% H_2O mixture, which flowed through a copper block sample holder. Temperature was monitored continuously at the sample.

For both quantum yield measurements [5,6] and tests of the Stepanov relation, [7,8] absorption and emission spectra were taken on the same sample. Absorption spectra were taken either immediately before or after the corresponding fluorescence measurement. Samples were diluted to 0.1 optical density at 675 nm with 0.05M Tricine, pH=7.8. Quantum yield was measured relative to a standard dye, Nile Blue in methanol. Calculations involved in these measurements will be discussed in chapter 3.

Polarization measurements were made using Glan Thompson polarizers for both excitation and emission. Emission was detected at right angles to the excitation beam. To correct for any polarization bias in the detection system, measurements were performed in the following manner [9]: Initially, excitation was vertically polarized and the emission was detected in both horizontal and vertical directions (I_{VV} and I_{VH}). Then, horizontally polarized excitation was used and again emission was detected in both horizontal and vertical polarizations (I_{HH} and I_{HV}). Let S_H and S_V represent the

horizontal and vertical light sensitivities of the emission monochromator and detector;
thus $I_{VV} = kS_V I_\parallel$ and $I_{VH} = kS_H I_\perp$. K represents a proportionality constant
accounting for the quantum yield of the sample and other factors. Then,

$$\frac{I_{VV}}{I_{VH}} = \frac{S_V I_\parallel}{S_H I_\perp}$$

where $I_\parallel$ and $I_\perp$ represent sample emission intensity detected parallel and perpendicular
to the excitation polarization. Similarly, $I_{HV} = kS_V I_\perp$ and $I_{HH} = kS_H I_\perp$; $I_\perp$ appears in
both expressions because detection at 90° causes both vertical and horizontal emission
components to be oriented perpendicular to the horizontally polarized excitation. Thus,

$$\frac{I_{HH}}{I_{HV}} = \frac{S_H I_\perp}{S_V I_\perp} \quad \text{and} \quad \frac{I_{VV} I_{HH}}{I_{VH} I_{HV}} = \frac{I_\parallel}{I_\perp}$$

Additionally, $S_H/S_V = 1/G$; this G factor is defined as the ratio of the sensitivity of the
detection system for horizontally and vertically polarized light. It can be measured
independently; however, in these measurements the polarization bias was eliminated by
recording four spectra and taking the appropriate ratio. [9] Polarization is defined as:

$$P = \frac{I_\parallel - I_\perp}{I_\parallel + I_\perp}$$

For all polarization spectra the sample was maintained at 5° C. Sample concentration
was 0.01 mg [Chl]/ml in a solution containing 50% glycerol and 50% 0.05M Tricine,
pH=7.8.

2. Time-Resolved Measurements

a. Instrumentation

Fluorescence decays were measured using the method of time-correlated single
photon counting. [9-11] A mode-locked (Spectra Physics 342) Argon ion laser
(Spectra Physics 171 or 2040-15) providing a train of pulses at a repetition rate of 82
MHz was used to drive a tunable cavity-dumped dye laser (Spectra Physics 375, 341).
For all measurements DCM was used as the lasing dye, yielding a lasing wavelength
range from 625-675 nm. For most of the experiments, pulses from the cavity dumper
were issued at a rate of 823 kHz; certain experiments were done at a repetition rate of
4.1 MHz and will be so indicated in the ensuing text. The pulse width as measured by
auto correlation is between 15-20 ps. The configuration of the instrument is depicted
in figure 2.2 Part of the excitation beam was sent to a fast photodiode (Antel
Optronics, AR-S2) and sampling oscilloscope (Textronix 7603, 7S11, 7T11), which
allowed for continuous monitoring of the pulse shape, width and stability during the
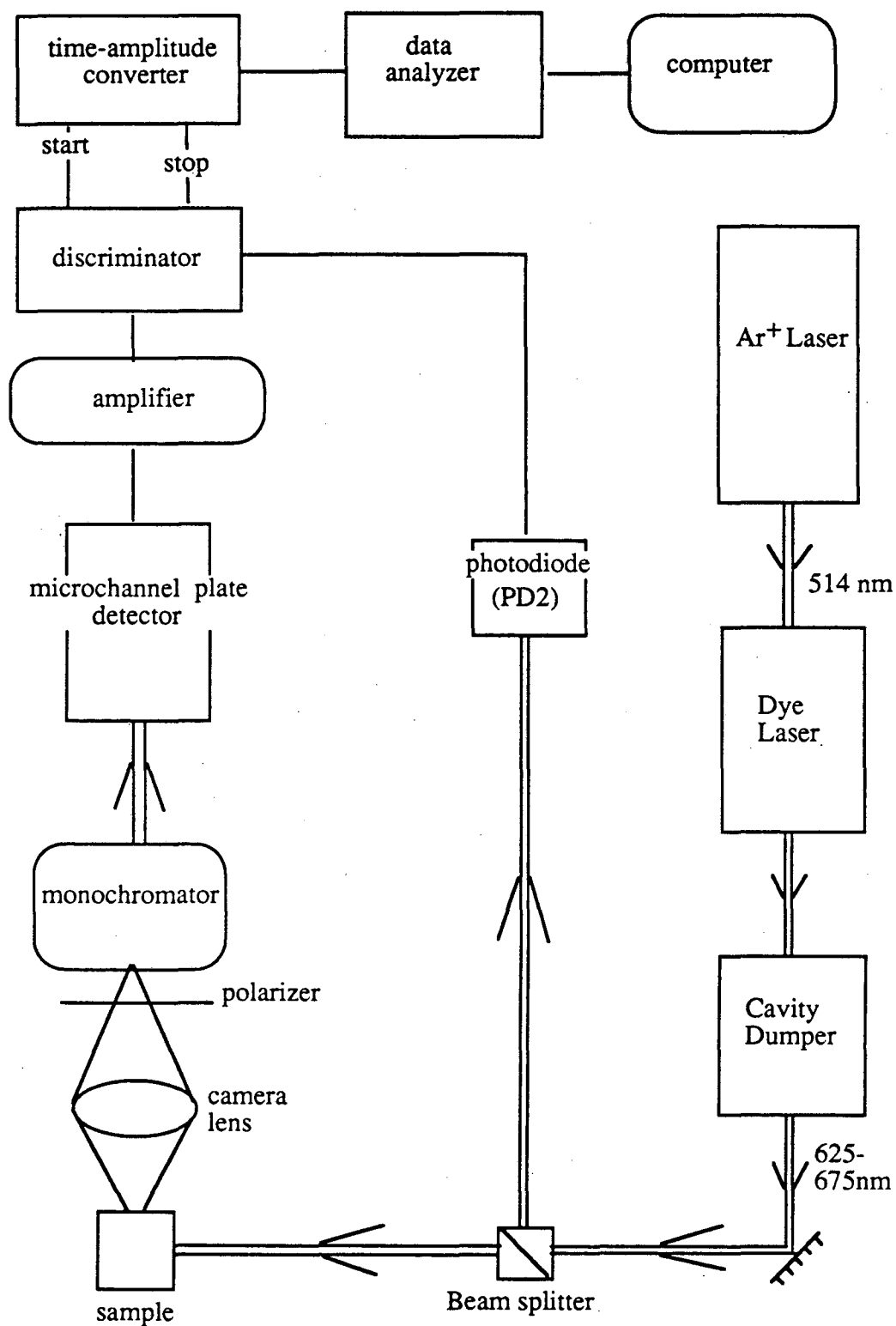course of the decay measurement. The beam was split off again to a second fast

Figure 2.2: Single Photon Counting apparatus. Lasing wavlenghts as indicated. Arrows show direction of optical beam. Further details in text.

photodiode (PD2) with a 100 ps risetime to generate the stop pulse for reverse single photon counting. The signal from this photodiode is immediately sent through an amplifier-discriminator. The majority of the excitation beam is sent to the sample box, where approximately 5% is sent to a photodiode in order to monitor the intensity of the beam close to the sample. Fluorescence is collected at right angles by an 85 mM camera lens (Nikon) and is then sent through a DH-10 Instruments SA monochromator. Prior to the monochromator the emission is sent through a sheet polarizer, set at 54.7°, in order to eliminate any anisotropic bias in the measurement. The majority of the measurements were done using 1 mm slits giving a wavelength resolution of 4 nm. A Hamamatsu R2809U-11 microchannel plate photomultiplier tube (MCP-PMT) with an S-25 spectral response was used for detection of the fluorescence. This 2 stage MCP-PMT has a 55 ps transit time spread allowing for detection of extremely fast pulses. A correction file for the wavelength dependence of the emission monochromator and detector was generated using a standard lamp (Optronics Laboratories 425C) as was done with the steady state fluorimeter. Signals from the detector were sent directly to an Hewlett-Packard 8447F amplifier with a 0.1-1300 MHz bandwidth. After 1 stage of amplification the signal is sent to a Tennelec 454 Constant Fraction Discriminator (CFD). Due to the relatively fast risetimes of the pulse, the CFD has been modified to increase the time resolution of the response. An external delay has been converted into an internal delay. The length of this delay was adjusted empirically for the fastest time response by monitoring the width of the instrument response function (IRF). Additionally, the input range selection jumper has been removed to eliminate any reflections which would contribute to a broadening of the time response.

The fluorescence pulse or start pulse is sent directly to the time-amplitude converter (EG&G Ortec 457). The stop pulse, taken from PD2, goes through two delay boxes (Ortec 425) before it arrives at the time-amplitude converter (TAC), in this manner the same excitation pulse triggers both the start and stop pulse. It was observed that count rates higher than 1 kHz broadened the instrument response function (IRF). This effect has also been observed by Hart et al.[12], who concluded that the time to amplitude conversion was influenced by the count rate. By imposing a gating period of 125 µs in which the TAC was effectively turned off, Hart et al. eliminated TAC rate dependence for count rates up to 8000 Hz. We observed that a 150 µs gating period was necessary to eliminate broadening of the time response. A pulse obtained from the true START output of the TAC triggered an Interstate

Electronics Corporation P22 pulse generator which produced a 150 μs gating pulse, used to suppress the TAC for that time period. This gating pulse limited the count rate to at most 6700 Hz. Typically, data were taken at 4000 Hz with an IRF between 50-60 ps. The width of the IRF was independent of the count rate using this configuration. For this method of data acquisition, the start pulse or the fluorescence pulse starts a voltage ramp, which is then stopped by the stop pulse or the laser pulse. In this manner a specific voltage corresponds to the difference in time between the start and stop pulses.

Voltage signals from the TAC were sent directly to a Northern Econ Series II MCA, where a histogram of pulses was built up. In general, data collection was terminated after 10,000 counts were amassed in the peak channel. In certain cases 20,000 counts were collected in order to improve signal/noise. The underlying supposition behind these measurements is that the probability distribution for emission of a single photon after excitation corresponds to the actual intensity versus time distribution of all of the photons produced subsequent to excitation. Therefore, by measuring single photon emission after several excitation flashes, a probability distribution can be constructed.

b. Data Analysis

These data were analyzed by a sum of exponentials using an iterative deconvolution program based on a non-linear least squares fitting routine. These programs were kindly provided by Dr. A. Holzwarth of the Max-Planck Institut für Strahlenchemie-Mülheim. Each of the decays is fast enough to have the width of the pulse and the time response of the detector and the electronics be an integral part of the decay. In order to evaluate the "true" fluorescence decay we employ a method of iterative deconvolution. [13]

$$F(t) = \int_0^t g(t-\tau)\, f(\tau)\, d\tau$$

In this expression F(t) is the measured decay, g(t) represents the actual decay rate and f(t) represents the excitation intensity function and the detector response function. τ represents the real time of the measurement. Using simulated data comparison of this method with either the method of moments or Fourier transforms indicates that it is the most effective at recovering the original parameters of the model function. [13] Thus, in the following experiments it was very important to have an accurate representation

of the excitation pulse profile and the detector response. The instrument response function (IRF) was obtained by scattering the excitation beam off a solution of non-dairy creamer suspended in H_2O. Typically, the IRF would be measured before and after the measurement of the fluorescence decay.

For the single analysis the fluorescence decay was described in terms of a sum of simultaneous exponential decays,

$$F(t) = \sum_i \alpha_i \exp{-(t/\tau_i)}$$

where F is the fluorescence intensity, α_i, the amplitude and τ_i, the lifetime of the individual components. [14] The amplitude can be either positive or negative and α_i and τ_i are optimized to obtain the best fit between calculated and experimental functions. Optimization is done using a Marquardt-type non-linear least squares algorithm. The quality of the fit is judged by two criteria. One criterion is a calculation of the weighted sum of the squares of the deviations of the experimental points from the calculated fitting function. This quantity is then divided by the degrees of freedom of the measurement, yielding a reduced chi-squared (χ^2) value which ideally should be 1.0. Typically, in single photon counting experiments, a good fit will have a reduced χ^2 between 0.8 and 1.2. Values significantly lower than 1.0 are indicative of an insufficient number of counts. [10] Values of 1.2 or greater typically signify the need for an additional component in the model function. In general, data analyzed in these experiments had reduced χ^2 values between 1.0 and 1.2.

In addition to the reduced χ^2 parameter the quality of the fit was also assessed by a plot of the weighted squared residuals. The residuals are weighted in the following manner:

$$w_i = \frac{\dfrac{1}{F_o(t_i)}}{\dfrac{1}{n}\sum_{i=1}^{n}\dfrac{1}{F_o(t_i)}}$$

where F_o is the experimentally obtained fluorescence decay, n is the number of time intervals in the experimental data and i indicates the specific time interval. Thus, greater weight is given to points where the experimental variance is less; in single photon counting this variance corresponds to the number of counts in the time interval. By weighting the residuals, a more accurate estimation of the error in the fit can be obtained. [15] In these experiments the weighted residuals were visually inspected for any non-random deviations about the zero axis. When both criteria were satisfied the fit was deemed acceptable (figure 2.3).

λ_{ex}=670nm λ_{em}=690nm

χ^2=1.007   SHIFT: 0.075

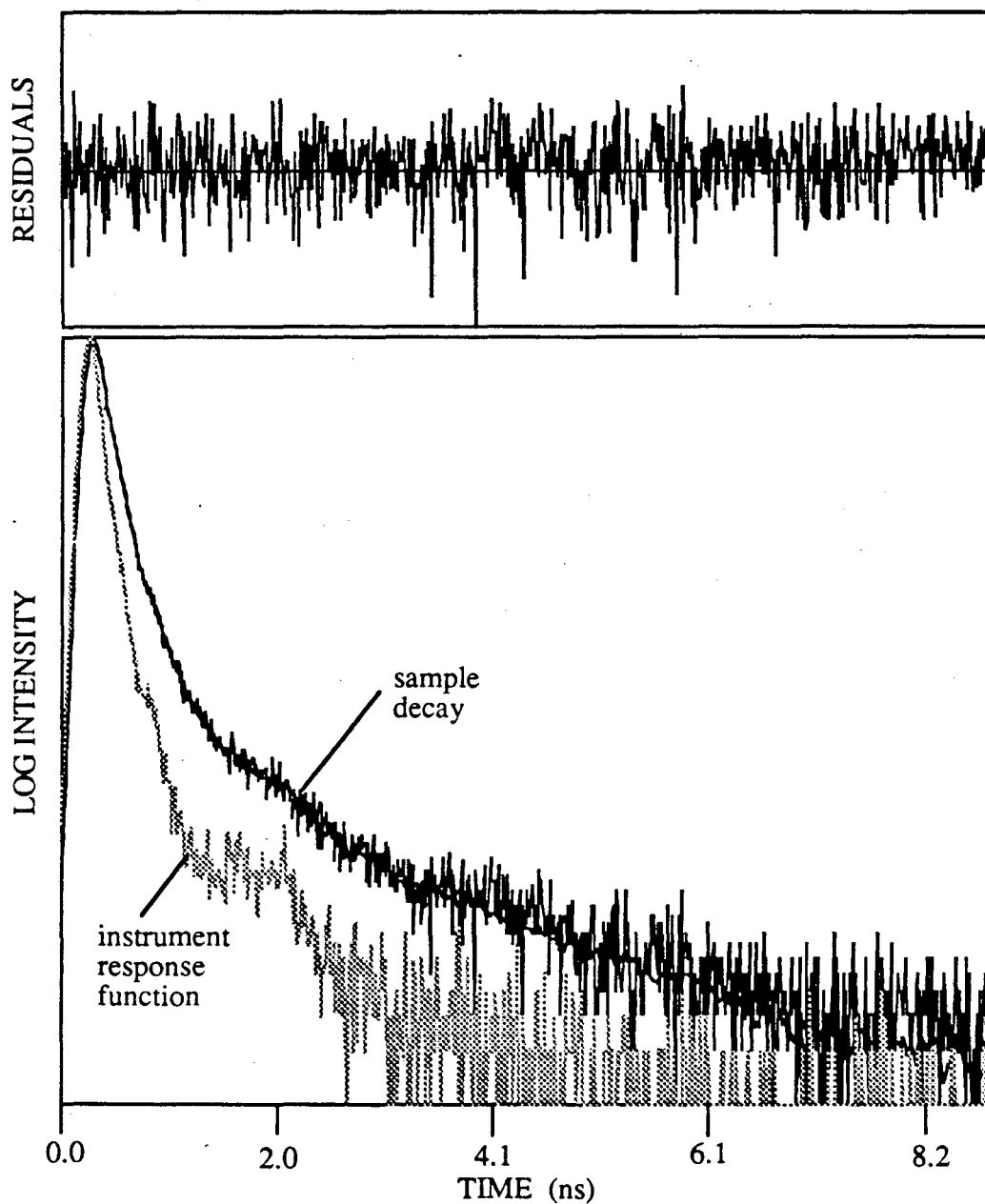| τ(ns):	0.029	0.090	1.860	0.327
α_t:	30.81	5.711	0.022	0.412

Figure 2.3: Sample time-resolved emission decay. Measured fluorescence decay of PSI-200 with calculated fit and instrument response function. 10,000 counts were collected in the peak channel. Decay deconvolved to 4 componets as shown above.

Additionally, time-resolved data were analyzed by the global analysis method. [16,17] This analysis technique also uses the method of iterative deconvolution with optimization via a non-linear least squares algorithm. Fluorescence decays are again described in terms of sums of simultaneous exponential rises and decays. The primary difference between the single and global analysis methods arises from the different constraints that are placed on the free floating parameters. When the global analysis method was used, a set of decays was measured at 5 nm intervals under the same conditions. The decays are then analyzed simultaneously with the lifetimes constrained to be constant for the corresponding decay components at all wavelengths. The primary advantage of this technique stems from the overdetermination of the parameters, resulting in a better determination of the minimum. The dimensionality of the fitting problem is reduced from $2 \times N \times n$ to $N \times n + 2$ where N is the number of decays being analyzed and n the number of decay components. This method is more likely to reveal inadequacies in the model function as well as to improve the stability and precision of each parameter. For each data set the decays were analyzed individually, and then it was verified that the lifetimes were constant across the emission range before the global analysis method was applied. Consistency with respect to lifetime and reduced χ^2 values was monitored specifically. The decay component amplitudes at each wavelength obtained from the global analysis were corrected for data collection time, excitation intensity and the wavelength dependence of the emission monochromator and detector. Decay-associated spectra (DAS) refer to corrected amplitudes plotted as a function of emission wavelength.

3. References for Chapter II

1. Laemmli, H.K., (1970) *Nature* (Lond.) **227**, 680-685.

2. Hiyama, T. and Ke, B. (1972) *Biochim. Biophys. Acta* **267**, 160-171.

3. Duggan, X.J., DiCesare, J. and Williams, J.F., (1983) *ASTM Special Technical Publication*, **822**, 112-126.

4. Nothnagel, E.A., (1987) *Anal. Biochem.*, **163**, 224-237.

5. Demas, J.N. and Crosby, G.A. (1971) *J. Phys. Chem.*, **75**, 991-1024.

6. Taylor, D.G. and Demas, J.N. (1979) *Anal. Chem.*, **51**, 717-722.

7. Stepanov, B.I., (1957) *Soviet Physics-Doklady*, **2**, 81-84.

8. Van Metter, R.L. and Knox. R.S. (1976) *Chem. Phys.*, **12**, 333-340.

9. Lakowicz, J.R., (1983) Principles of Fluorescence Spectroscopy, New York: Plenum Press.

10. O'Connor, D.V., Phillips, D., (1984) Time-correlated Single Photon Counting, Miami: Academic Press, Inc.

11. Chang, M.C., Courtney, S.H., Cross, A.J., Gulotty, R.J., Petrich, J.W. and Fleming, G.R., (1985) *Anal. Instrumentation*, **14**, 433-464.

12. Hart, D.E., Anfinrud, P.A. and Struve, W.S., (1987) *J. Chem. Phys.*, **86**, 2689-2696.

13. McKinnon, A.E., Szabo, A.G. and Miller, D.R., (1977) *J. Phys. Chem.*, **81**, 1564-1570.

14. Ware, W.R., Doemeny, L.J. and Nemzek, T.L., (1973) *J. Phys. Chem.*, **77**, 2038-2048

15. Grinvald, A. and Steinberg, I.Z., (1974) *Anal. Biochem.*, **59**, 583-598.

16. Wendler, J., John, W., Scheer, H. and Holzwarth, A.R., (1986) *Photochem. Photobiol.*, **44**, 79-85.

17. Knutson, J.R., Beechem, J.M. and Brand, L., (1983) *Chem. Phys. Lett.*, **102**, 501-507.

Chapter III: Steady-state Fluorescence Characterization of Photosystem I Preparations from Higher Plants and Cyanobacteria

The fluorescence properties of a photosystem I (PSI) preparation from spinach containing approximately 200 chlorophyll (Chl) per reaction center were investigated. The preparation, characterized both spectroscopically and biochemically, contained the peripheral light harvesting antenna associated with PSI. In this study steady-state fluorescence measurements were performed as a function of temperature. An emission maximum at 690 nm and a long wavelength shoulder from 710 to 740 nm were observed. The fluorescence yield at 690 nm is temperature independent, while the yield of the long wavelength shoulder increases dramatically with decreasing temperature. Temperature dependent measurements have also been done on a cyanobacterial PSI complex, for which similar results have been obtained. Cyanobacteria lack the peripheral light harvesting antenna of higher plants and thus provide a good complex for comparison with PSI-200.

Recently, several excellent reviews on PSI have been published discussing electron transfer properties and polypeptide composition. [1-7] Intact PSI complexes have been isolated with different amounts of core and peripheral antenna pigments associated with the reaction center. [8-10] A peripheral light harvesting complex (LHC-I) containing Chl b is associated with PSI. This light harvesting complex contributes significantly to the long wavelength emission characteristic of PSI at low temperature. [9,11,12] The core antenna and reaction center are associated with two high molecular mass peptides of approximately 84 kDa, which bind the primary electron transfer components and 100 Chl a molecules. [13-15] The LHC-I complex contains polypeptides in the 20-24 kDa range and possibly other lower molecular weight polypeptides. This complex consists of 100 Chl a and Chl b molecules in a ratio of approximately 4:1. The majority of the Chl b in PSI is found in the LHC-I complex [8,9,15,16]; although, it has been reported that Chl b is contained in a 10 Chl reaction center preparation. [17] In this study the role of Chl b in stimulating long wavelength emission is specifically addressed.

1. *Isolation*

Spinach. The PSI complex (PSI-200) containing the reaction center and a full complement of the antenna was isolated from spinach according to the procedure described by Mullet et. al. [8] with some modifications. All procedures were carried

out at 4°C with limited light exposure. Chloroplasts were prepared by grinding market spinach leaves in buffer (0.3M sucrose, 0.01M NaCl, 5.0 mM $MgCl_2$ and 50.0 mM N-tris[hydroxymethyl]- methyl glycine (Tricine), pH=7.8), filtering through 4 layers of cheesecloth, followed by centrifuge spin (1000xg; 5 min). Chloroplasts were resuspended (50.0 mM sorbitol, 0.75mM EDTA, pH=7.8) and then concentrated by centrifugation (11,000xg; 5 min). This step was repeated. Resulting pellets were resuspended (50.0 mM sorbitol, 5.0 mM Tricine, pH=7.8) and then centrifuged (19,000xg; 15 min) to remove soluble components. Pellets were then diluted with ice cold H_2O to a Chl concentration of 0.7-0.8 mg/ml with a Triton-X-100 concentration of 1.0-1.2% (w/v). These conditions differ depending on the nature of the spinach and the season. This detergent chloroplast mixture was shaken for 1 h at room temperature in a water bath protected from light and then centrifuged (44,000xg; 30 min). The resulting supernatant was immediately loaded onto a 0.1-1.0M linear sucrose density gradient containing 0.02% Triton-X-100 and centrifuged (100,000xg; 16 h). The band of interest occurred at the interface between the 2.0M sucrose cushion and the linear gradient.

Cyanobacteria. PSI particles were isolated from *Synechococcus* sp., a thermophilic organism, following the procedure of McDermott et al. [17] with minor modifications. PSI was extracted from thylakoids at a Chl concentration of 0.8 mg/ml with 1.0% (w/v) Triton-X-100. The solution was spun at 1000xg for 10 min. The resulting supernatant was loaded onto 0.1-1.0 M linear sucrose density gradients containing 0.01M Trizma, pH=7.8, 1.0 mM EDTA and 0.02% Triton-X-100 and centrifuged (90,000xg; 16 hrs). Lower bands contained the material of interest. To obtain material completely free of phycobilisomes sometimes it was necessary to repeat the sucrose density gradient step.

2. Results

The PSI preparation used for these spectroscopic studies is stable and photochemically active. It contains approximately 200 Chl/ P700 and has a Chl a/b ratio of 8:1. The presence of Chl b is confirmed by prominent shoulders at 472nm and 650nm in the absorption spectrum (figure 3.1). SDS-PAGE was used to characterize the polypeptide composition. Reaction center and peripheral antenna polypeptides were observed, as well as low molecular weight polypeptides which bind Fe-S centers, A and B. [19,20]. It has been shown that the two large molecular weight polypeptides, gene products of psaA and psaB, hold the reaction center P700, A_0, A_1
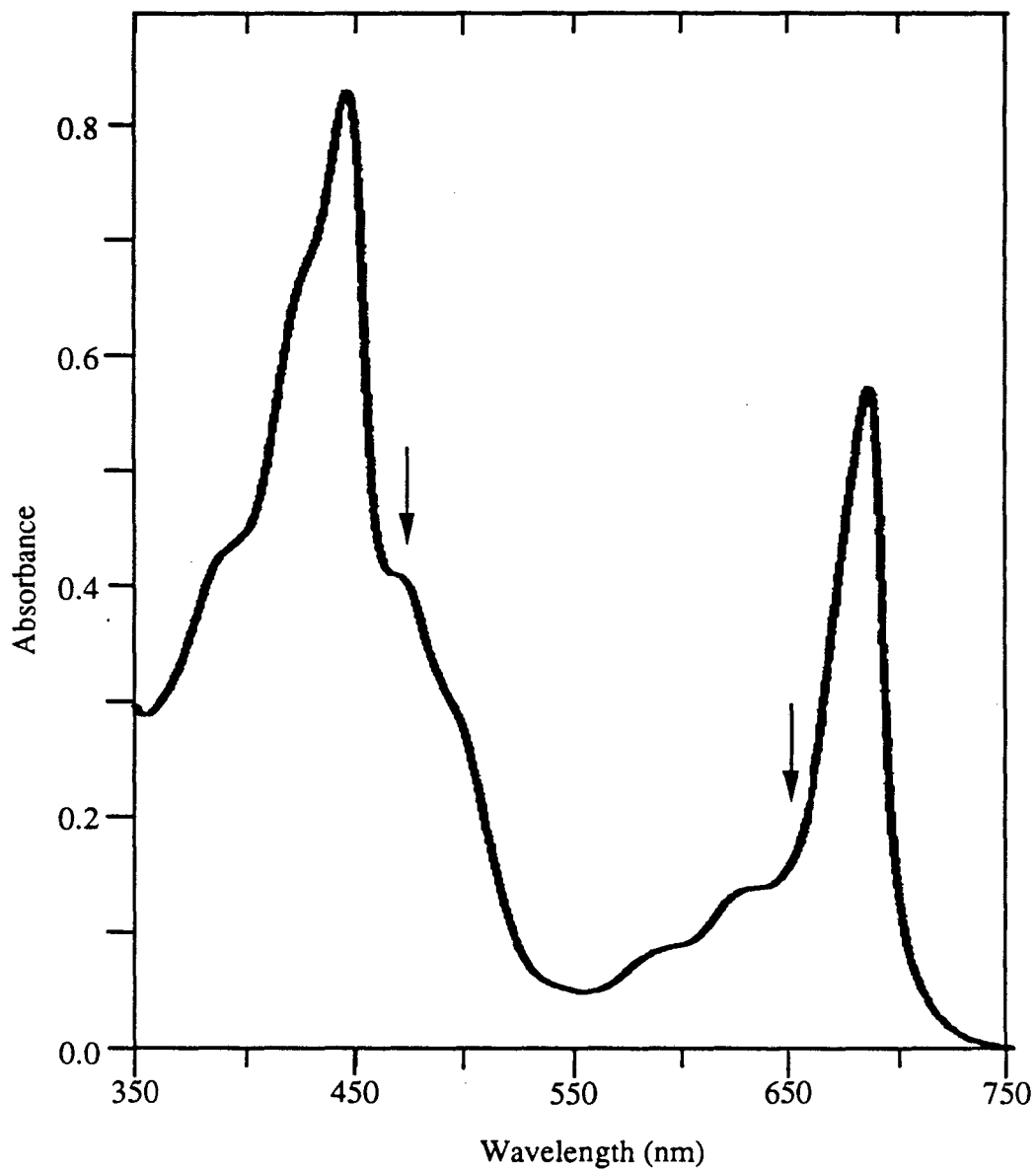
Figure 3.1: Absorbance Spectrum of PSI-200. Absorbance maxima are located at 440 and 680 nm. Arrows indicate absorption maxima of Chl b. Sample was diluted to [Chl] = 0.01 mg/ml in 0.05M Tricine, pH=7.8.

and Fe-S center, X. [14,21] Recent X-ray absorption spectroscopy and Mossbauer spectroscopy results indicate that all three Fe-S centers contained in PSI are [4Fe-4S] centers. [18, 22, 23] Chemical cross-linking studies have demonstrated that the 19 kDa protein interacts with plastocyanin [24] and that the 22 kDa polypeptide serves as a docking protein for ferredoxin. [25,26]. Due to the large antenna complement and the relatively low amounts of detergents used for isolation, PSI-200 represents a preparation which resembles PSI in vivo. [8,9]

The relative amounts of Chl/P700 were determined by photobleaching for both particles as described in chapter 2. For *Synechococcus* sp., the material was diluted to 0.01 mg Chl/ml in a medium containing 0.5 μM PMS, 0.01mM methyl viologen, 0.1 mM sodium ascorbate and 0.02 M Trizma, pH=7.5. By these measurements we estimate the higher plant PSI complex to contain approximately 200 Chl per reaction center and the cyanobacterial PSI complex to contain 100 Chl/P700. As cyanobacteria do not synthesize Chl b, this smaller core particle, hereafter referred to as PSI-100*, is completely lacking in Chl b. The emission spectrum of PSI-100* is quite different from that of PSI-200. PSI-100* has an emission maximum at 720 nm with a prominent shoulder at 690 nm. (figure 3.2) It is of interest that in this complex the majority of fluorescence emission observed occurs at lower energy than the excited state of the reaction center. It should be noted that the emission of similar particles from higher plants has an emission maximum at 690 nm with a much smaller shoulder at 720 nm. [27]

Additionally, in PSI-200 the relative fluorescence intensity of the long wavelength shoulder is dependent on excitation wavelength. At 295K excitation was done at 435, 472, 650 and 670 nm. The highest fluorescence yield was observed with excitation at 435 nm. (figure 3.3) Excitation spectra confirm that Chl b particularly sensitizes long wavelength emission at 77K. This effect is also seen in room temperature excitation spectra. Features at 705-715 nm are more prominent for emission at 735 nm. (figure 3.4) Excitation at the Chl b absorption maxima enhances the relative fluorescence yield of the long wavelength shoulder with respect to emission at 690nm. When excitation is at 472nm, there is an unknown amount of contribution from carotenoid absorption; however, carotenoids do not contribute to the absorption at 650 nm (figure 3.3). At 77K excitation of Chl b enhances F730/F690 relative to Chl a excitation.

Quantum yield measurements were performed following the method of Demas and Crosby for optically dilute samples. [28] Measurements were made relative to a
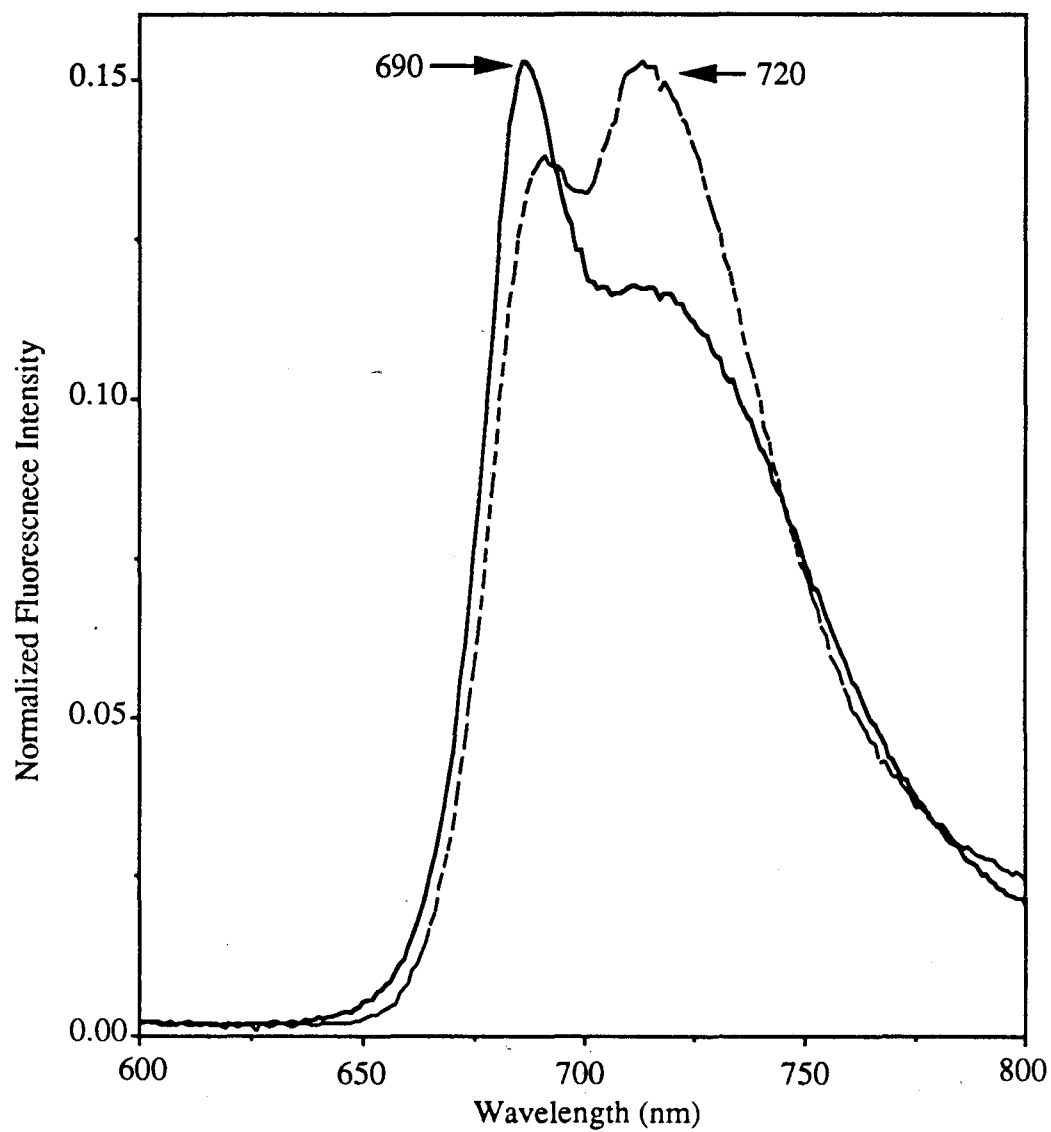
Figure 3.2: Comparison of fluorescence emission of PSI-100* and PSI-200.
Both spectra are taken at 295K and are normalized to their emission maxima.
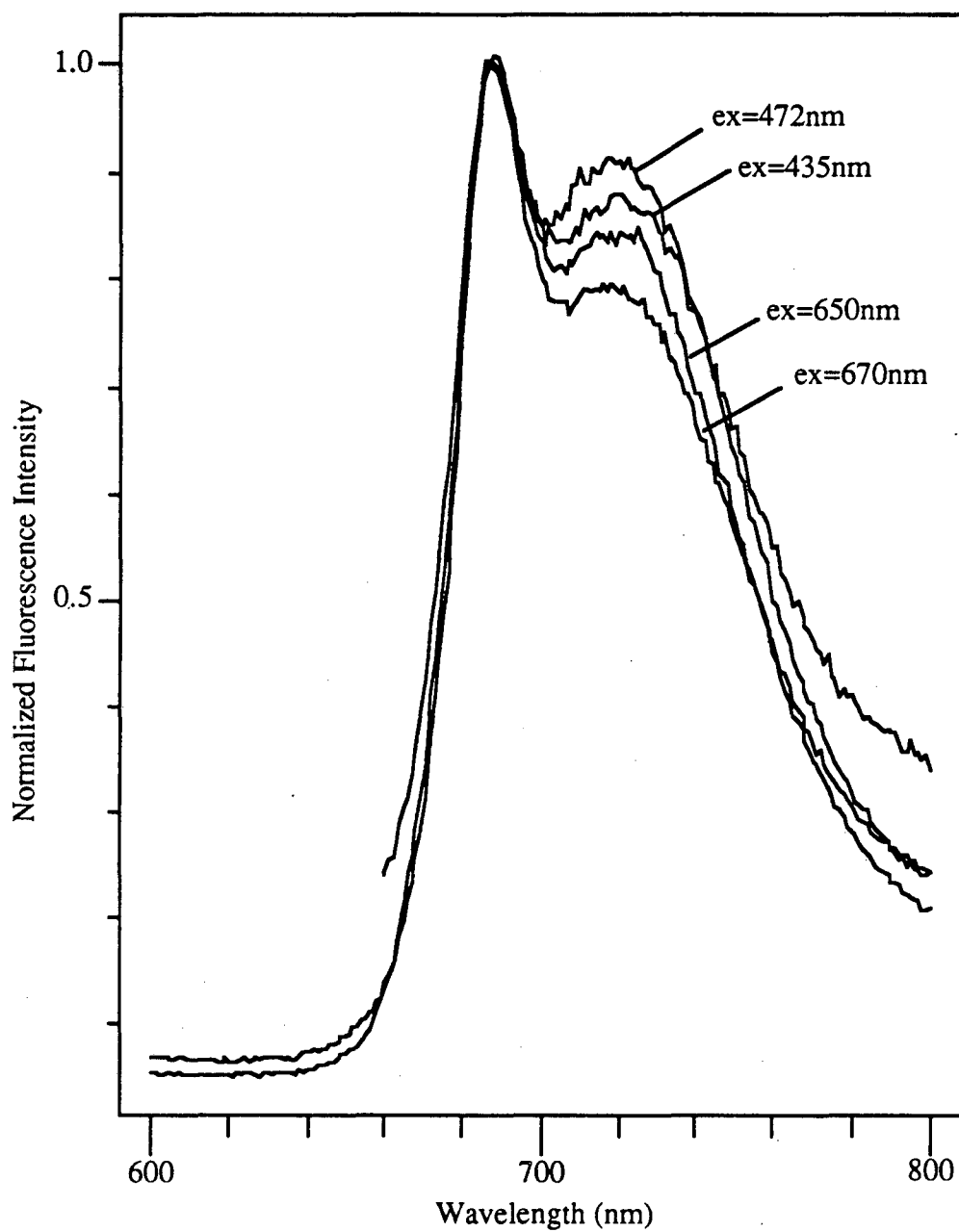Emission maximum of PSI-100* (----) at 720 nm and of PSI-200 (solid line)
at 690.

Figure 3.3: Dependence of F735 on excitation wavlength. Steady state emission spectra at 295K, normalized to emission maxima. Excitation at 435 nm, 472 nm, 650 nm or 670 nm. Sample diluted to 0.1 absorbance at 680 nm in 0.05M Tricine, pH=7.8.
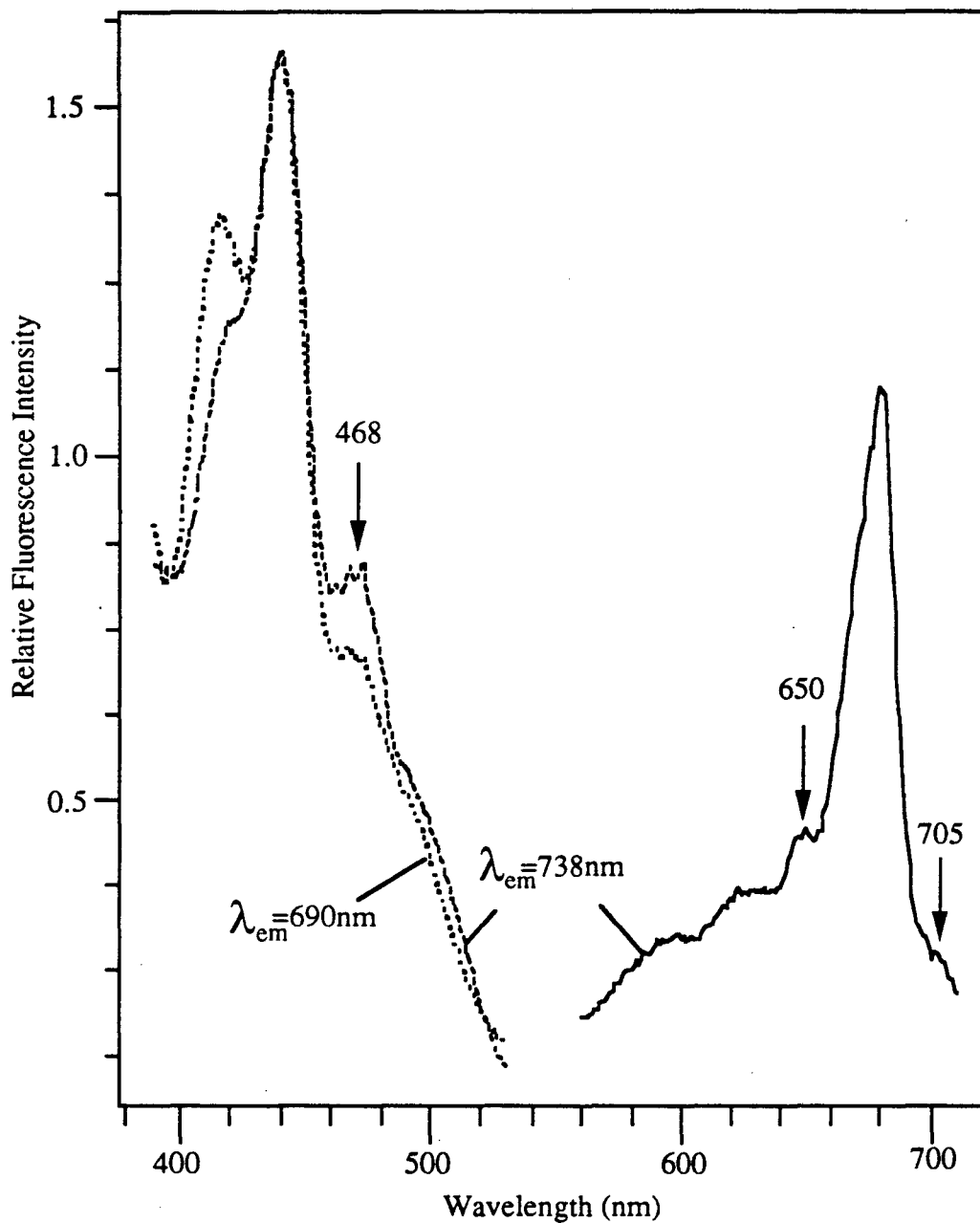
Figure 3.4: Excitation spectra of PSI-200 at 77K. Enhanced excitation at 468 nm, 650 nm and 705 nm observed for emission at 738 nm. Sample frozen to a cracked glass in 60% glycerol, 40% 0.05M Tricine, pH=7.8.

standard. These measurements rest on the premise that the luminescence observed for a given compound is proportional to the intensity of the incident light, I_0 multiplied by the fraction of light absorbed by the sample, B. Since the solution is optically dilute the fraction of light absorbed can be approximated by the absorbance of the sample, based on Beer's law.

$$Q_X = Q_R \left(\frac{A_R\ (\lambda)}{A_X\ (\lambda)}\right)\left(\frac{I_R(\lambda)}{I_X(\lambda)}\right)\left(\frac{n_X^2}{n_R^2}\right)\left(\frac{D_X}{D_R}\right)$$

Q represents the quantum yield; the subscript R refers to the reference compound, Nile Blue, which has a previously determined quantum yield of 1.0 ± 0.1. [29] A (λ) is the absorbance/cm for the solution at the exciting wavelength, λ. In most cases the absorbances of the two samples were approximately the same. In our measurements, because excitation of the sample and reference were done at the same wavelength and consecutively, it was assumed that $I_R\ (\lambda) = I_X\ (\lambda)$. The average refractive index, n, is incorporated into the equation to compensate for refraction at the cuvette interfaces. For the standard solution, Nile Blue in methanol, n was assumed to be 1.329, the value for pure methanol. For the sample the assumption was made that the index of refraction was equal to that of the bulk medium, $H_2O = 1.333$. Although the chromphores of the photosynthetic materials are contained within a protein matrix, the correction is for the interface between the cuvette and the bulk medium and therefore this represents a valid approximation. The quantum yield measured for PSI-200 serves as a point of comparison with the quantum yield of the isolated LHC-I complex, as both measurements were made in the same manner utilizing the same assumptions. The quantum yield of LHC-I will be discussed in chapter 5. Finally, D is the integrated area under the corrected emission spectrum. For measurements done on PSI-200 with excitation at 670 nm the quantum yield was determined to be 0.025 ± 0.003 and for $\lambda_{ex} = 650$ nm the quantum yield was 0.028 ± 0.006. It is thought that the error is larger in the 650 nm measurement because the observed fluorescence is so much lower due to the decreased absorption cross-section. Thus, within the error of the measurement the quantum yields at the two excitation wavelengths are approximately the same.

The Stepanov relation between absorption and emission spectra was tested for both the PSI-200 and the PSI-100* complex. This formulation predicts a linear relation between low energy absorption bands and emission spectra based upon considerations of blackbody radiation and the attainment of equilibrium vibrational distributions in both the ground and excited state. Primary assumptions of the relation

are that thermal equilibrium has been obtained prior to fluorescence and that the fluorescent system is homogenous. In this manner the vibrational distribution in the ground state is reflected in the excited electronic state, resulting in the mirror symmetry commonly observed between absorption and emission spectra. [30] The ground and excited state are in vibrational equilibrium at an ambient temperature, T. The relation can be formulated as:

$$F(\nu) \equiv \ln\left[\frac{W(\nu)}{\nu^3 A(\nu)}\right] = \frac{-h\nu}{k_B T} + D(T)$$

$W(\nu)$ is the luminescent power of a molecule at frequency, ν, or in our case $h\nu$ times the emission probability per second. $A(\nu)$ is the absorption coefficient at ν, T is the absolute temperature, k_B is Boltzmann's constant and $D(T)$ is a function which is independent of frequency. For our measurements, made with a fixed bandpass as a function of wavelength, an additional λ^2 factor must be introduced when representing data as a function of frequency, since the bandpass is variable in frequency. [31]

$$I(\tilde{\nu}) = \lambda^2 I(\lambda)$$

For our measurements, the relation takes on the following form:

$$F(\tilde{\nu}) \equiv \ln\left[\frac{W(\tilde{\nu})hc}{\tilde{\nu}^4 A(\tilde{\nu})}\right] = \frac{-hc\tilde{\nu}}{k_B T} + D(T)$$

For PSI-200 a linear Stepanov plot can be obtained over the region of highest overlap between absorption and emission, 650-710 nm, giving a Kennard-Stepanov temperature, $T_{ks} = 366 \pm 12$ K. (figure 3.5A) Because these measurements were made at RT this temperature is significantly elevated from ambient. For PSI-100* a linear plot can also be obtained over a slightly different wavelength region, 665-730 nm. (figure 3.5B) The redder region of overlap is caused by the red-shifted emission maximum in these particles. The T_{ks} calculated for PSI-100*, 313 ± 4 K is also elevated from ambient, although not to the same extent as for PSI-200. Van Metter and Knox [32] discuss the possible reasons for these non-ambient Kennard-Stepanov temperatures, which have also been observed in large aromatic molecules. [33] Specifically, two possibilities are proposed, the first of which is inhomogeneous broadening, caused by the presence of two or more emitting species. The other explanation for an elevated T_{ks} is that the calculated temperature is the temperature of the excited state during the fluorescence lifetime. In this case a Boltzmann distribution is obtained in the excited state corresponding to the elevated temperature, T '. This "warm fluorescence" explanation has been invoked when higher excitation energies lead to a higher Kennard-Stepanov temperature. [32] In our data excitation in the Soret
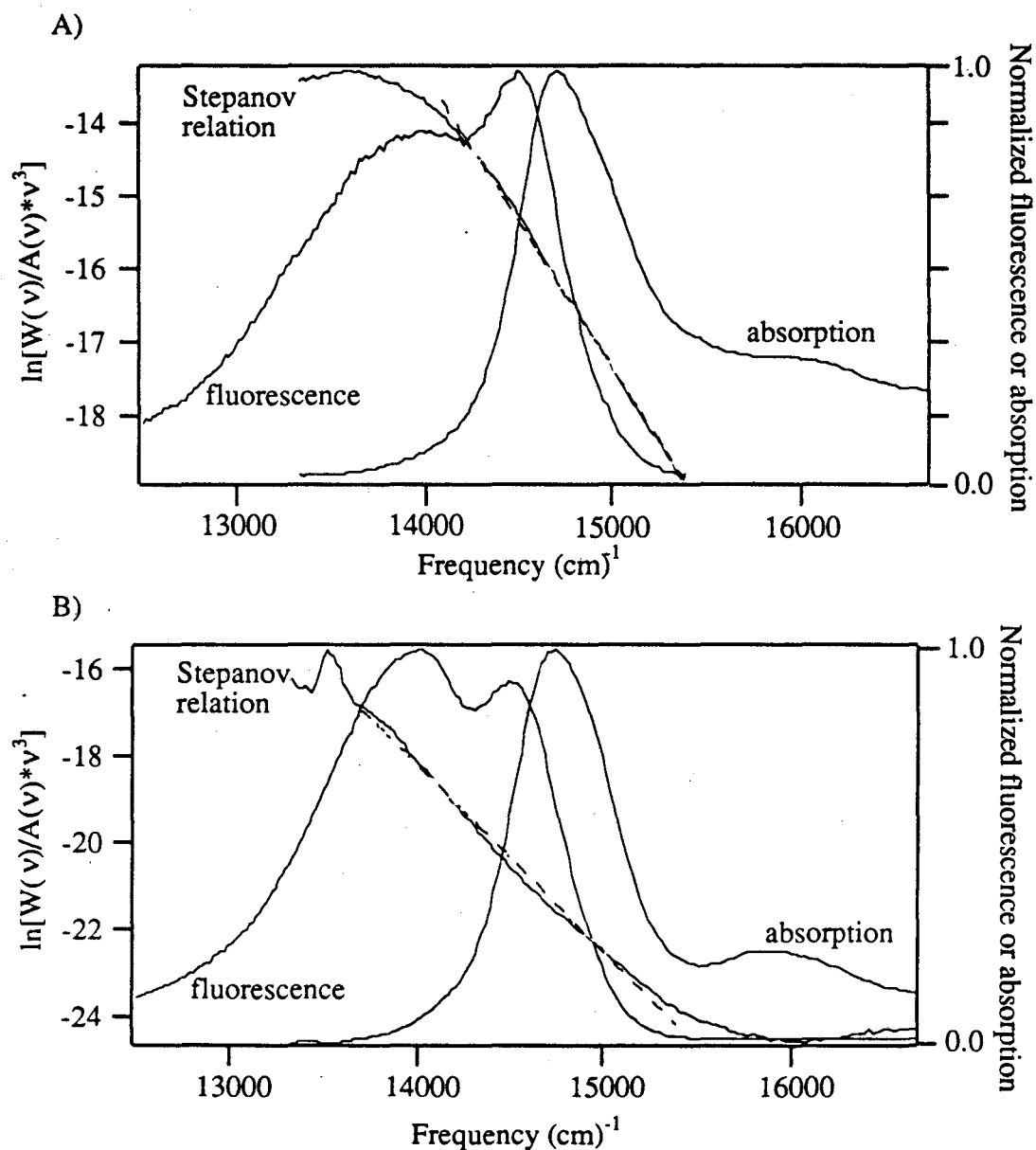
Figure 3.5: Stepanov relation applied to PSI-100* and PSI-200. The relation was calculated as described in the text. A linear fit is depicted with a dashed line through the data. For PSI-200 (figure 3.5A) the data was fit from 650 nm to 710 nm, giving a Kennard-Stepanov temperature of $366 \pm 12K$. For PSI-100* (figure 3.5B) data was fit to the relation from 665 nm to 730 nm, giving a Kennard-Stepanov temperature of $313 \pm 4K$. It can be seen that the data deviate from the fit when either the fluorescence intensity or the absorbance is very small.
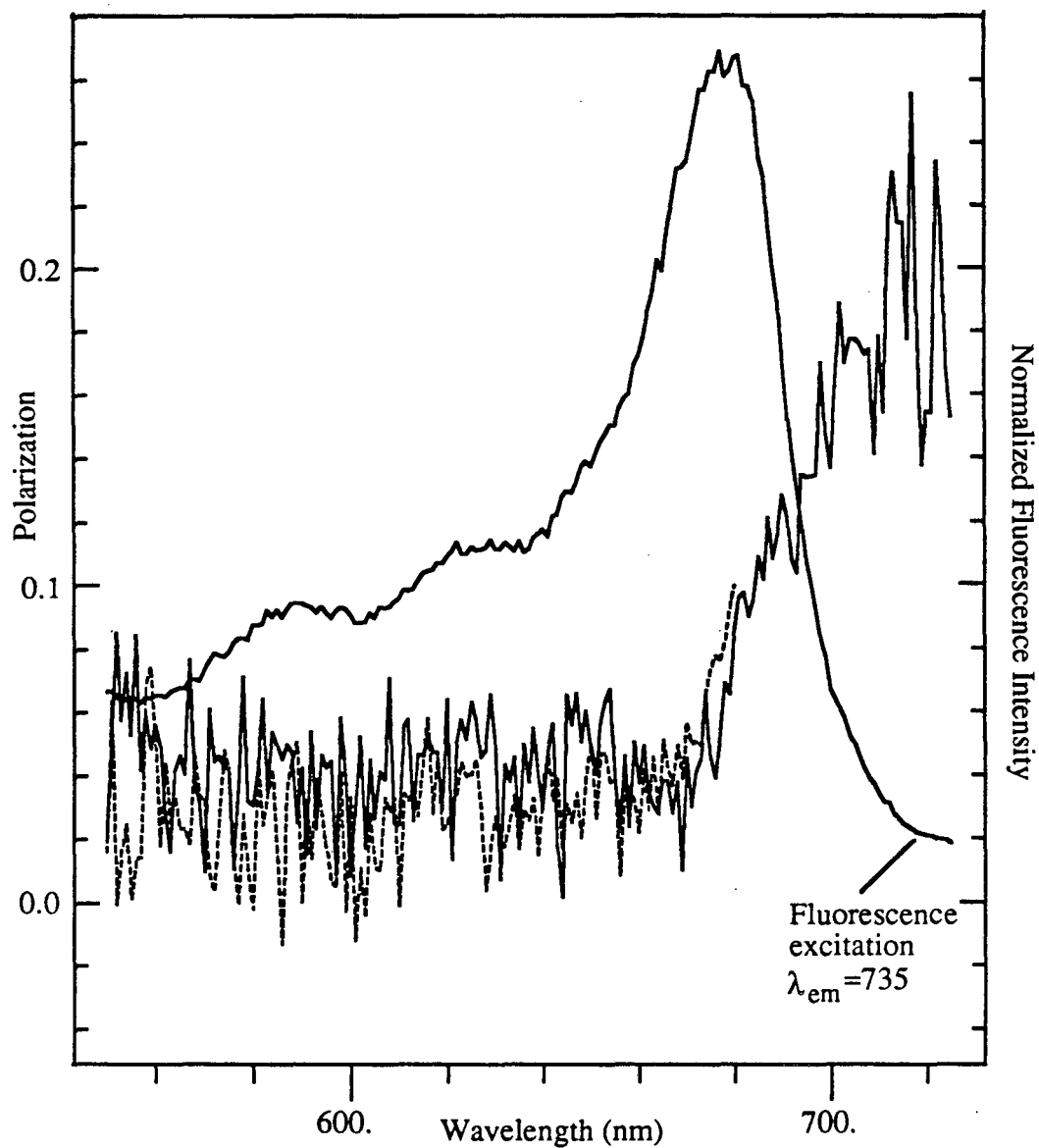
Figure 3.6: Excitation polarization spectra of PSI-200. Emission at 690 nm depicted with dashed line. Emission at 735 nm, solid line. Steady state excitation spectrum taken with emission at 735 nm. T=278 K. Sample in 40% 0.05M Tricine, pH=7.8, 60% glycerol.

region or in the red absorption bands give the same calculated T_{ks}, indicating that we are not observing "warm fluorescence". It appears that the heterogeneous nature of the emission bands in both complexes are giving rise to the elevated temperatures observed.

Excitation polarization spectra were obtained for the PSI-200 complex, as described in chapter 2. From figure 3.6 it can be seen that for emission either at 690 nm or at 735 nm from 550 to 675 nm the polarization value is essentially zero. This value indicates that the emission arising from those excitation wavlengths is essentially depolarized, due to energy transfer processes. For emission at 735 nm, in the range 680 to 705 nm the polarization rises to a value of approximately 0.2 and then remains constant from 705 to 725 nm. Higher values of polarization indicate that the relative angle between absorption and emission dipoles is getting progressively smaller. This increase is commensurate with either the same fluorophore giving rise to both absorption and emission or energy transfer between two colinear transition dipoles. [34] In the ideal case of parallel transition dipoles the polarization would be 0.5. For this system the polarization value is significantly lower. We attribute this lower value to spectral overlap of F735 with depolarized emission at shorter wavelengths. It is well-documented [8] that core PSI antenna complexes have a fluorescence emission at 720 nm. It is possible that overlap between F720 and F735 leads to a lower polarization value, or energy transfer processes could also serve to depolarize this emission.

Temperature dependent fluorescence measurements

In both complexes, PSI-100* and PSI-200, far-red emission increases dramatically as the temperature decreases. We have investigated this phenomenon over two temperature ranges for the PSI-200 complex and over one narrow temperature range for PSI-100*.

273-324 K. Figure 3.7 shows the effect of temperature on PSI-100*. The relative changes in fluorescence intensity were reverisble up to 324 K; as the temperature is increased, F720 decreases until F690 becomes the emission maximum. At 324 K the emission spectrum resembles that of PSI-200 at room temperature, where F735 has almost the same intensity as F690. For the thermophile F690 does not become the emission maximum until 309 K. The spectra are not normalized and thus, it can be seen that the intensity of F690 is independent of temperature. The temperature dependence is observed only for the far-red emission. In PSI-200 (figure

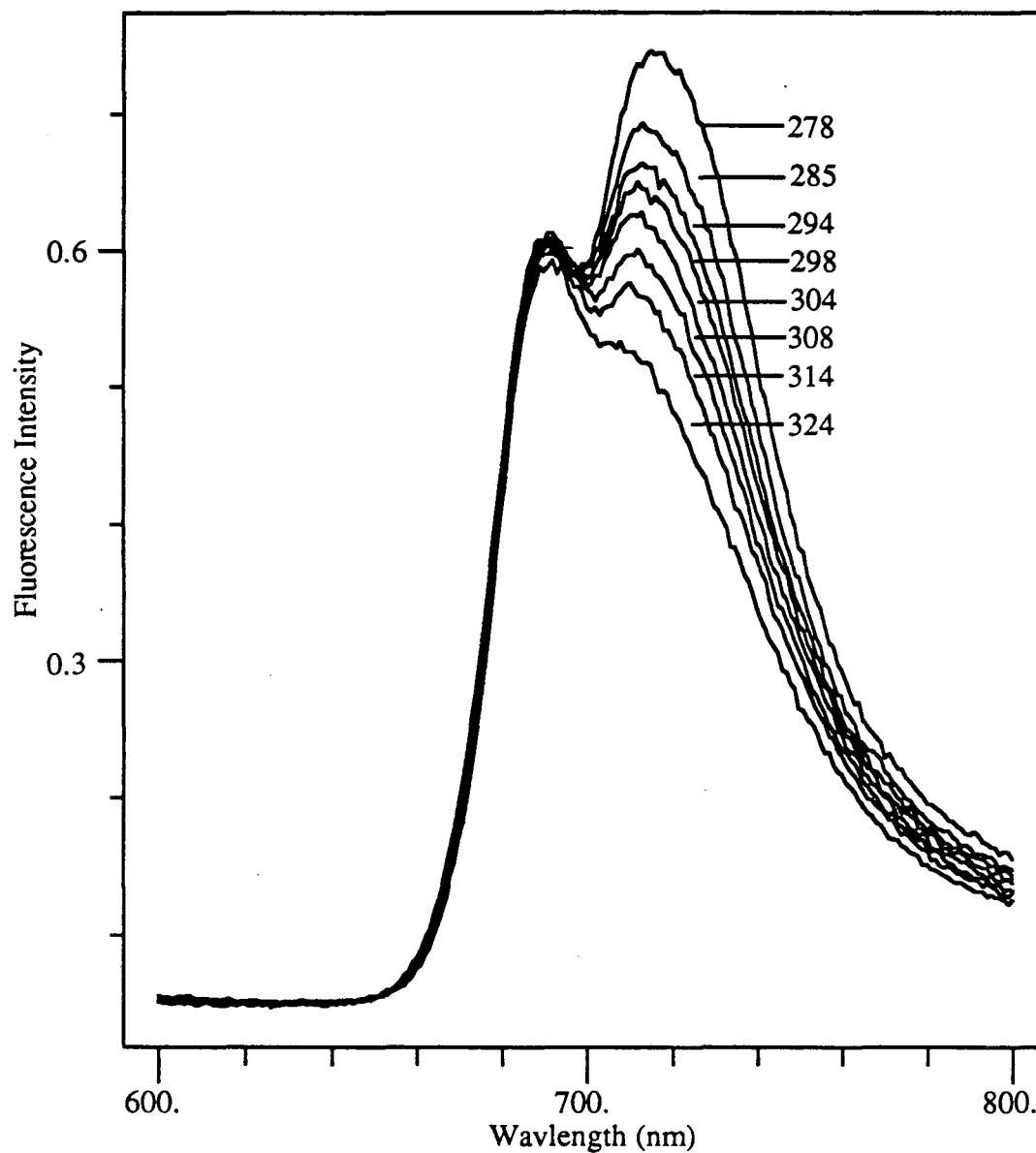Figure 3.7: Temperature dependence of PSI-100* fluorescence. Temperature shown in Kelvin. All measurements made on the same sample. Excitation done at 435 nm. Sample diluted 5 fold in 40% 0.05M Tricine, 60% glycerol.
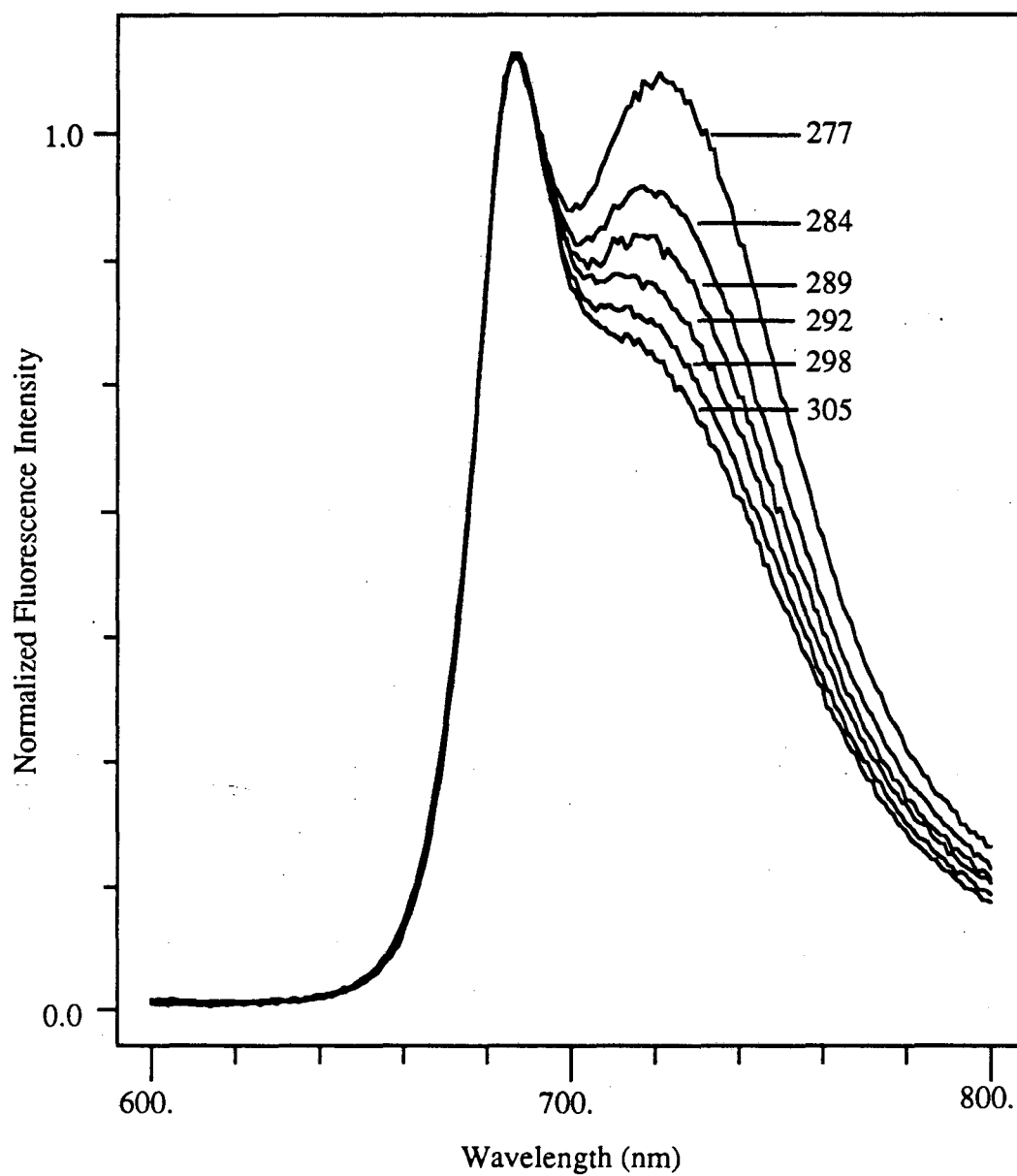
Figure 3.8: Temperature dependence of PSI-200 fluorescence from 277-305 K. Excitation done at 435 nm. Spectra are normalized to their maximum. Sample diluted 10 fold in 40% 0.05M Tricine, pH=7.8, 60% glycerol.

3.8) reversible temperature dependent fluorescence changes were observed to a maximum temperature of 304 K. From their respective fluorescence behavior it appears that PSI-100* is more stable at higher temperatures. In PSI-200 F720-F735 does not dominate the emission spectrum until the temperature is lower than 273 K.

In both cases we have attempted to quantify the fluorescence behavior by utilizing the Arrhenius equation. In an ideal case where fluorescence is the only process of de-activation from the excited state, the lifetime of the excited state or radiative lifetime is,

$$\tau_R = 1/k_F = 1/A_{BA}$$

where, k_F is the fluorescence rate constant and A_{BA} is the Einstein A coefficient for spontaneous emission. However, if there are several possible pathways of de-excitation it is necessary to include them in the determination of the fluorescence lifetime.

$$\tau_F = \frac{1}{k_F + k_{IC} + k_{IS} + k_Q}$$

In this expression k_{IC}, k_{IS} and k_Q represent the rate constants for intersystem crossing, internal conversion and quenching, respectively. The fraction of excited states which return to the ground state via fluorescence is the fluorescence quantum yield, which can be expressed as:

$$\Phi_F = \frac{k_F}{k_F + k_{IC} + k_{IS} + k_Q} = \frac{\tau_F}{\tau_R}$$

where τ_F is the observed fluorescence decay time and τ_R is the intrinsic radiative lifetime. The fluorescence yield is then directly proportional to the fluorescence rate constant.

From our time-resolved emission measurements on PSI-200 (chapter 4) we have determined that the increase in fluorescence yield arises primarily from an increase in decay amplitude rather than lifetime. Additionally, fluorescence measurements on the isolated LHC-I (chapter 5) indicate that a non-radiative quenching mechanism, independent of the reaction center is operational in these antenna. Therefore, we have incorporated these results into the modelling of of our temperature dependent steady-state fluorescence measurements. In a possible mechanistic scheme we introduce an initially excited species X, which can decay by two possible pathways, either non-radiative quenching or excitation transfer generating an excited state, C735*, which subsequently fluoresces.

$$\xrightarrow{h\nu} B \longrightarrow X \xrightarrow{k_{c735}} C735^* \longrightarrow F735$$
$$\downarrow k_Q$$
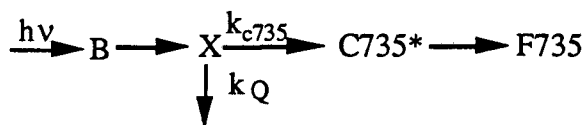
As a first approximation we have simplified the system to two fluorescing species, F690 and F735. From the temperature dependent spectra it is observed that F690 remains relatively constant over the temperature range employed. The temperature dependence of the system is attributed to k_Q. Assuming that k_{c735} is rate limiting, the increase in F735 can be directly related to the decay processes of X.

$$\frac{d[F735]}{dt} = k_{c735}[X] \qquad [X] = [X]_0 \exp{-(k_Q + k_{c735})}$$

In this scheme, the population of C735* will increase at lower temperatures without dramatically affecting the lifetime, because of the temperature dependence of k_Q. Using a similar mechanism for F690, $k_{Q'}$ represents the temperature independent quenching of Y, the precursor to C690*. Thus, the ratio of the two yields can be expressed as:

$$\frac{\Phi735}{\Phi690} = \frac{k_{c735}[X]_0}{k_{c690}[Y]_0} \frac{(k_{Q'} + k_{c690})}{(k_Q + k_{c735})}$$

Since k_Q is the only temperature dependent rate constant, this expression can be re-written:

$$\frac{\Phi690}{\Phi735} B \left(1 - \frac{1}{k_{Q'}}\right) = A \exp{(-Ea/RT)} = \frac{k_Q}{k_{Q'}}$$

$$B = \frac{[X]_0 \, k_{c735}}{[Y]_0 \, k_{c690}} \left(1 + \frac{k_{c690}}{k_{Q'}}\right)$$

In these expressions $\Phi690$ and $\Phi735$ represent the area of those deconvoluted emission bands. Using the method of spectral subtraction, we have estimated the area of the fluorescence bands, F735 and F690, at a given temperature. A is a pre-exponential factor which is temperature independent, R is the gas constant and E_A is the activation energy. From the experimentally determined value for the quantum yield of fluorescence (0.028) it is evident that non-radiative quenching is the dominant mechanism of de-excitation near room temperature. As a result the term $1/k_{Q'}$ is quite small relative to 1 and can be neglected at these temperatures. For *Synchococcus,* sp. (figure 3.9) a linear fit to the above expression can be obtained with a squared correlation coefficient of 0.99. The activation energy obtained is 2.0 kcal/mole or 710 cm^{-1}. For the PSI-200 complex from spinach (figure 3.10) a linear correlation is also observed. It is important, however, to realize that there is more than 1 component which is emitting in the long wavelength region, which we are not deconvolving in this

Figure 3.8: Arrhenius plot of the temperature dependence of PSI-100*. The natural log of the decovolved emission areas, F690/F720 are plotted as a function of 1/T. Solid line indicates linear fit to the data, giving an activation energy of 710 cm^{-1}. Original data shown in figure 3.6.

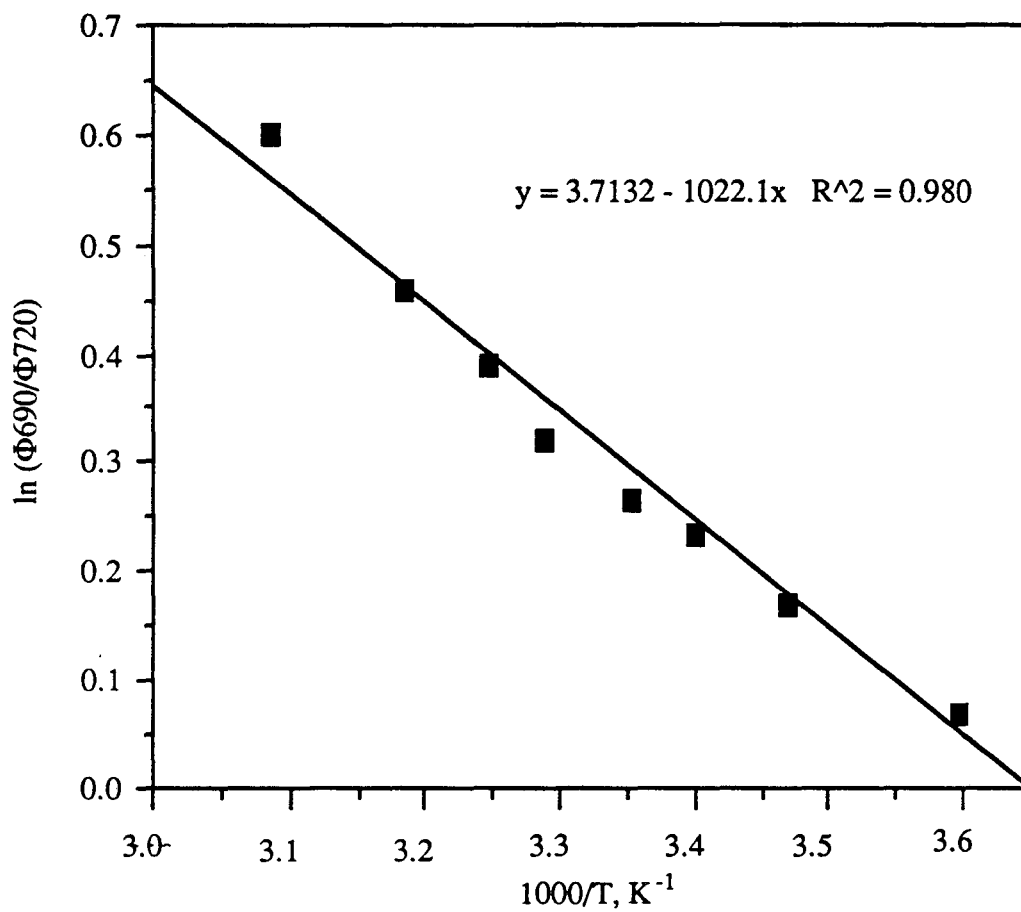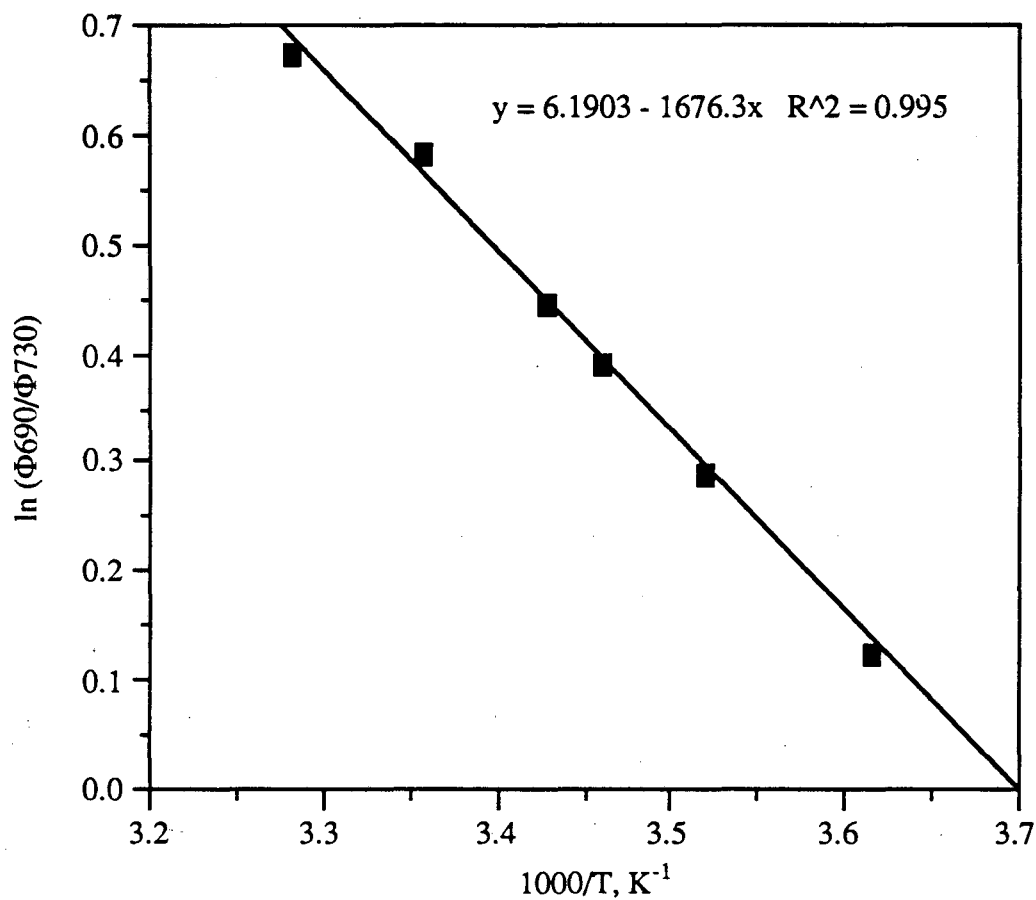$$y = 6.1903 - 1676.3x \quad R^2 = 0.995$$

Figure 3.10: Arrhenius plot of the temperature dependence of PSI-200.
The natural log of the deconvolved emission areas, F690/F730, are plotted
as a function of 1/T. The solid line indicates the linear fit to the data, giving
an activation energy of 1170 cm . Original data shown in figure 3.7.

method. We have monitored the intensity of F735 across the putative emission band and it appears that the two species F720 and F735 have approximately the same temperature dependence over this narrow temperature range. We did not deconvolve F720 from the spectra, because it is not directly observed in this preparation. For $\Phi690/\Phi735$ of PSI-200 an activation energy of 1170 cm^{-1} is calculated.

77-298K. PSI-200 at room temperature exhibits an emission maximum at 690 nm with a shoulder from 710 to 740 nm; at 77K the emission maximum is red-shifted to 738 nm with a shoulder at 690nm. In figure 3.11 it can be seen that the intensity of F735 increases approximately 20 fold as a function of decreasing temperature; whereas F690 remains relatively small. Changes in the apparent intensity of F690 result in part from instabilities in the glass at temperatures between 77K and 250K. The maximum of the long-wavelength emission becomes progressively red-shifted as the temperature is decreased, which is suggestive that more than one component is contributing to this fluorescence. This temperature dependent fluorescence behavior is not a property of Chl a *in vitro*. [35] We conclude that for the PSI complex the fluorescence behavior is directly related to changes in excitation quenching and energy transfer dynamics.

4. Discussion

Our results confirm and extend those that have been previously reported. Our spectral data agree well with the biochemical evidence [8,11,12] which indicates that the longest wavelength emission in PSI arises primarily from the peripheral light harvesting antenna. We have observed both at 295K and at 77K that excitation at the absorption maxima of Chl b enhances fluorescence at 735 nm. As Chl b is found only in LHC-I in PSI, this complex appears to be directly connected to the longest wavelength emission observed at both RT and 77K.

Excitation polarization spectra indicate that species absorbing in the 705-725 nm range are giving rise to emission at longer wavelengths. These components are specifically observed in the 77K excitation spectra and comprise a relatively small portion of the antenna pool judging from the absorption spectra. These chromophores absorb at lower energies than the reaction center, P700 and at lower energies than the majority of antenna Chl. For emission detected at 735 nm, highest polarization values (0.2) are still relatively low, indicating that the emission is quite depolarized. Since PSI-200 has more than one antenna pool, it is possible that the depolarization is occuring because of energy transfer from F720 to F735. Alternatively, depolarization could be arising because of overlap between the two long-wavlength emission bands in
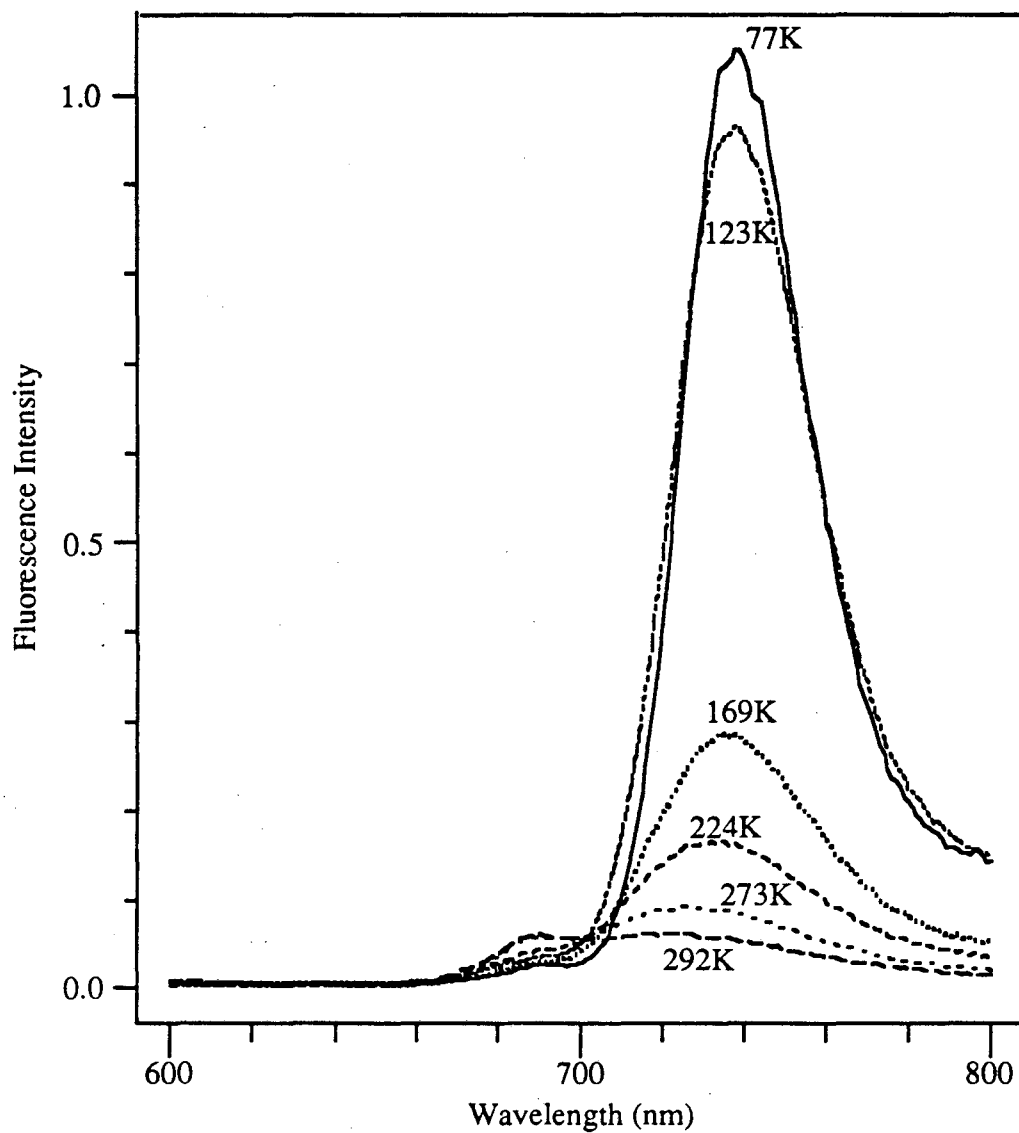
Figure 3.11: Temperature dependence of PSI-200 fluorescence, 77-292K. Excitation was done at 435 nm. All spectra were taken on the same sample. Sample diluted approximately 5 fold in 40% 0.05 M Tricine, pH=7.8, 60% glycerol.

the emission region monitored. For λ_{em} = 690, the polarization rises slightly between 680 and 690 nm. This rise could represent emission from pigments which absorb in that region or it could reflect some overlap between F735 and F690, causing an apparent increase in F690 polarization. Time-resolved anisotropy measurements could distinguish between these two cases. For both λ_{em} = 690 and λ_{em} = 735 excitation in the 550-680 nm range leads to depolarized emission, suggestive of energy transfer processes.

Linear dichroism and polarized emission spectroscopy have been performed on similar PSI particles. [36] In those studies the highest dichroic ratio (1.57) was observed at 697 nm. The region between 705-725 was less dichroic with a value of 1.54. In our measurements for emission at 735 nm, it appears that the polarization value at 697 nm is less than that observed at 705-725 nm. From measurements done on a Chl-b-less barley mutant Tapie et al. determined that F720 and C697 do not originate from the same pigment bed. Additionally, their data indicate that C697 and F735 have an identical orientation relative to the thylakoid plane. Signal to noise is somewhat low for our polarization measurements due to the relatively low quantum yield; yet, our data do not support this conclusion. Our data indicate that F735 arises from chromophores absorbing in the 705-725 nm range.

We have also applied the Stepanov relation to the data, which determines if the excited state is in thermal equilibrium relative to the ground state. We observe that linear plots can be generated in the region of highest overlap between absorption and emission; however, temperatures calculated are elevated from ambient. It has been reported that elevated Kennard-Stepanov temperatures can be attributed to inhomogeneous broadening of the emission band. [32] For these PSI complexes the heterogeneous nature of the antenna pools, F690, F720 and F735 could be the primary source of the elevated T_{ks}. In PSI-100* the T_{ks} is only 10-15° elevated from ambient as opposed to the 50° in the PSI-200 complex. From the steady state emission spectra it is obvious that more of the emission is arising from a lower energy antenna pool in PSI-100*. Since more of the energy resides on lower energy pigments, the emission is more homogeneous, resulting in a lower Stepanov temperature. Additionally, in PSI-100* it appears that only one long wavelength emitting species is present, leading to a less heterogeneous emission band compared to PSI-200. Alternatively, it is possible there is a higher degree of thermal equilibrium in the excited state leading to a T_{ks} close to ambient. It is interesting to note that at lower temperatures, the calculated T_{ks} also gets correspondingly lower; although, it still remains elevated from the temperature at

which data was taken.

Temperature dependent fluorescence

Over a relatively small temperature range we observe that both PSI-200 and PSI-100* exhibit dramatic changes in emission characteristics. In PSI-200 the emission maximum is shifted almost 50 nm to the red as the temperature is lowered to 77K. Additionally, the fluorescence yield increases approximately 20 fold over this 200 degree temperature range. In both complexes the intensity of F690 remains relatively constant while longer wavelength emitting pigments demonstrate temperature dependent changes in intensity. Not surprisingly, PSI-100* isolated from a thermophilic organism, has a higher degree of thermal stability than the PSI-200 isolated from spinach. Interestingly, when comparing the emission spectrum of PSI-100* with that of similar PSI particles isolated from higher plants, F720 is still noticeably enhanced even at elevated temperatures. We speculate that this increased emission at 720 nm confers a higher degree of thermal stability to the organism. From an evolutionary point of view it is of note that higher plants have developed an additional antenna complement with a set of even lower energy pigments. It appears then that these chromophores represent an important element of the antennal system.

We observe Arrhenius behavior for PSI-200 and PSI-100*. In both cases, the ratio of the yield at 690 nm relative to the yield at 720 or 735 nm was plotted as a function of temperature in order to calculate an E_A. For the PSI-100* complex, an activation energy of 710 cm^{-1} is obtained over the temperature range 278-324 K. In contrast, over a smaller temperature range 277-305 K, the PSI-200 complex has an activation energy of 1170 cm^{-1}. In summary, for both species F690 is temperature independent and emission at longer wavelengths is highly temperature dependent. In spinach the yield of F735 increases approximately twenty fold from RT to 77K. Both species exhibit Arrhenius behavior; although, PSI-200 has a higher activation energy than that obtained for PSI-100*. Time-resolved emission and excitation spectroscopy will be presented in chapter 4, following which a model for transfer energetics will be discussed.

4. *Summary*

1. Excitation and emission spectra indicate that Chl b, primarily found in LHC-I, specifically enhances F735 at 295 and 77 K.

2. Excitation and excitation polarization spectra demonstrate that components absorbing in the far-red region (705-725 nm) predominantly contribute to F735.

3. The Stepanov relation, when applied to PSI-200 and PSI-100*, results in an elevated T_{ks}. We attribute this behavior to heterogeneity in the antenna pools of both species. PSI-100* has a lower T_{ks}, resulting from the increased emission of lower energy antenna species and more homogenous emitting pigments.

4. For both species the intensity of F720-F735 increases with lower temperature, while the intensity of F690 is independent of temperature. The change in $\Phi690/\Phi735$ as a function of temperature shows Arrhenius behavior. PSI-200 has a higher activation energy than PSI-100*, presumably as a result of its lower energy antenna pool.

5. References for Chapter III

1. Malkin, R. (1982) *Ann. Rev. Plant Physiol.*, **33**, 455-479.
2. Rutherford, A.W. and Heathcote, P. (1985) *Photosynthesis Res.*, **6**, 295-316.
3. Malkin, R. (1987) in The Light Reactions (J. Barber, ed.) Amsterdam: Elsevier Science Publishers, 495-524.
4. Golbeck, J.H. (1987) *Biochim. Biophys. Acta*, **895**, 167-204.
5. Golbeck, J.H. (1988) in Light Energy Transduction in Photosynthesis: Higher Plants and Bacterial Models (Stevens, S.E. and Bryant, D.A., eds.) American Society of Plant Physiologists, 243-258.
6. Lagoutte, B. and Mathis, P. (1989) *Photochem. Photobiol.*, **49**, 833-844.
7. Margulies, M.M. (1989) *Plant Science*, **64**, 1-13.
8. Mullet, J.E., Burke, J.J. and Arntzen, C.J. (1980) *Plant Physiol.*, **65**, 814-822.
9. Lam, E., Ortiz, W., Mayfield, S. and Malkin, R. (1984) *Plant Physiol.* **74**, 650-655.
10. Bassi, R. and Simpson, D.(1987) *Eur. J. Biochem.*, **163**, 221-230.
11. Haworth, P., Watson, J.L. and Arntzen, C.J. (1983) *Biochim. Biophys. Acta*, **724**, 151-158.
12. Lam, E., Ortiz, W. and Malkin, R. (1986) *FEBS Lett.*, **168**, 10-14.
13. Fish, L.E. and Bogorad, L. (1986) *J. Biol. Chem.*, **261**, 8134-8139.
14. Golbeck, J.H., Parrett, K.G., McDermott, A.E. (1987) *Biochim. Biophys. Acta*, **893**, 149-160.
15. Malkin, R. (1986) *Photosynthesis Res.*, **10**, 197-201.
16. Ortiz, W., Lam, E., Ghirardi, M. and Malkin, R. (1984) *Biochim. Biophys. Acta*, **766**, 505-509.
17. Breton, J. and Ikegami, I. (1989) *Photosynthesis Res.*, **21**, 27-36.
18. McDermott, A.E., Yachandra, V.K., Guiles, R.D., Britt, R.D., Dexheimer, S.L., Sauer, K. and Klein, M.P. (1988) *Biochem.*, **27**, 4013-4020.
19. Høj, P.B. and Moller, B.L. (1986) *J. Biol. Chem.*, **261**, 14292-14300.
20. Oh-oka, H., Takahashi, Y., Wada, K., Matsubara, H., Oh-yama, H. and Ozeki, H. (1987) *FEBS Lett.*, **218**, 52-54.
21. Golbeck, J.H., Parrett, K.G., Mehari, T., Jones, K.L. and Brand, J.J. (1988) *FEBS Lett.*, **228**, 268-272.
22. McDermott, A.E., Yachandra, V.K., Guiles, R.D., Sauer, K., Klein, M.P., Parrett, K. and Golbeck, J.H. (1989) *Biochem.*, **28**, 8056-8059.

23. Petrouleas, V., Brand, J.J., Parrett, K.G., and Golbeck, J.H. (1989) *Biochem.*, **28**, 8980-8983.

24. Wynn, R.M. and Malkin, R. (1988) *Biochem.*, **27**, 5863-5869.

25. Zanetti, G. and Merati, G. (1987) *Eur. J. Biochem.*, **169**, 143-146.

26. Zilber, A. and Malkin, R. (1988) Plant Physiol., 88, 810-814.

27. M.F.J. Talbot, personal communication.

28. Demas, J.N. and Crosby, G.A. (1971) *J. Phys. Chem.*, **75**, 991-1024.

29. Taylor, D.G. and Demas, J.N. (1979) *Anal. Chem.*, **51**, 717-722.

30. Stepanov, B.I. (1957) *Soviet Physics-Doklady*, **2**, 81-84.

31. Lakowicz, J.R. (1983) Principles of Fluorescence Spectroscopy, New York: Plenum Press, 42-43.

32. Van Metter, R.L. and Knox. R.S. (1976) *Chem. Phys.*, **12**, 333-340.

33. Klochkov, V.P. and Korotkov, S.M. (1967) *Opt. Spectrosk.*, **22**, 345, 189-194.

34. Lakowicz, J.R. (1983) Principles of Fluorescence Spectroscopy, New York: Plenum Press, 111-153.

35. Goedheer, J.C. (1964) *Biochim. Biophys. Acta*, **88**, 304-317.

36. Tapie, P., Choquet, Y., Breton, J., Delepelaire, P. and Wollman, F.A. (1984) *Biochim. Biophys. Acta* **767**, 57-69.

Chapter IV: Time-resolved Fluorescence Spectroscopy of PSI-200

Excitation dynamics of PSI-200 as measured by time-correlated single photon counting will be discussed in this chapter. Measurements were performed at 295 and 77 K. Both time-resolved emission and excitation spectroscopy were done on the complex. In each case at 295 K a 4-component fit was necessary to describe the data; whereas, at 77 K, an additional 40-50 ps rise component, indicative of fluorescence induction was needed. The kinetic measurements demonstrate that the increase in fluorescence yield as a function of decreasing temperature arises primarily from an increase in decay component amplitude rather than an increase in lifetime.

1. *Introduction*

The dynamics of energy transfer between antenna pigments and reaction centers of photosynthetic systems has motivated many spectroscopic studies in recent years (reviews: [1-4]). The occurrence of uphill energy transfer to the reaction center from a long wavelength absorbing pigment [5] causes PSI to be a particularly interesting system for study. Time-resolved emission and excitation spectroscopy using the method of single-photon counting is a useful tool for unravelling the mechanisms of energy transfer within photosynthetic systems. Analysis of fluorescence decay kinetics can provide information relating to structure, dynamics of energy transfer and photochemical trapping within a photosynthetic unit. Recently, single-photon counting measurements have led Owens et al. [6] to conclude that a linear relation exists between trapping times and antenna size, indicating that in PSI core preparations excitation migration is nearly diffusion limited. Although many time-resolved fluorescence studies have been done on chloroplasts at low temperature [5,7-13] and on PSI reaction-center enriched preparations, [9,10,14-19] comparatively few studies have been done on PSI preparations containing more than 100 Chl/reaction center at low temperature. [9,10,17] More recently, the method of transient absorption spectroscopy and photochemical hole-burning studies have been done on similar PSI preparations. [20-22] PSI-200 was isolated in the same manner as discussed in chapter 3 and kinetic measurements were made as described in chapter 2.

2. *Results*

In this study all measurements were performed on a PSI preparation from spinach containing 200 Chl/P700. Time-resolved emission spectroscopy was done at

room temperature and at 77K. A time-resolved excitation profile was generated at 278 K. Fluorescence decays at 295K were adequately described by 4 components: <30 ps, 80-100 ps, 270-330 ps, and 1.3-1.8 ns. At 77K the fluorescence decay kinetics was deconvolved to 5 components: 40-50 ps rise, and decays of 250-280 ps , 1.0-1.1 ns , 2.4-2.5 ns and 4.8-5.3 ns. Based on steady state measurements the fluorescence yield at 740 nm increases about 20 fold with decreasing temperature; kinetic data demonstrate that this increase is a result of larger component amplitudes rather than longer lifetimes. Additionally, the ratio of fluorescence yield at 735 nm (F735) to the yield at 690 nm (F690) increases when the excitation is at 650 nm relative to excitation at 670 nm. This effect is observed at both 295K and at 77K. This enhanced yield at longer wavelengths reflects an increase in the amplitude of the 80-100 ps component at room temperature and the longer lived components at 77K. Steady state measurements confirm the results obtained in the kinetic studies. Because 650 nm is the absorption maximum for Chl b, we conclude that Chl b plays an integral role in stimulating long wavelength emission in PSI.

The time-resolved fluorescence decay measurements on PSI-200 were taken over the emission wavelength range 685-740 nm. Excitation was done at either 650 nm or 670 nm. The data obtained were analyzed globally using both a 3-exponential and a 4-exponential model. Owens et al. [16] report decays which fit to 3 components for smaller PSI complexes, with antenna complements between 50 and 100 Chl. We find that the PSI-200 complex with an extended antenna requires an additional component. The weighted residuals of the global fits are shown in figures 4.1 and 4.2. It is apparent from the plot of the weighted residuals and a comparison of the χ^2 values that the 4 exponential model best satisfies the data at room temperature.

In contrast to Owens et al. [16] we find that the lifetime of the shortest decay component is relatively independent of emission wavelength, regardless of the excitation wavelength. The single wavelength analysis lifetimes for each component are independent of emission wavelength within the experimental uncertainty ($\pm$ 10%) and are in good agreement with the lifetimes obtained from global analysis (see Table 4.1).

Fluorescence yields for λ_{ex}=675 nm, generated from global analysis, are plotted vs. wavelength in figure 4.3. The fluorescence yield of each component is defined as:

$$\Phi_i = \alpha_i \tau_i$$

The <30 ps component constitutes approximately 90% of the amplitude, corresponding

$\lambda_{ex}=670nm$ $\chi^2=1.4052$

740nm
735nm
730nm
725nm
720nm
715nm
710nm
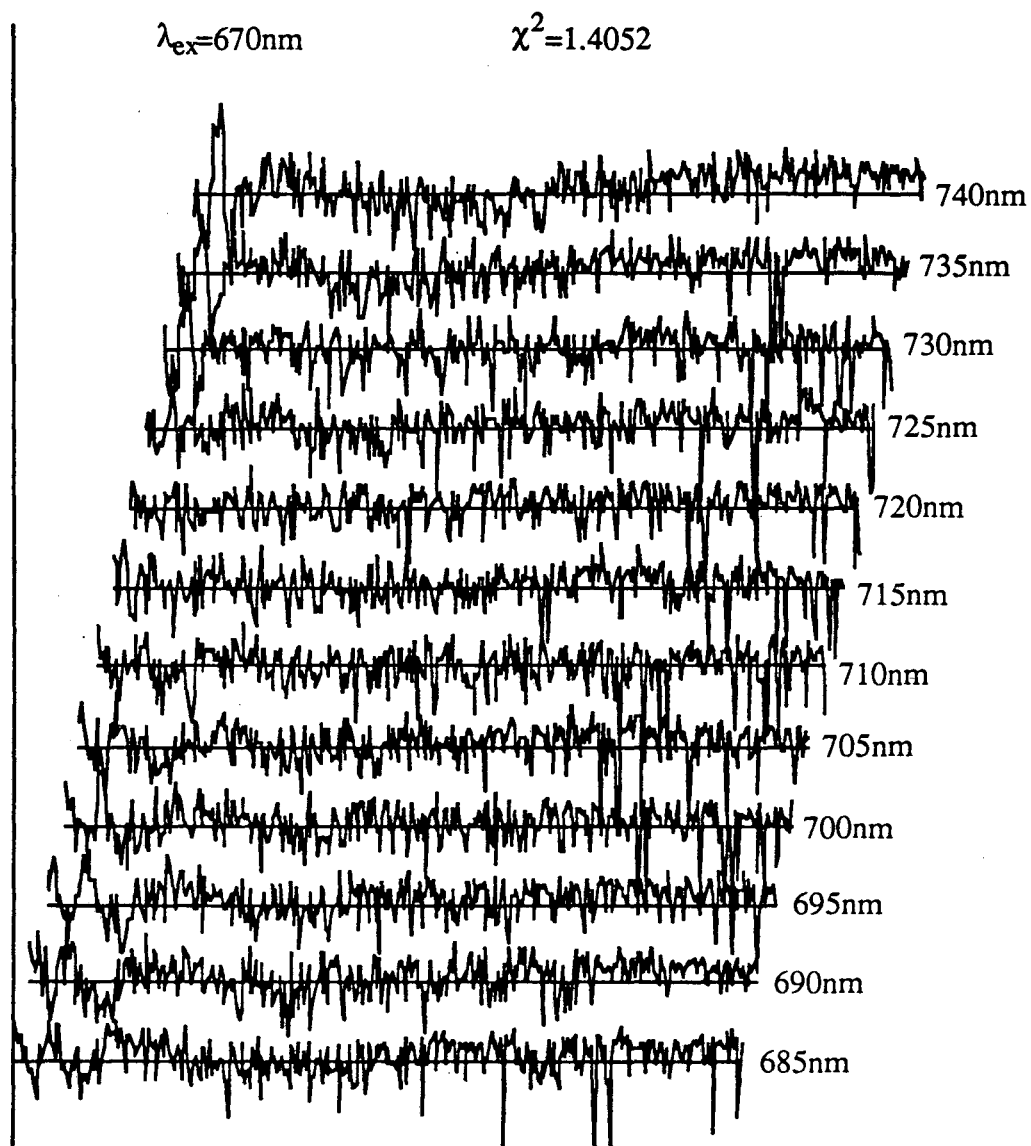705nm
700nm
695nm
690nm
685nm

Figure 4.1: Residuals from global analysis: 3 components. Weighted residuals from global analysis of a set of decays using a 3 exponential model. Reduced chi-squared of 1.40. Excitation done at 670 nm. Emission range from 685 nm to 740 nm. PSI-200 sample diluted to 0.01 mg Chl/ml in 0.05M Tricine, pH=7.8.

$\lambda_{ex}=670nm$ $\chi^2=1.1649$

740nm
735nm
730nm
725nm
720nm
715nm
710nm
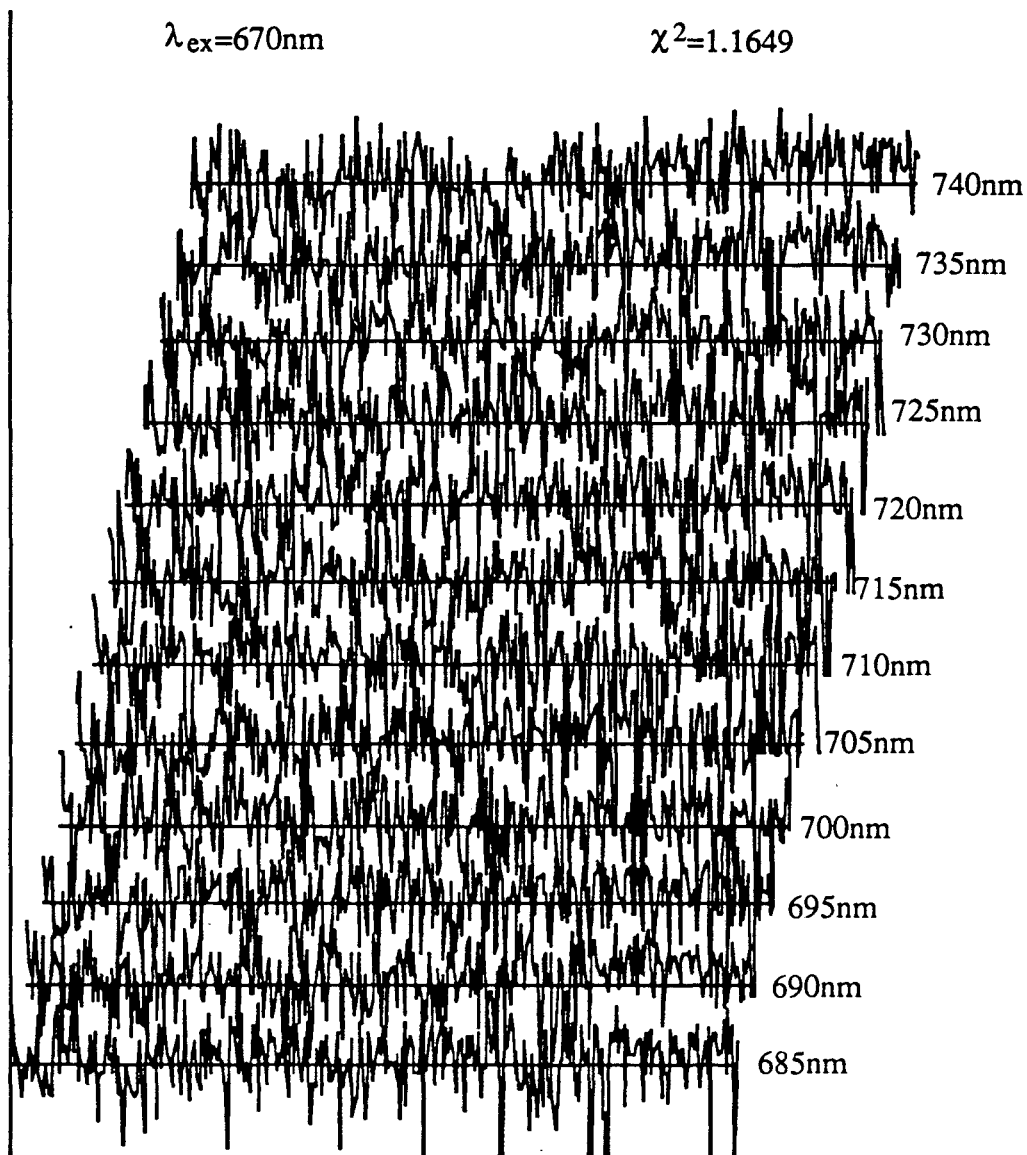705nm
700nm
695nm
690nm
685nm

Figure 4.2: Residuals from global analysis: 4 components. Weighted residuals from global analysis of same set of decays as in figure 4.1 using a 4 exponential model. Reduced chi-squared of 1.16. Scale expanded by a factor of two relative to figure 4.1. Excitation done at 670 nm, over the wavlength range 685 nm to 740 nm.

TABLE 4.1

Decay-Associated Spectra obtained from Global Analysis
of Fluorescence Kinetics from PSI-200

Kinetic components	1	2	3	4	5
Temperature=295K					
Global analysis lifetimes (ns)	0.018[a] $\pm$0.010	0.085[b] $\pm$0.010	0.30 $\pm$0.04		1.53 $\pm$0.19
Emission maximum (nm)	695	720	-		<685
Temperature=77K					
Global analysis lifetimes (ns)	0.045[c] $\pm$0.005	0.27 $\pm$0.02	1.05 $\pm$0.07	2.48 $\pm$0.06	4.99 $\pm$0.21
Emission maximum (nm)	695 (pos. amp.) 735 (neg. amp.)	720	725-730 (broad)	750	<680

Average lifetimes obtained from single wavelength analyses:
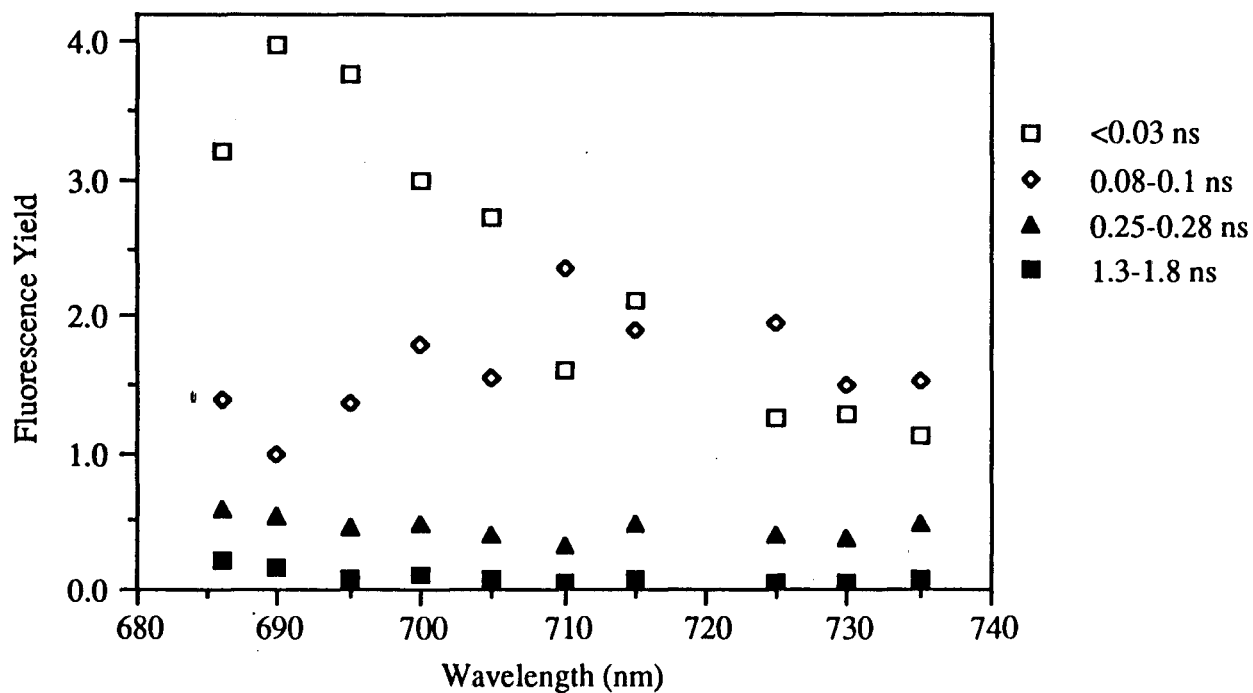[a]0.024 ns
[b]0.102 ns
[c]0.049 ns

Figure 4.3: Decay associated spectrum of PSI-200. Excitation was done at 675 nm. Decays were analyzed using a 4-exponential model. Data were taken at 295K. The fluorescence yield of each component is plotted as a function of wavelength. Sample was diluted to [Chl]=0.01 mg/ml in 0.05M Tricine, pH=7.8.

to 70% of the fluorescence yield at its emission maximum at 695 nm. This component, although at the limit of our time resolution, dominates the decay profile owing to its large amplitude. The 80-100 ps component contributes approximately 60% of the overall yield at its emission maximum at 720 nm. The corrected yield arising from the middle component, 270-330 ps, is relatively wavelength independent and contributes 10% to the yield. The slowest component, 1.3-1.8 ns appears to have an emission maximum wavelength shorter than 685 nm and adds at most 4% to the total fluorescence yield.

Figure 4.4 depicts a decay associated spectrum from global analysis, where λ_{ex}=650 nm. The ratio of the fluorescence yields Φ 730/Φ 690 for the 80-100 ps component increases when excitation is at 650 nm relative to that for excitation at 670 nm. This enhancement of the long wavelength fluorescence through Chl b excitation is seen in both the kinetic measurements and the steady state measurements. Our data are suggestive that Chl b particularly sensitizes long wavelength emission, reflected by the increase in relative yield of the 80-100 ps decay component.

Figure 4.5 shows a decay associated spectrum of PSI-200 at 77K with λ_{ex}=670 nm. The decays were analyzed by global analysis using a 5 component model. From global analysis it was determined that a 4 exponential model was not sufficient to describe the data. The lifetime of each of the components is 2 to 3 times longer than those observed at room temperature. In the slower components the dominant effect of lowering the temperature appears to be an increase in amplitude, although, in the faster components the amplitudes are relatively unaffected.

The fastest component, 50 ps, comprises about 95% of the amplitude at 695 nm. This component also exhibits a negative amplitude, indicative of fluorescence induction, at wavelengths longer than 720 nm. The maximum of the negative amplitude occurs at 735 nm. Additionally, a fast decay of 250-280 ps is observed which has an emission maximum at 720 nm and contributes 55% of the amplitude at that wavelength. The slowest decay component, 4.8-5.3 ns, has an emission maximum at wavelengths <680 nm and contributes at most 3% to the overall amplitude. The 1.0-1.1 ns component has a broad maximum at 725-730 nm and contributes about 40% to the total amplitude. The 2.4-2.5 ns decay peaks at 750 nm, comprising approximately 70% of the total amplitude. In a comparison of decay associated spectra (figure 4.5 and 4.6) the ratio of the amplitudes of the slower decay components (0.25 ns, 1.1 ns, 2.4 ns) from 720 nm to 740 nm to the amplitude of the fast decay (0.05 ns) at 695 nm is larger when excitation is at 650 nm.
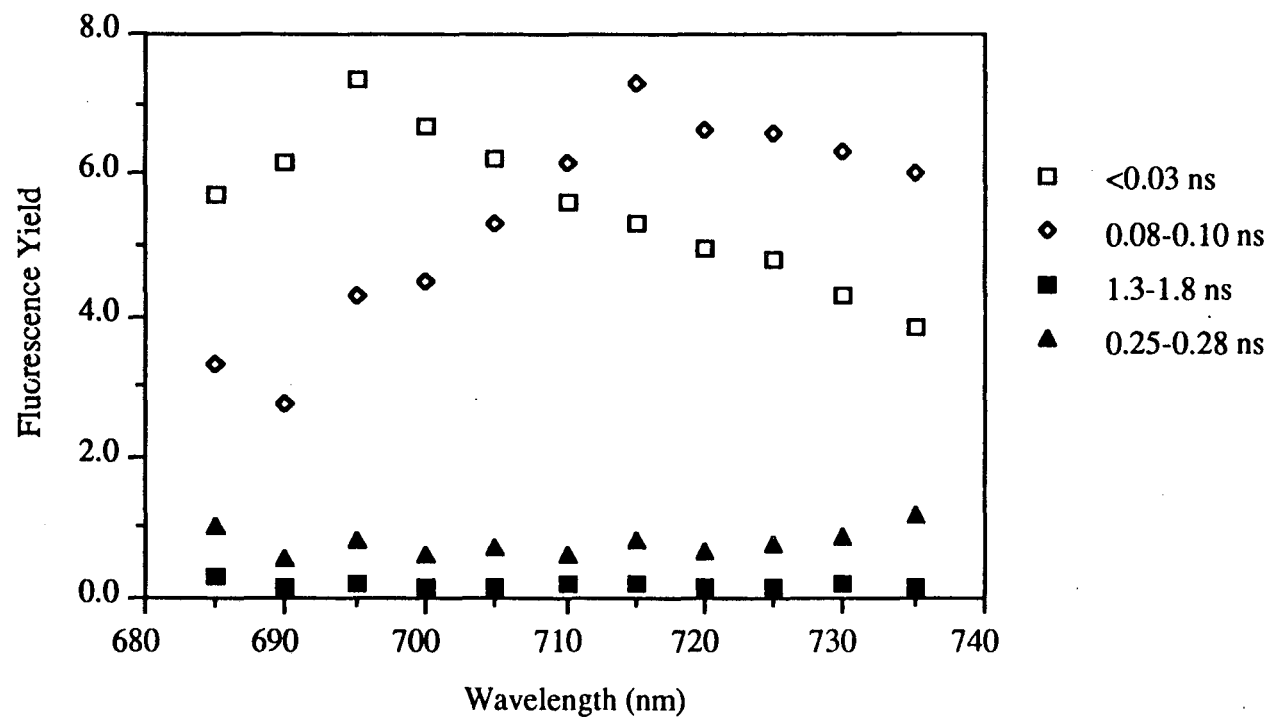
Figure 4.4: Decay associated spectrum of PSI-200. Excitation done at 650 nm. Decays analyzed as in figure 4.3. Data were taken at 295K. The fluorescence yield of each component is plotted as a function of wavelength. Sample preparation as in figure 4.3.
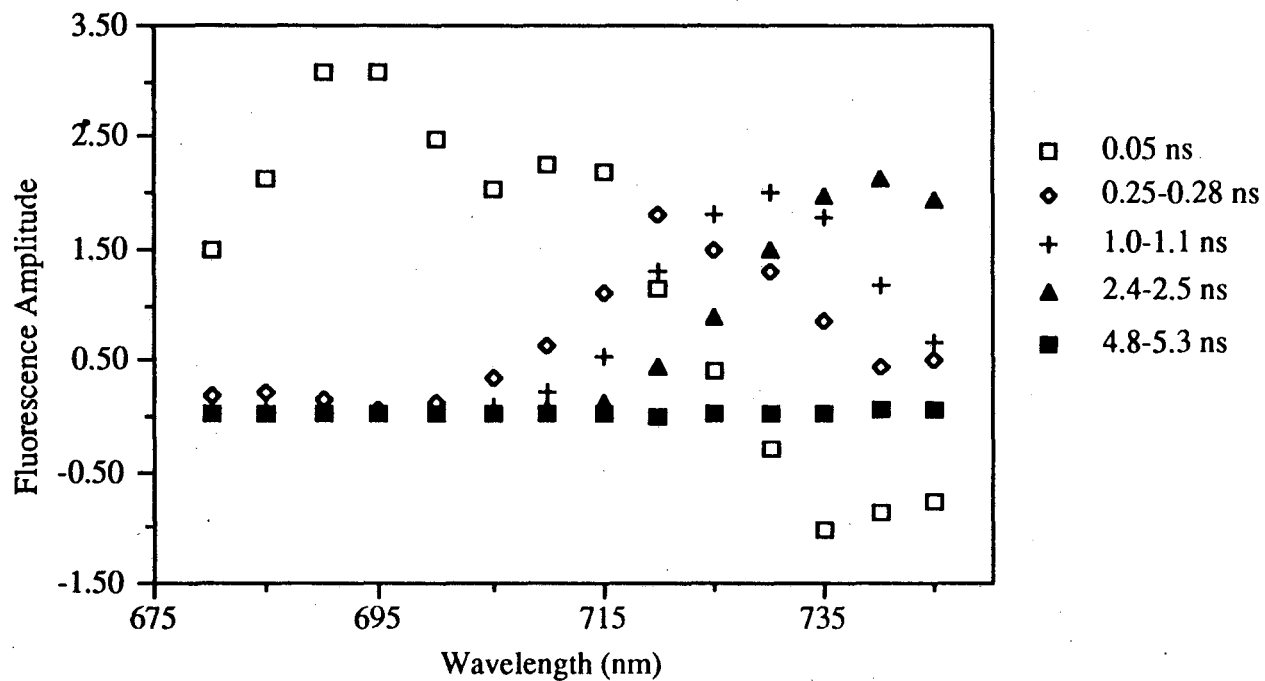
Figure 4.5: Decay associated spectrum of PSI-200 at 77K. Excitation done at 670 nm. Decays were fit to a 5-exponential model using global analysis. Corrected fluorescence amplitudes are plotted as a function of emission wavelength.
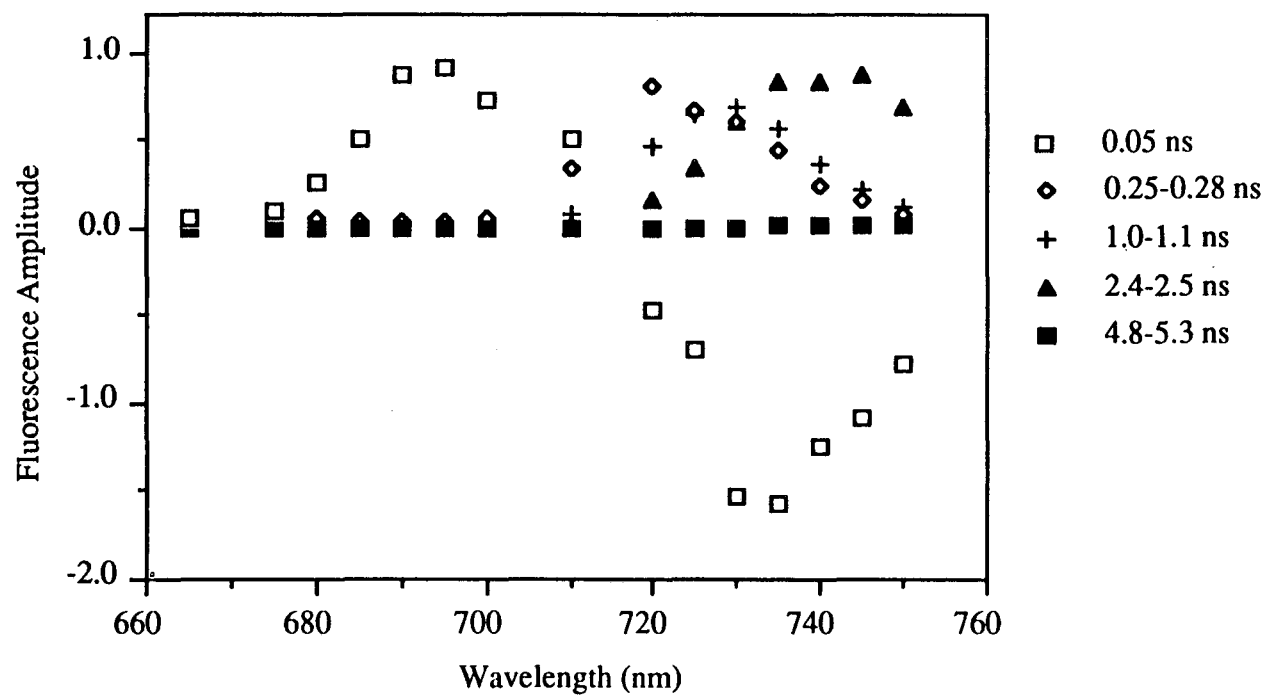
Figure 4.6: Decay associated spectrum of PSI-200 at 77K. Excitation was done at 650 nm. Decays were analyzed as in figure 4.5. Sample was frozen to a cracked glass in 60% glycerol, 40% 0.05M Tricine, pH=7.8.

Emission at either 690 nm or 735 nm was monitored using different excitation wavelengths. Decay-associated spectra recorded in this manner will be referred to as time-resolved excitation spectra. We observe that the time-resolved excitation spectra exhibit the same four lifetimes as the emission spectra. We report a slightly faster lifetime in the time-resolved excitation measurements relative to the time-resolved emission measurements, because they were made using a detector with a significantly faster time-response. Therefore, we can report the fastest lifetime with greater confidence and estimate it at 25 ± 6 ps. Most notably, in contrast to Holzwarth et al. [19], we do not observe a rise time in the long wavelength region of the spectrum. For similar PSI particles they report a rise component of 22 ps, which is comparable to the 25 ps decay component we observe. Our measurements were performed at both room temperature and 278 K and, for certain decays, up to 40,000 counts were collected in the peak channel. Due to experimental constraints it was not possible to apply the global analysis to the data; therefore, potentially we are not successful at deconvolving the rise component. We observe, however, that only Holzwarth et al. [19] have been able to resolve rise components [16,18,21] in PSI particles at temperatures close to room temperature.

The time-resolved excitation spectra confirm what was previously detected in the time-resolved emission spectra. (figures 4.7 and 4.8) For λ_{em} = 690 nm, the 25 ± 6 ps component contributes primarily to the emission and the shape of its excitation dependence indicates that it arises mainly from Chl a antenna molecules. Similarly, the 80-100 ps component shows distinct enhancement at 650 nm for emission at either 690 nm or 735 nm. The excitation spectrum of the 370-460 ps component has distinct similarities with that of Chl a. The wavelength behavior of the 3 ns component is less clear; although, it does resemble that of Chl a. We attribute this component to non-functional antenna pigments or dissociated Chl, which is membrane bound. It contributes less than 5% to the overall yield at any excitation wavelength. This component has a longer decay than in the time resolved emission spectra. This effect might be a result of our increased time resolution in the excitation spectra. Since the fastest components are more effectively recovered, they have less influence on the lifetime of the longer lived components. The intermediate decay lifetime is similarly lengthened, although not to the same extent.

As in the emission data, the amplitude of the decay is completely dominated by the fastest component. We observe, however, that the amplitude of this component is considerably diminished when λ_{em} = 735 nm, as expected from the emission data.
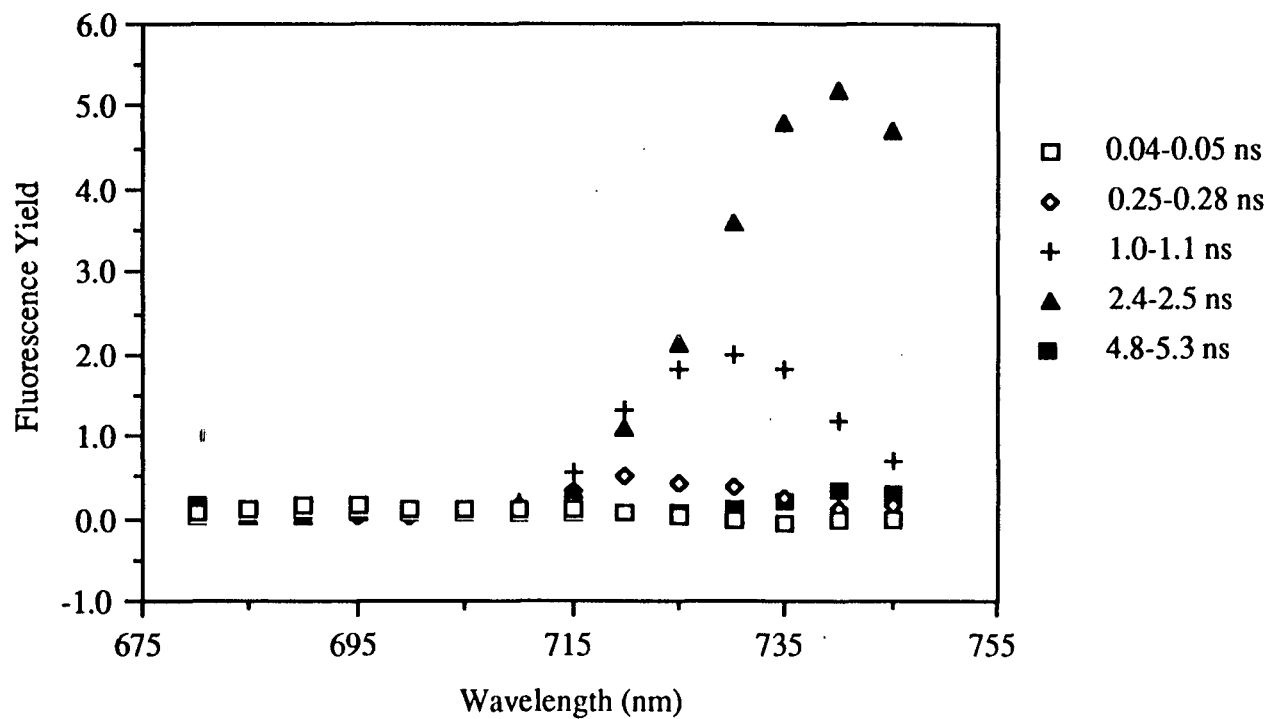
Figure 4.9: Decay associated spectrum of PSI-200. Excitation was done at 670 nm. Decays were analyzed as in figure 4.5. Fluorescence yield is plotted as a function of wavelength.

Figure 4.7: Decay associated excitation spectrum of PSI-200. Emission was monitored at 690 nm. Each decay was analyzed individually to a 4-exponential model. Fluorescence yield is plotted as a function of wavelenth. Sample diluted to 0.01 mg Chl/ml in 0.05M Tricine, pH-7.8. Data were taken at 278 K.

The amplitude does show an increase at 650 nm for this component. One possibility for this enhancement stems from the low amplitude of this component at longer wavelen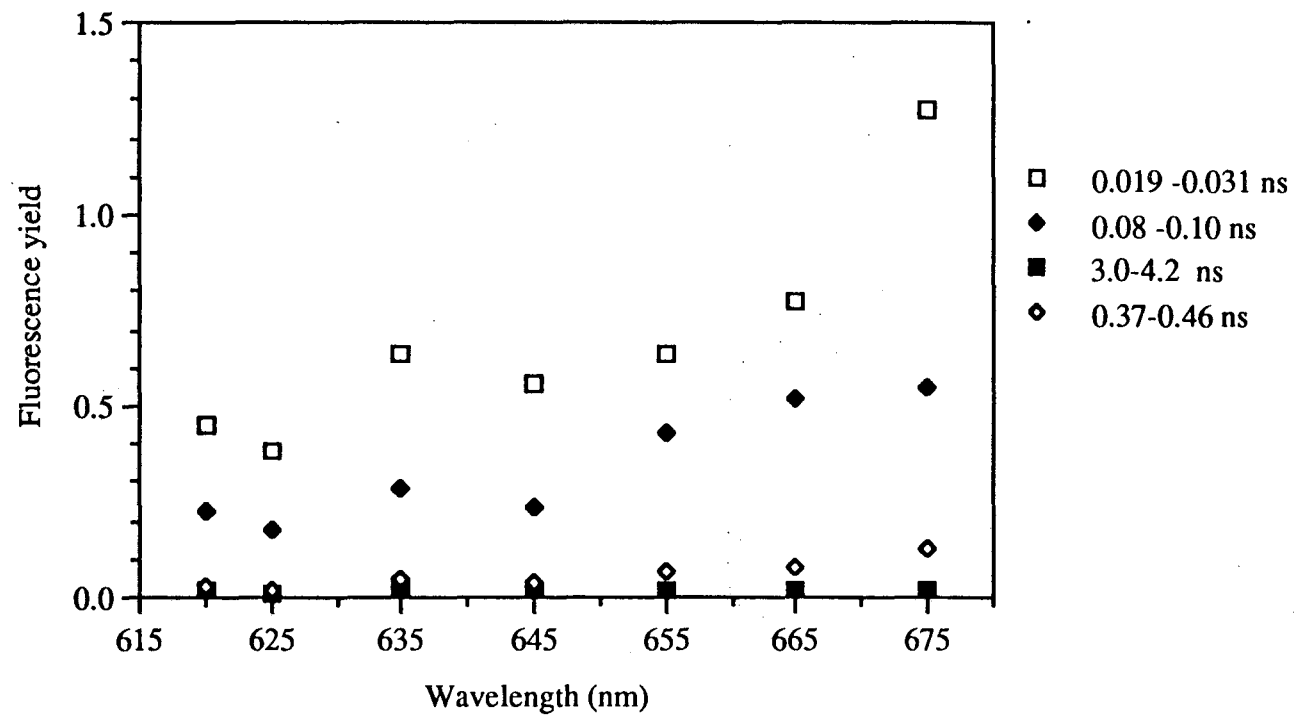gths. It is possible that the resolution of the two fastest components is not complete at this wavelength and the higher amplitude of the 80-100 ps component affects the amplitude of the 25 ps component. It is also possible that we are observing some energy transfer processes. Thus, the excitation spectra support what has been previously detected in the emission spectra: 1) decay kinetics are dominated by the fastest component, whose amplitude is 2 to 3 times smaller for emission at longer wavelengths. 2) the 80-100 ps component is specifically associated with an antenna pool containing Chl b and its amplitude is enhanced at F735. 3) the longest lived component appears to represent emission from non-functional antenna molecules, consisting primarily of Chl a. It is important to realize that the transfer components detected in the time-resolved excitation and emission spectra are the dominant ones in the system. Other components may be present, but are difficult to resovle either due to low amplitude or comparatively fast lifetimes.

3. *Discussion*

Mimuro et. al. have made time-resolved spectroscopic measurements on PSI complexes similar in antenna size and isolation procedure to the PSI-200 preparation. [9.10] The lifetimes obtained in the present work agree with the 4 components they used to deconvolute room temperature data. [9] Measurements at 77K by Mimuro [10] were deconvoluted to 7 components, including three designated F720, F735 and F747. The emission peaks of the slower decay components obtained in our study correlate with the 3 longest wavelength components identified by Mimuro.

Wittmershaus (1987) reports lifetimes of 11 ps and 89 ps for PSI particles using a streak camera to observe room temperature emission at 685 nm; at 77K lifetimes of 12 ps and 305 ps are reported. Their data were fit to only 2 exponential decay components. The effect of temperature on the amplitudes of these components was not addressed.

The lifetimes presented in this study correlate well with those observed by other researchers [9,10,16-19] on similar PSI particles from spinach and other organisms. The primary discrepancy with current results arises because we do not detect any rise components at room temperature, which were observed by Holzwarth et al. [19] in both cyanobacteria and spinach. It is possible that we do not have the time resolution to resolve this component within our signal to noise; although, the lifetime

of our fastest decay component corresponds well with their reported rise component. A second discrepancy arises in the detection of intermediate decay components. Using PSI preparations with some peripheral antenna attached, transient absorption [21] and single photon counting experiments [16] have obtained intermediate decays of 150 to 300 ps. We resolve one relatively fast component, 80-100 ps and one intermediate decay, 270-330 ps (370-460 ps-excitation spectra). Both emission and excitation spectroscopy results demonstrate that the 80-100 ps component displays enhanced amplitude when excited at 650 nm. Holzwarth et al. [19] detect two relatively fast components, 65 and 135 ps, which have a significant amplitude in the long wavelength region; they did not address the Chl b dependence. We suggest that since only three kinetic components were deconvolved in the Owens et al. [16] and Struve et al. [21] work, they were not able to resolve kinetic components 2 and 3, (table 4.1) which we observe. Additionally, our time resolved spectroscopy results support steady state results which show enhanced F735/F690 with excitation at the Chl b absorption maxima.

We observe from kinetic measurements at 77K that the exponential decay component amplitudes are the dominant factor for the dramatic increase in yield. We believe that the increase in amplitude reflects an increase in photon capture cross-section of the long wavelength emitters, caused by a decrease in the rate of non-radiative fluorescence quenching at lower temperatures. The fluorescence decay lifetimes increase by a factor of 3; however, the yield increases by approximately 20 fold between 290 and 80K. The majority of the fluorescence yield increase appears to arise from the increased amplitudes of the 1.0 and 2.5 ns decay components which peak at 730 nm and 740 nm. (figure 4.9) Studies of the temperature dependence of a PSI complex (CPI) with a smaller antenna indicated that, in that case also, the increased yield arises primarily from an increase in amplitude of the longer lived decay components (1.8 ns). [23]

We propose that the kinetic component 1, (F690, see Table I) arises from Chl a molecules, which are closely coupled to the reaction center (core antenna). Component 2 (F720) reflects emission from longer wavelength absorbing pigments. Biochemical fractionation suggests that these pigments are located on the reaction center-containing polypeptides. At 295K Chl b excitation increases the yield of component 2, implying that the peripheral light harvesting antenna transfers energy to this antenna complex. Excitation transfer from F735 to F720 is not resolved in our measurements, as we observe no rise time. We assign the slowest decay component to dissociated Chl or to
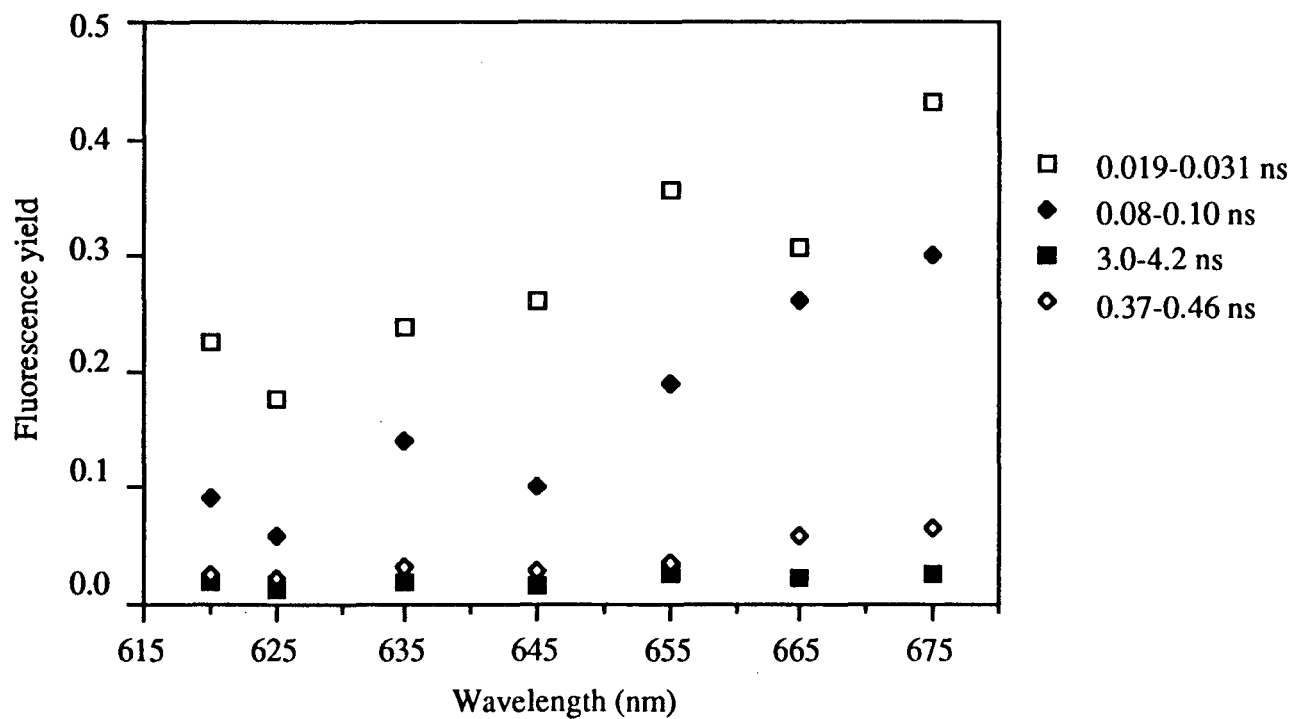
Figure 4.8: Decay associated excitation spectrum of PSI-200. Emission monitored at 735 nm. Data were analyzed individually to a sum of 4-exponentials. Sample conditions as in figure 4.7

antenna which lack a functional trap. Such slowly decaying fluorescence amounts to no more that 3% of the total amplitude and less than 10% of the yield. We attribute kinetic components 3 (F735) and 4 at 77K to the peripheral light harvesting antenna.

Recent work based upon time-resolved experiments done with oxidized and reduced reaction center is suggestive of energy transfer from C680/F690 to P700 via an intermediate C697/F720. [18] At room temperature we do not detect any rise components, which would support this energy transfer pathway. The temperature dependence of the system, particularly in the isolated light harvesting complex (as discussed in chapter 5), indicates that a temperature dependent quenching intermediate does exist. We suggest, however, that this quenching process operates via a radiationless mechanism, possibly representing formation of a triplet state or changes in protein conformation. Malkin and Bearden [24] observed that P700 was effectively oxidized by 730 nm laser light; yet, in a similar experiment they did not oxidize P680. Hiyama and Ke [25] have shown previously that the quantum efficiency of P700 for far-red light is near unity. We speculate that at room temperature the rate of back transfer from these lower energy pools is high; therefore they are efficient at absorbing energy and channelling it to the reaction center. The reaction center represents only one quenching mechanism within the complex. Experiments done on PSI-core reaction center particles [23] show little to no change in fluorescence intensity as a result of opening or closing the reaction center. Thus we propose alternate mechanisms of fluorescence quenching in the antenna, which are highly temperature dependent. As a result at lower temperatures quenching is substantially less efficient and more excitation is diverted to F720 and F735, increasing the effective photon-capture cross-section of these two components. The increased cross-section results in the increase in amplitude of the corresponding components observed in the time-resolved fluorescence relaxation. Data obtained on the isolated LHC-I (chapter 5) support the presence of a quenching intermediate in that system. Temperature dependent measurements on PSI complexes [23], devoid of LHC-I, display similar temperature dependent behavior. We speculate that more than one fluorescence quencher exists in the antennna separate from teh reaction center. We suggest a model (figure 4.10) for energy transfer within PSI, which attempts to explain both the increase in lifetime and amplitude at lower temperatures. Searle et. al. [14] have proposed a model for a smaller antenna system; we have modified and extended this model to encompass the system used in this study. Our model consists of 3 distinct emitting forms: F690, F720 and F735 and a photochemical trap, P700. It is
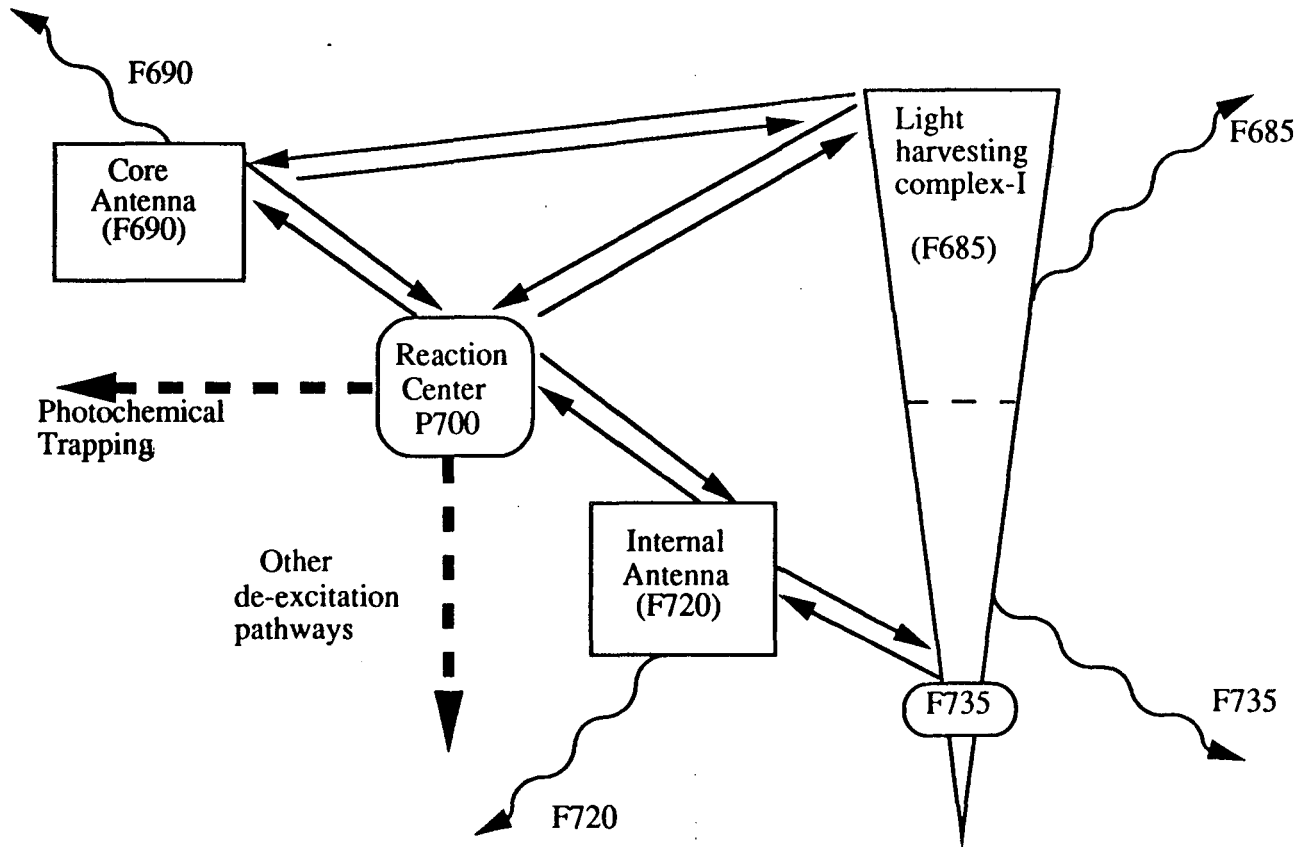
Figure 4.10: Proposed model of excitation transfer within PSI-200. Transfer from core antenna (F690) is temperature independent. Transfer from F720 or F735 to the reaction center is endothermic.

recognized that the light harvesting antenna contains a pool which emits at 685 nm. We speculate that this pool transfers energy directly to antenna (F690) located closer to the reaction center and this process is temperature independent. Transfer energetics withing the isolated LHC-I will be discussed in chapter 5. Chl contained on the reaction center polypeptides, which emit at 690 nm, are referred to as core antenna. For the purposes of this model, we subsume F685 into the fluorescence from the reaction center core antenna, F690. We propose that the efficiency of fluorescence quenching decreases with decreasing temperature. The fluorescence quenching is not explicitly depicted in this model as it is not clear at what point it occurs. Additionally, excitation transfer from F735 to F720 and from F720 to F690 and P700 are both endothermic and temperature dependent. Temperature dependent increases in fluorescence intensity of these components support this contention. At lower temperatures fluorescence is a primary decay path for excited F720 and F735 . We assume that most of the excitation arises from absorption by the main antenna Chl molecules and visits the reaction center before reaching F720 or F735. Excited F690 decays by temperature independent transfer to P700 or by fluorescence. The increase in lifetime at lower temperatures reflects the decrease in rate constant for energy transfer to the reaction center.

Thus, we suggest that the temperature dependence of PSI-200 arises from temperature dependent changes in fluorescence quenching. It is not clear how these proposed non-radiative quenchers are related to excitation transfer to the reaction center. The fluorescence behavior of the isolated light harvesting complex (chapter 5) suggests that the quencher operates independently of the reaction center. These temperature dependent changes result in more excitation reaching lower energy pigments, causing the increase in decay component amplitude observed experimentally in PSI-200. Quantum yield measurements using far red light indicate that the low energy pigments are effective at transferring energy to the reaction center at room temperature. We speculate that the quenching mechanism prevents excitation transfer from low energy pigments to the reaction center at lower temperatures. At this time the nature of the quenching mechanism is undetermined but it will be discussed further in chapter 5.

4. *Summary*

1. At RT both time-resolved excitation and emission spectra are successfully deconvolved to four components. At 77K a five component exponential model is

required to satisfy the data.

2. The increase in fluorescence yield at lower temperature arises primarily from an increase in decay component amplitude rather than longer lifetime. Although, an increase in lifetime is also observed.

3. Excitation kinetic data indicates that the 80-100 ps component is sensitized by Chl b excitation relative to Chl a excitation. Emission data demonstrates that this component has enhanced emission at 735 nm, confirming the relation between Chl b and F735 first observed in steady state emission data (chapter 3).

4. We suggest a model for the data in which the fastest component (30 ps) reflects excitation from the core antenna, F690. Transfer from F690 to the trap is temperature independent. Excitation transfer from F735 and F720, energetically uphill to the trap, is endothermic and highly temperature dependent. Large increases in fluorescence intensity of F735 and F720 at lower temperature are attributed to the presence of a fluorescence quenching mechanism, which is inefficient at lower temperature.

5. References for Chapter IV

1. Bose, S. (1982) *Photochem. Photobiol.*, **36**, 725-731.
2. Holzwarth, A.R. (1987) in The Light Reactions (J. Barber, ed.), Amsterdam: Elsevier Science Publishers, 95-157.
3. Zuber, H. (1985) *Photochem. Photobiol.*, **42**, 821-844.
4. Holzwarth, A.R. (1986) *Photochem. Photobiol.*, **43**, 707-725.
5. Butler, W.L., Tredwell, C.J., Malkin, R. and Barber, J. (1979) *Biochim. Biophys. Acta,* **545**, 309-315.
6. Owens, T.G., Webb, S.P., Mets, L., Alberte, R.S., Fleming, G.R. (1987) *Proc. Natl. Acad. Sci. USA*, **84**, 1532-1536.
7. Reisberg, P., Nairn, J.A. and Sauer, K. (1982) *Photochem. Photobiol.*, **36**, 657-661.
8. Wittmershaus, B., Nordlund, T.M., Knox, W.H., Knox, R.S. and Breton, J. (1985) *Biochim. Biophys. Acta*, **806**, 93-106.
9. Mimuro, M., Yamazaki, I., Tamai, N., Yamazaki, T. and Fujita, Y. (1987) in Primary Processes in Photobiology (T. Kobayashi, ed.), Berlin: Springer, 23-32.
10. Mimuro, M. (1988) in Photosynthetic Light Harvesting Systems (H. Scheer and S. Schneider, eds.), Berlin: W. de Gruyter, 589-600.
11. Beddard, G.S., Fleming, G.R., Porter, G., Searle, G.F.W. and Synowiec, J.A. (1979) *Biochim. Biophys. Acta*, **545**, 165-174.
12. Gulotty, R.J., Mets, L., Alberte, R.S. and Fleming, G.R. (1985) *Photochem. Photobiol.*, **41**, 487-496.
13. Holzwarth, A.R. (1987) in Progress in Photosynthesis Research (J. Biggins, ed.), Vol. I, The Hague: Martinus Nijhoff, 73-76.
14. Searle, G.F.W., Tamkivi, R., van Hoek, A., Schaafsma, T.J. (1988) *J. Chem. Soc., Faraday Trans. 2*, **84**, 315-327.
15. Owens, T.G., Webb, S.P., Eads, D.D., Alberte, R.S., Mets, L. and Fleming, G.R. (1989) *Biophys. J.*, **56**, 95-106.
16. Owens, T.G., Webb,S.P., Alberte, R.S., Mets, L. and Fleming, G.R. (1988) *Biophys. J.*, **53**, 733-745.
17. Wittmershaus, B. (1987) in Progress in Photosynthesis Research (J. Biggins, ed.), Vol. I, The Hague: Martinus Nijhoff, 75-82.

18. Sparrow, R., Brown, R.G., Evans, E.H. and Shaw, D. (1990) *J. Photochem. Photobiol. B: Biology*, **5**, 445-455.

19. Holzwarth, A.R., Haehnel, W., Ratajczak, R., Bittersmann, E. and Schatz, G.H. (1990) in Current Research in Photosynthesis (M. Baltscheffsky, ed), Vol. II, The Netherlands: Kluwar Academic Publishers, 611-614.

20. Causgrove, T.P., Yang, S. and Struve, W.S. (1988) *J. Phys. Chem.*, **92**, 6121-6124.

21. Causgrove, T.C., Yang, S. and Struve, W.S. (1989) *J.Phys. Chem.* **93**, 6844-6850.

22. Gillie, J.K., Small, G.J. and Golbeck, J.H. (1989) *J. Phys. Chem.* **93**, 1620-1627.

23. Tabbutt, S. (1987) in Spectroscopic Studies of Energy Transfer in Photosynthetic Reaction Centers of Higher Plants, PhD. Thesis, Berkeley: Lawrence Berkeley Laboratory Report (LBL-24017), 105-165.

24. Malkin, R. and Bearden, A.J. (1975) *Biochim. Biophys. Acta*, **396**, 250-259.

25. Hiyama, T. and Ke, B. (1971) *Arch. Biochim. Biophys.*, **147**, 99-108.

Chapter V: Spectroscopic Characterization of an Isolated Light Harvesting Complex of Photosystem I: Steady-state and Time-resolved Measurements

In this chapter the isolation and spectroscopic characterization of the peripheral light harvesting complex of PSI will be described. This light harvesting complement to PSI has been identified and isolated in both higher plants and green algae. [1-13] Although, the specific fluorescence characteristics differ from species to species, in all cases the fluorescence from these peripheral antenna systems occurs at longer wavelengths than the reaction center, P700. It has been observed for *Lemna gibba* [8] that all of the pigment resides on one polypeptide, however in spinach and barley [4,7] it has been reported that more than one polypeptide contains pigment. The antenna complex does not assemble during growth under intermittent light conditions nor in Chl-b-less mutants. [13,14] Thus, Chl b, an important element of light harvesting, appears to play a structural role in protein assembly as well. In spinach the isolated light harvesting complex (LHC-I) displays similar spectroscopic behavior to the native PSI complex, PSI-200. We have isolated this antenna complement in order to investigate the spectroscopic origins and function of the long wavelength fluorescence, F735, of PSI. We have employed steady-state and time-resolved fluorescence spectroscopy to characterize the isolated LHC-I. Time-resolved emission studies have been done at 77K and room temperature. Additionally, the temperature dependent behavior of F735 has been specifically addressed over a relatively narrow temperature range.

1. *Isolation*

LHC-I was isolated from PSI-200 following the method of Haworth et. al. [2] with some minor modifications. PSI-200 fractions were collected off linear sucrose density gradients, as described in chapter 3. These fractions were assayed by fluorescence to insure complete separation from LHC-II and were then pooled and stored at -20°C for a period no longer than a month. PSI-200 material from two or three preparations was often collected prior to proceeding to the isolation of LHC-I, to obtain enough material for spectroscopic measurements. The pooled fractions of PSI-200 were dialyzed against 0.05M Sorbitol at 4°C in the dark for 18 h. The aggregated material was pelleted by centrifugation (12,000xg; 10 min). Pellets were then diluted with ice cold H_2O to a Chl concentration of 0.5 mg/ml. At this time dodecyl-β-D-

maltoside (1.5 mg/ml) and zwittergent-16 (2.0 mg/ml) were added to the solution. The detergent mixture was shaken for 1 h in the dark at 0°C and immediately loaded onto a 0.1-1.0M linear sucrose density gradient containing 0.025% dodecyl-β-D-maltoside and 0.02M Tricine, pH=7.8. The gradients were centrifuged at 85,000xg for 18.5 h. The isolated antenna band was located at the top of the gradient immediately below a free Chl band. A second band on the gradient contained primarily reaction center. It was found that the detergent concentrations used in the sucrose gradient for optimal separation of the light harvesting complex were insufficient to separate the reaction center completely from the peripheral antenna. However, as a result of the low concentrations of detergents used for the isolation, the complex appears to be relatively intact . Purity of the material was assessed by SDS-PAGE as described in chapter 2. The Bio-Rad silver stain procedure was used to detect protein bands and to insure the complete absence of reaction center in these preparations.

2. *Results*

The isolated light harvesting complex contains four polypeptides, 24, 21, 17 and 11 kDa and the 21 kDa is sometimes observed as a doublet. [13] Although, the exact distribution of pigments is uncertain, recent biochemical studies show that the majority of the Chl b is located on one protein. [9,10] Using the method of Arnon, [15] Chl concentrations were determined and the complex was found to have a Chl a/Chl b ratio of 3 or 4:1. Absorption spectra confirm the presence of Chl b with pronounced shoulders at 650 and 472 nm. (figure 5.1a) The primary difference between the absorption spectra of PSI-200 and LHC-1 is the enhanced absorbance at 654 nm in LHC-I, reflecting the higher relative amount of Chl b. By the simple process of subtraction, with both spectra normalized at 440 nm, it is observed that PSI-200 has an enhanced absorption at 500 nm, which is suggestive of a larger amount of carotenoid in the holocomplex. (figure 5.1b) LHC-I contains only lutein [9]; PSI-200, however, contains β-carotene also. [16] This β-carotene is reflected in our difference spectrum. CD studies indicate that the carotenoid present is not in the normal trans configuration. It is unclear whether pigment-protein interactions are also contributing to the CD spectrum.[17] Interestingly, in the subtracted spectrum PSI-200 has a pronounced absorption at 685 nm. This absorption peak is at longer wavelength than the main red absorption peak for the light harvesting complex. The main absorption of PSI-200 occurs at longer wavelength than LHC-I indicating that the majority of Chl in LHC-I absorbs at higher energy than the antenna associated with the
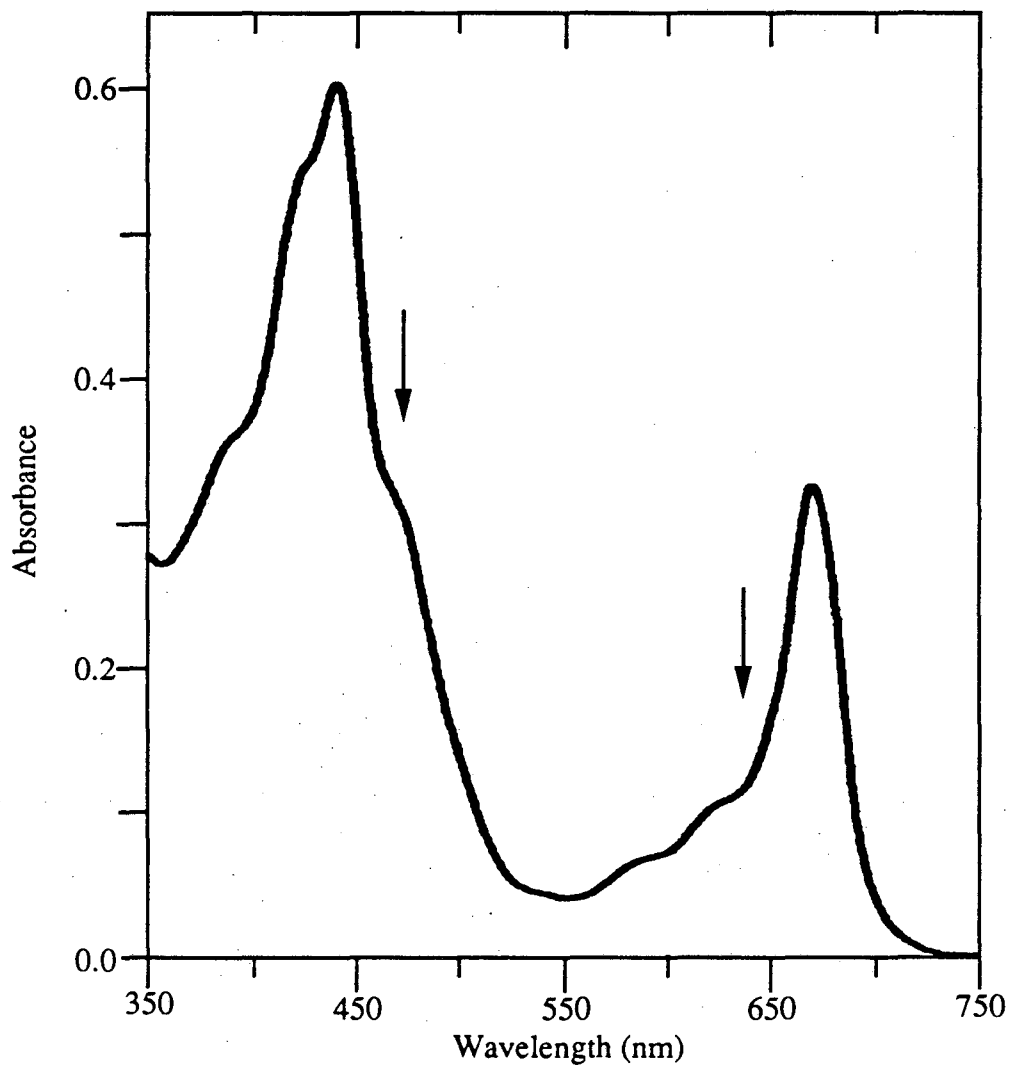
Figure 5.1a: Absorption Spectrum of LHC-I. Sample was diluted in 0.05M Tricine, pH=7.8 to 0.01 mg Chl/ml. Absorption pathlength was 0.4 cm. The absorption maxima occur at 440 nm and 672 nm. Chl b absorption at 472 nm and 650 nm indicated by arrows.
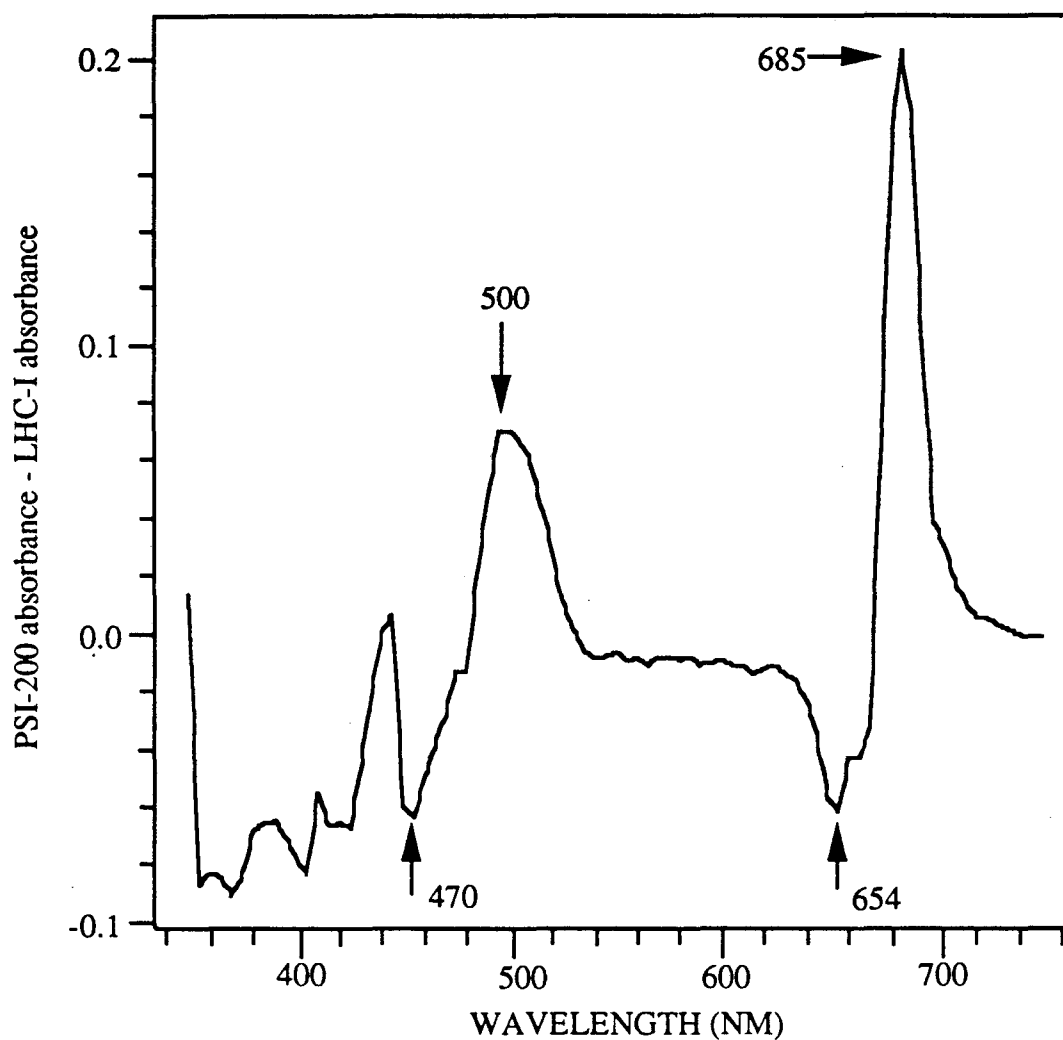
Figure 5.1b: Absorption Difference Spectra of PSI-200 and LHC-I. Both spectra were normalized at 440 nm and then subtracted. Samples diluted to 0.01 mg Chl/ml with 0.05M Tricine, pH=7.8. The carotenoid absorption at 500nm, Chl b absorption features at 470 nm and 654 nm, and Chl a absorption at 685 nm are indicated with arrows.

reaction center. Absorption at longer wavelengths, 700-730 nm, in LHC-I is relatively low, implying that the concentration of low energy pigments within LHC-I is small in comparison with the rest of the Chl.

Steady State Fluorescence Measurements

At room temperature the LHC-I complex has an emission maximum at 685 nm (F685) with a broad shoulder ranging from 710-740 nm. At 77K a dramatic shift in wavelength emission maximum from 685 nm to 733 nm (F730) is observed. (figure 5.2) This emission maximum at 733 nm is at higher energy than the 738 nm (F735) peak observed for PSI-200 as reported in chapter 3. Additionally, the LHC-I complex has a pronounced shoulder at 685 nm, compared to the relatively weaker short wavelength emission observed at 77K in PSI-200. This shoulder could serve to blue-shift the emission maximum. It is also possible that dissociated Chl released in the isolation procedure shifts the emission maximum to higher energy than what is observed for the reaction center complex.

Quantum yield measurements have also been performed on the isolated light harvesting complex. These measurements were done with the excitation wavelengths, 650 and 670 nm. In each case the emission scan was started 10 nm to the red of the exciting light in order to avoid any scattering artefacts. All scans were ended at 800 nm. Both emission and absorption measurements were made concurrently with the standard dye, Nile Blue 690. Calculations were done as described in chapter 3, utilizing the same assumptions. An additional problem encountered with these complexes relative to the reaction center complex is the presence of dissociated Chl within the preparations. This problem is not significant in the reaction center preparation; however, the process of isolating the antenna from PSI-200 releases some Chl, which is then difficult to separate from the pigment-protein complex. The presence of this non-functional Chl influences the fluorescence yield; therefore, we corrected the yield for this contaminant by estimating the amount within the preparation. Specifically, the contribution to the yield was estimated from the yield of the longest-lived component deconvolved from the time-resolved measurements, typically between 10 and 20 percent of the emission at 680 nm. The wavelength dependence of this emission was determined from the decay-associated spectra (DAS). This constructed spectrum was then subtracted from the original steady-state fluorescence spectrum yielding a corrected emission. The area of the corrected emission was integrated for the quantum yield calculation. For excitation at 670 nm,
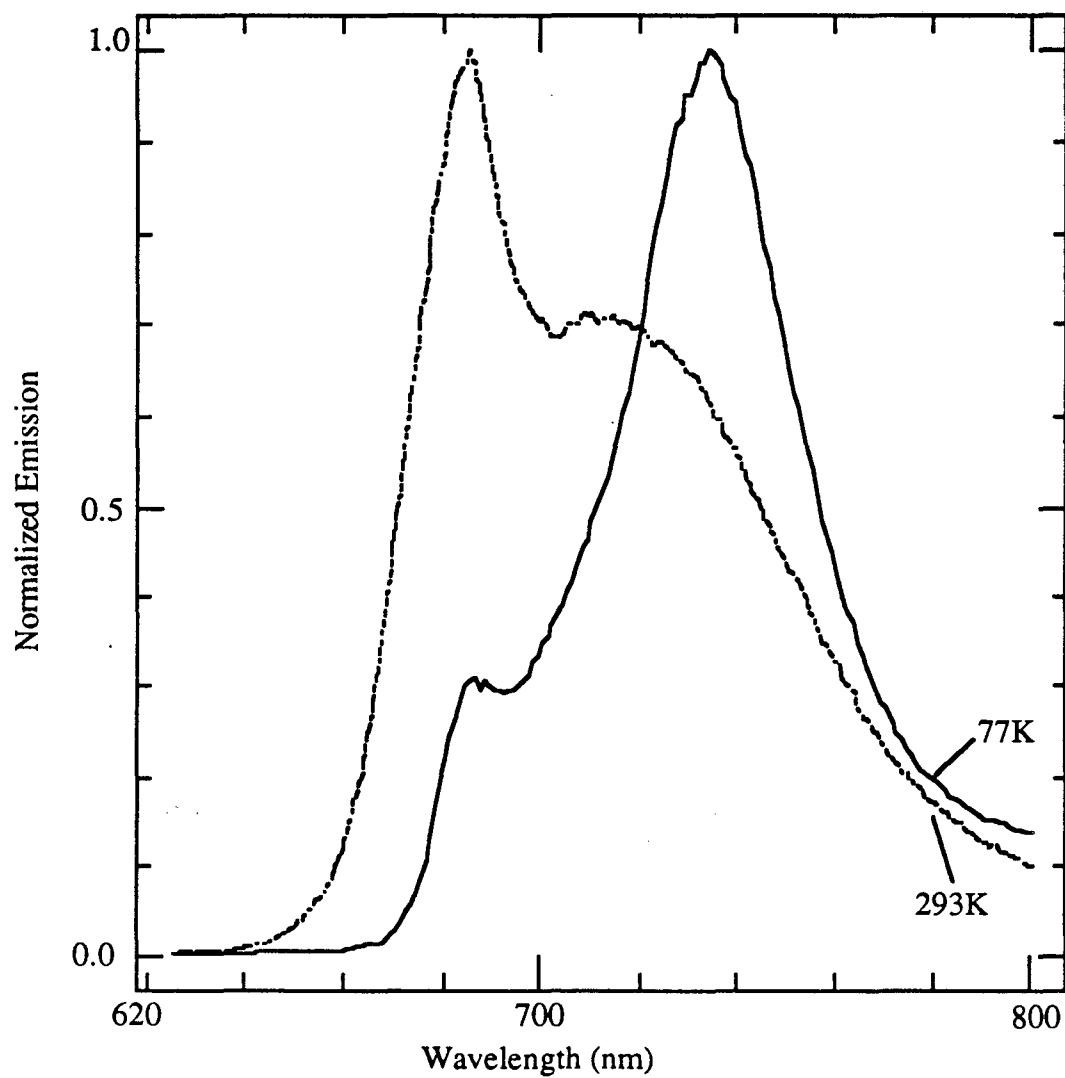
Figure 5.2: Steady state fluorescence emission of LHC-I at 293K and 77K. Excitation done at 435 nm. Sample originally in 0.1-0.2 M sucrose diluted 5 fold. 293K: Sample dilution done with 0.05 M Tricine, pH=7.8. 77K: Sample dilution done with 40% 0.05M Tricine, pH=7.8, 60% glycerol.

the quantum yield, Φ_F, was calculated to be 0.27 ± 0.06. When the exciting light was at 650 nm, Φ_F = 0.24 ± 0.05. Thus, within the error of the measurement, the quantum yields at 650 nm and at 670 nm are the same. It is apparent however that the value of the yield is approximately 10 fold higher for LHC-I than for PSI-200. These data indicate that the presence of the reaction center complex acts as a uniform quencher of fluorescence emission from LHC-I.

Measurements were also performed to test the validity of the Stepanov relation [18,19] within this complex. These measurements were done in the same manner as described in chapter 3. Approximately linear plots were observed over the range of highest overlap between absorption and emission (650-700 nm). In the red edge of the absorption band, where the actual absorbance is quite small, the plots displayed a noticeable degree of curvature. (figure 5.3) The Kennard-Stepanov temperature (T_{ks}) calculated from these plots, 363K ± 5K is significantly elevated from the temperature at which the measurements were conducted, 298K. The temperature obtained is similar to the T_{ks} observed for the PSI-200 complex, although it is substantially higher than that observed for PSI-100*. In both PSI-200 and LHC-I the emission spectrum is quite heterogeneous. In LHC-I F730 is almost two-thirds the intensity of F685. The curvature in the Stepanov plot could reflect the two different emitting species. When the Stepanov relation was applied to isolated LHC-II, the light harvesting complex of PSII, in the region of highest overlap a linear plot was obtained giving a T_{ks} = $T_{ambient}$ = 297K. [20] It is of interest that the two isolated light harvesting complexes of green plants do not exhibit the same Stepanov behavior. Similar measurements performed on phycobilisomes, however, also yielded a T_{ks} elevated relative to $T_{ambient}$. [21] The Kennard-Stepanov temperatures obtained in that case compare favorably with those obtained from the chlorophyll proteins of PSI.

Excitation spectra of LHC-I were taken at 77K. (figure 5.4) Peaks at 468 nm and 650 nm, the absorption maxima of Chl b, are noticeably enhanced for F735 in comparison with that for F685. Our data correlate well with biochemical evidence which indicates that Chl b is intimately connected with fluorescence at longer wavelengths. [3,5,10] An additional feature of the excitation spectra is a small shoulder observed between 703-708 nm. This shoulder may reflect the presence of a long wavelength absorber originally proposed by Butler to be responsible for emission at 720 nm in whole leaves. [22] We assign this pigment to C705, although there could be more than one spectral component. Both Chl b and C705 enhance F735 in LHC-I. This feature was also observed in the 77K excitation spectrum of PSI-200.
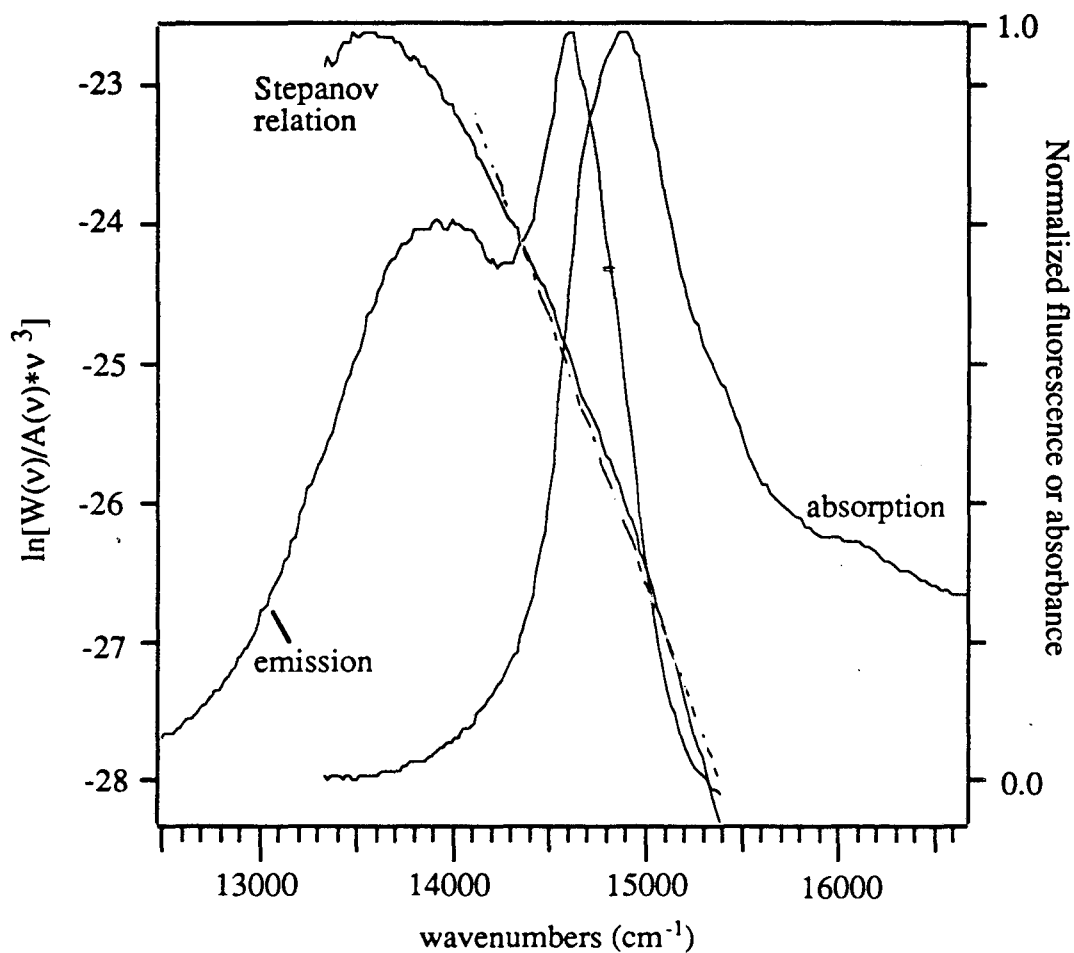
Figure 5.3: Stepanov Relation applied to LHC-I. The Stepanov relation was calculated as described in the text, using the absorption and emission spectra depicted. All measurements were done on the same sample. A linear fit (dashed line) was applied to the region of highest overlap, 650-700 nm. This fit yielded a Kennard-Stepanov temperature of 363K ± 5K.
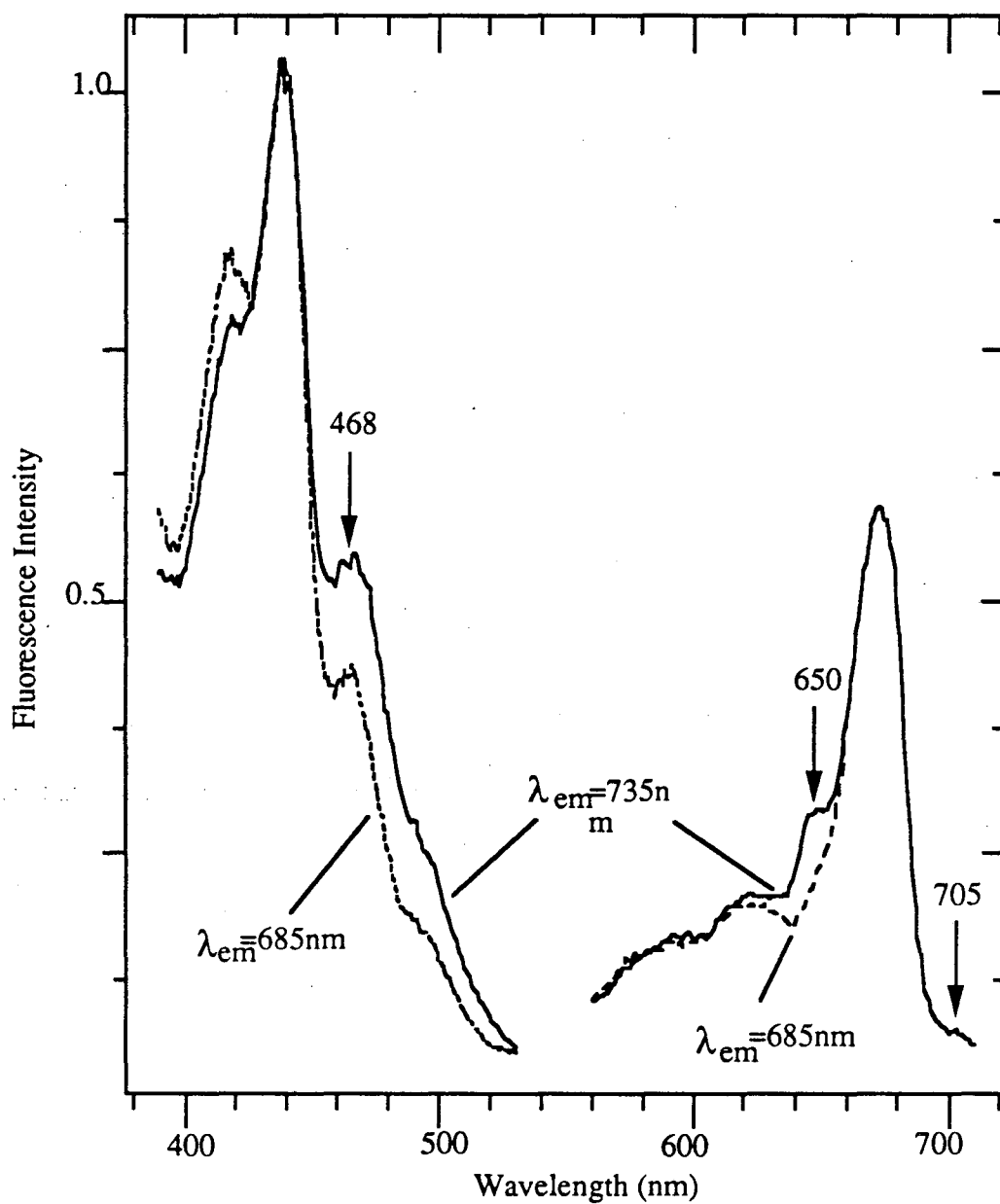
Figure 5.4: Steady state excitation spectra of LHC-I. Spectra were taken at 77K with emission at 685 or 735 nm. Samples frozen to a cracked glass in 40% 0.05 M Tricine, pH=7.8, 60% glycerol. Excitation at Chl b absorption maxima, 468 nm and 650 nm, and at 705 nm are enhanced for emission at 735 nm.

Excitation polarization studies have also been done on the LHC-I complex. (figure 5.5) For 735 nm emission a polarization value of approximately zero is observed using excitation wavelengths from 600 nm to 675 nm. The polarization then rises over the wavelength range 675 nm to 705 nm, reaching a value of 0.3 from 705 nm to 725 nm. In general, polarization values of 0.3 or more indicate that the relative angle between absorption and emission dipoles is small. [23] High polarization values imply that absorption and emission are occurring at the same chromophore or that excitation transfer is limited to a set of chromophores with nearly parallel transition moments. The polarization spectrum for emission at 735 nm resembles that obtained for PSI-200, as discussed in chapter 3. For LHC-I the maximum polarization value is higher, 0.3, compared with 0.2 for PSI-200. It appears that in LHC-I either the chromophores are more oriented or there is a smaller degree of depolarizing energy transfer processes. In linear dichroism studies Tapie et al. [24] also observed a higher dichroic ratio for isolated LHC-I relative to the holocomplex. Our data are indicative that LHC-I contains a smaller amount of the F720 emitting species, compared to PSI-200. We suggest that F720 potentially causes the depolarized emission at 735 nm observed in PSI-200.

In the 550-670 nm range the polarization values of F690 are lower than those obtained for emission at 735 nm. The lower polarization of the 690 nm emission reflects the presence of two different antenna species, one giving rise to F690 and one to F730. The rise observed from 670-680 in the excitation spectra for $\lambda_{em} = 690$ is similar to what is observed for PSI-200. We attribute the rise to either emission from pigments absorbing at those wavelengths or from overlap with F735. Polarization values of approximately zero are indicative of depolarized emission. In this instance the depolarization undoubtedly results from energy transfer processes occurring within the antenna complex. The polarized fluorescence observed from excitation wavelengths greater than 705 nm is indicative of emission arising from a pigment or pigments with an excited state lying at lower energy than those of the majority of the LHC-I Chl and probably lower than that of the reaction center of PSI.

The temperature dependence of LHC-I fluorescence has also been investigated. Figure 5.6a depicts the emission of the antenna complex as a function of temperature. It can be seen that the fluorescence yield of the complex increases as the temperature decreases. There is no concomitant increase in absorption cross-section as the temperature is lowered (data not shown). In Figure 5.6b the same data are depicted normalized to their emission maxima, demonstrating that the yield of F735 increases at

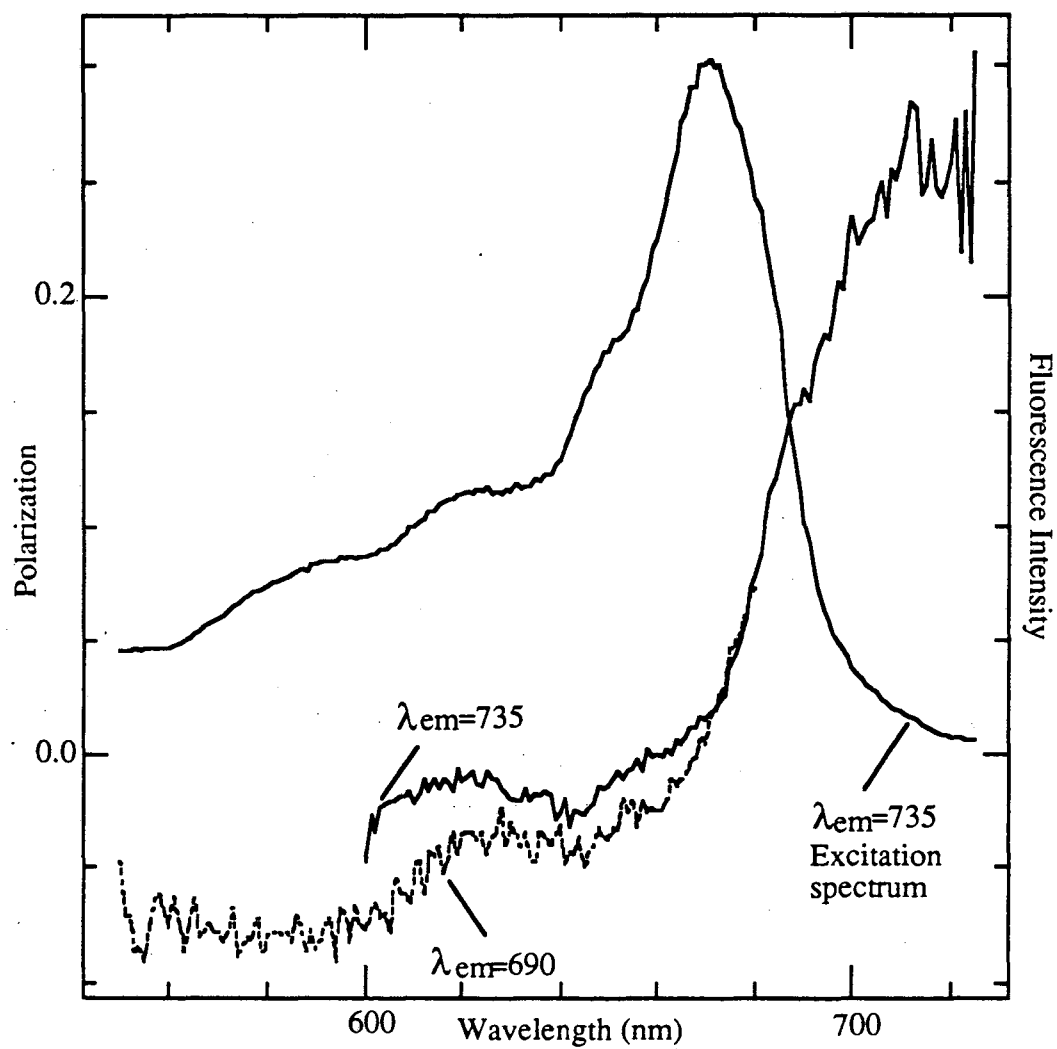Figure 5.5: Excitation polarization of LHC-I. Emission wavelengths at either 690 nm or 735 nm. Steady state excitation spectrum with emission at 735 nm. T = 278K. Sample in 40% 0.05 M Tricine, pH=7.8, 60% glycerol.

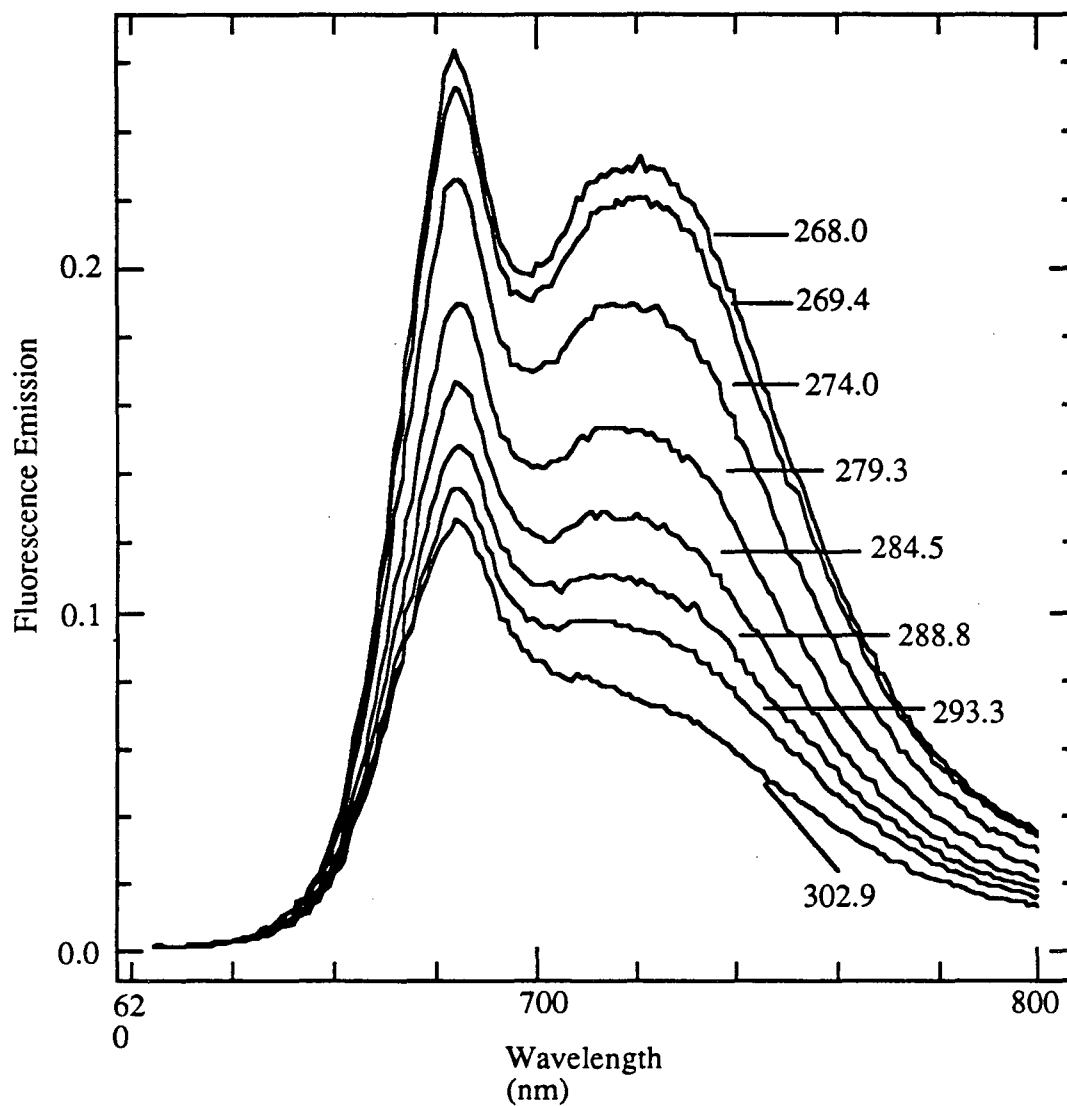Figure 5.6a: Temperature dependence of LHC-I. All spectra taken on the same sample at indicated temperatures (K). Sample diluted approximately 5 fold in 40% 0.05M Tricine, pH=7.8, 60% glycerol. Excitation done at 435 nm.
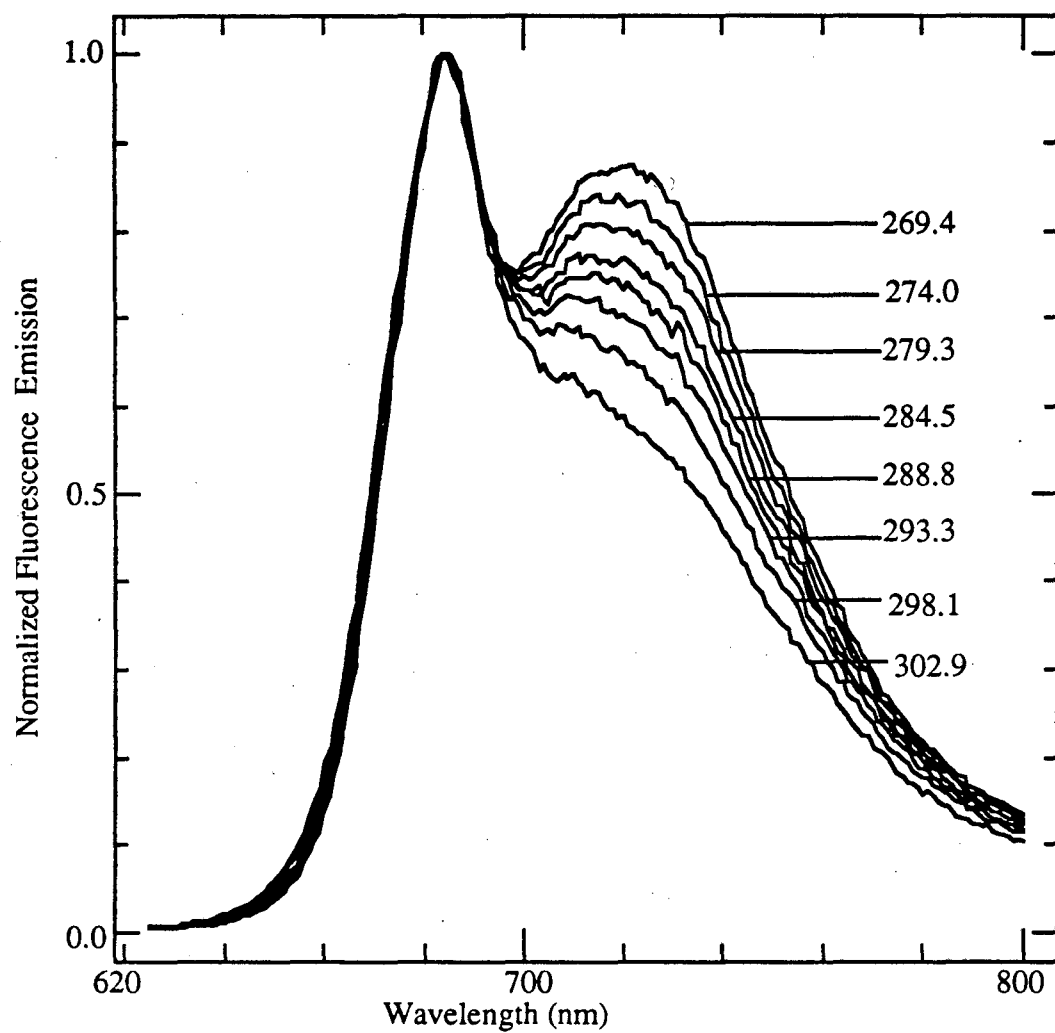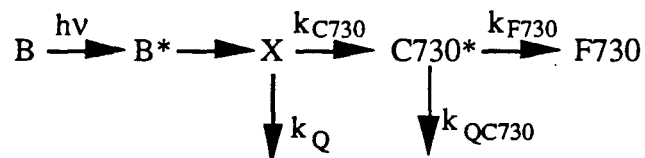
Figure 5.6b: Temperature dependence of LHC-I. All spectra taken on the same sample at indicated temperatures (K). Normalized steady state fluorescence emission. Sample preparation as in Figure 5.6a.

a greater rate than the fluorescence yield of F685. This behavior contrasts markedly with what is observed for PSI-200. For the reaction center containing complex, PSI-200, the fluorescence yield of the shorter wavelength component (F690) remains essentially temperature independent, while the yield of the long wavelength component increases dramatically, as described in chapter 3. The increase in fluorescence intensity as the temperature is decreased implicates a high temperature quenching mechanism for the excited state. Although, both F685 and F730 are temperature dependent in LHC-I, we suggest that F685 contains both temperature independent and temperature dependent fluorescence. This premise is supported by temperature-dependent kinetic data, discussed in subsequent sections. Emission bands were deconvolved by the method of spectral subtraction. We assume that F730 contains a negligible amount of temperature independent fluorescence. For F730 we propose a mechanistic scheme similar to the one proposed for PSI-200.

$$B \xrightarrow{h\nu} B^* \longrightarrow X \xrightarrow{k_{C730}} C730^* \xrightarrow{k_{F730}} F730$$

with $X \xrightarrow{k_Q}$ and $C730^* \xrightarrow{k_{QC730}}$

Using this scheme we are able to write the following rate equations:

$$\frac{d[C730^*]}{dt} = k_{C730}[X] - (k_{QC730} + k_{F730})[C730^*]$$

where k_{QC730} represents the rate constant for temperature independent quenching processes such as internal conversion and intersystem crossing. Similarly,

$$\frac{d[X]}{dt} = k_{BX}[B^*] - (k_{C730} + k_{QX})[X]$$

where k_{QX} is the rate constant for non-radiative temperature dependent fluorescence quenching. The fluorescence yield at 730 nm can then be expressed as:

$$F730 = \frac{k_{F730}k_{C730}k_{BX}[B^*]}{(k_{C730} + k_{QX})(k_{QC730} + k_{F730})}$$

Assuming that the temperature dependent changes primarily arise from k_{QX}, the above relation can be re-written:

$$\frac{k_{F730}k_{C730} k_{BX}[B^*]}{F730 (k_{QC730} + k_{F730})} = A \exp{-(Ea/RT)} + k_{C730} = k_{QX} + k_{C730}$$

k_{C730} is smaller than k_{QX} and is neglected in the calculation. A linear fit ($R^2 = 0.99$) can be generated to satisfy the data, when it is expressed in the above form. An activation energy of 1700 cm^{-1} is obtained. (figure 5.7) We propose the following scheme to account for the temperature dependence of F685:
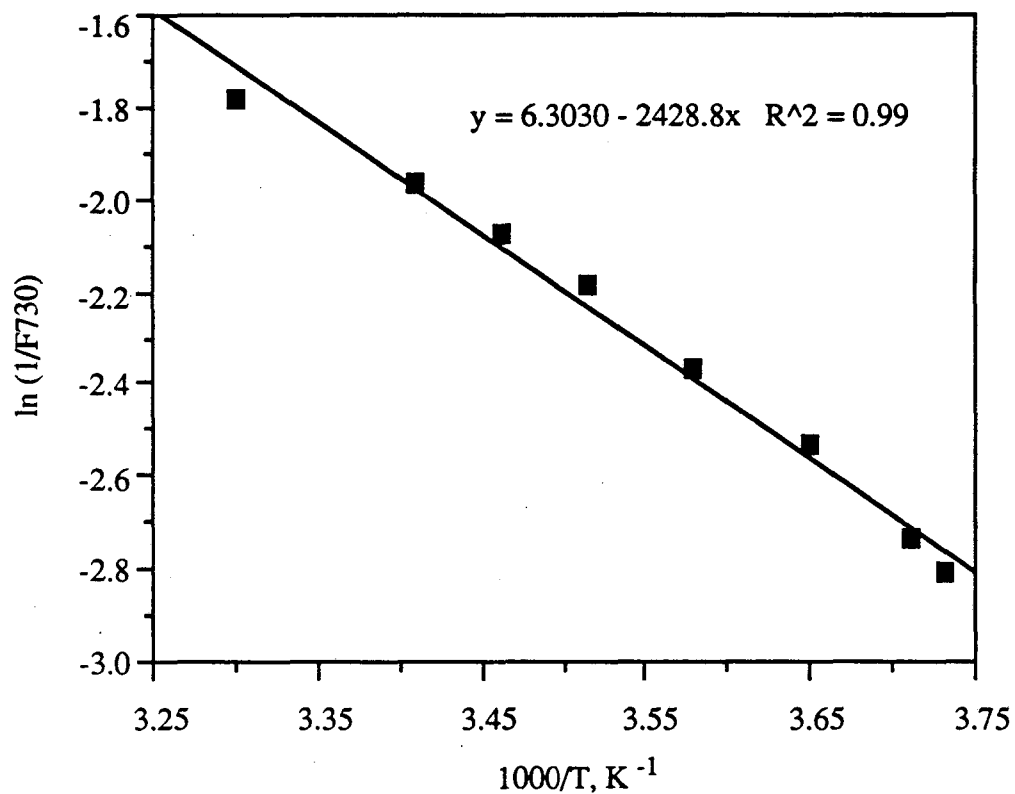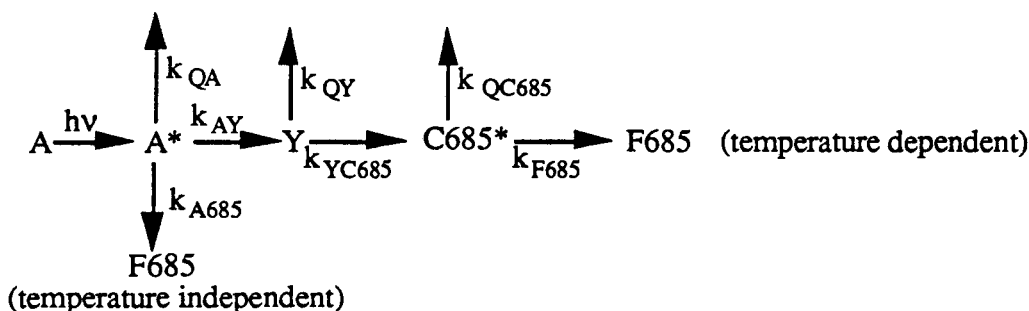
Figure 5.7: Arrhenius plot of F730. The natural logarithm of the inverse of F730 is plotted as a function of 1/T. Linear fit to the data is shown with a solid line. An activation energy of 1700 cm^{-1} is obtained.

$$A \xrightarrow{h\nu} A^* \xrightarrow{k_{AY}} Y \xrightarrow{k_{YC685}} C685^* \xrightarrow{k_{F685}} F685 \quad \text{(temperature dependent)}$$

with k_{QA}, k_{QY}, k_{QC685} (upward) and k_{A685} (downward)

$$F685$$
(temperature independent)

In this scheme k_{QA} and k_{QC685} represent temperature independent quenching processes, such as internal conversion and intersystem crossing. k_{QY} represents non-radiative quenching and is assumed to be the only temperature dependent process. By relating the rate equations for the concentrations of A*, Y and C690*, we obtain an expression in which the fluorescence yield at 685 nm can be related to the temperature dependent rate constant k_{QY}.

$$\left[\frac{C}{F685 - D}\right] - B = A \exp{-Ea/RT} = k_{QY}$$

$$C = \frac{\left(\Phi_A I_{ABS}\right)\left(k_{F685} k_{YC685} k_{AY}\right)}{\left(k_{F685} + k_{QC685}\right)\left(k_{AY} + k_{A685} + k_{QA}\right)}$$

$$D = \frac{\left(\Phi_A I_{ABS} k_{685}\right)}{\left(k_{AY} + k_{A685} + k_{QA}\right)}$$

$$B = k_{YC685}$$

We have determined that subtracting approximately 20% of the yield of F685 at 303K from all values gives an activation energy (1700 cm^{-1}) similar to what was obtained for F730. (figure 5.8) We observe that the 0.04 ns component resolved in kinetic measurements, (discussed in the next section) contributes approximately 20% to the fluorescence yield at 685 nm and less than 5% at 730 nm. We suggest that this component reflects the temperature independent emission present in the system. This formalism, however, is based on the premise that all other rate constants in the system are temperature independent. It is possible that other mechanisms could account for the observed temperature dependence. One possible mechanism arises from the decrease in spectral overlap of donor and acceptor as a result of the narrowing of absorption and emission bands with decreasing temperature. Alternatively, changes in chromophore orientation caused by temperature-dependent changes in protein conformation would also lead to a decrease in energy transfer and a subsequent

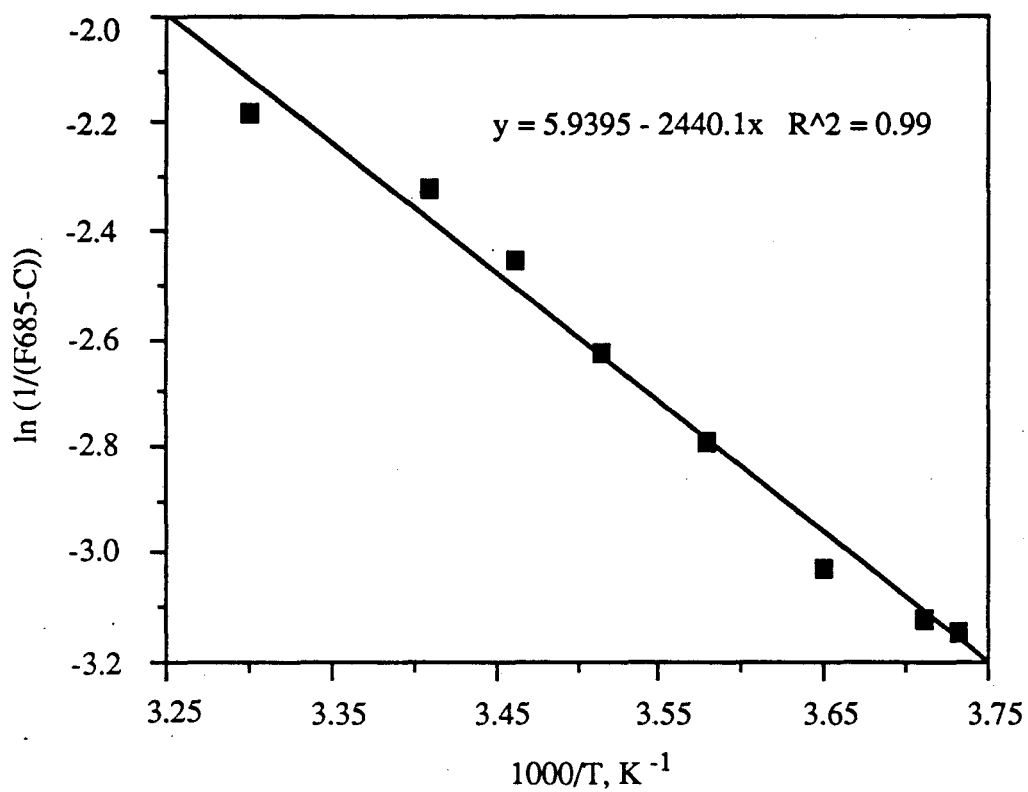Figure 5.8: Arrhenius plot of F685. The natural logarithm of the inverse of the F685 is plotted as a function of 1/T. Formulation of this expression is described in the text. Linear fit to the data is shown with a solid line. An activation energy of 1700 cm^{-1} is obtained.

increase in fluorescence yield.

Time-resolved fluorescence measurements

To probe the changes in excitation transfer as a function of temperature, we have also performed time-resolved fluorescence spectroscopy on the LHC-I complex. These measurements were done at two different excitation wavelengths, 670 nm and 650 nm, the absorption maxima of Chl a and Chl b, respectively. Fluorescence decays were measured over the entire emission spectrum at both 295K and 77K. Additionally, while monitoring emission at 690 nm and 735 nm, the fluorescence kinetics were examined over the temperature range from 298K to 268K. As in the reaction center containing complex, the lifetimes were determined by single wavelength decay analysis to be relatively independent of emission wavelength; therefore, the global analysis method was applied.

At both RT and 77K the fluorescence decays were fit to a sum of five exponentials. By inspection of the residuals and the χ^2 value, we determined that five components were necessary for fitting the data using global analysis. Figure 5.9 depicts representative residuals from global analysis fits using either a four or a five component model. Five component fits consistently gave more evenly distributed residuals and lower χ^2 values at all wavelengths. In figure 5.10 the decay component amplitudes are plotted as a function of wavelength for λ_{ex} = 670 nm. It can be seen that at 680 nm the decay amplitude is dominated by a relatively fast component, 0.03 ns. (see table 5.1) The amplitude of that component drops dramatically when the emission is measured at longer wavelengths. It is possible that this lifetime component may exhibit some rise behavior at longer wavelengths; however, it is not within our signal/noise to deconvolve it at this time. Additionally, we observe a component with a lifetime of 0.21 ns. This component has a very broad amplitude maximum, which peaks at 710-720 nm, contributing at most 50% of the amplitude. We also observe several longer-lived components This fact is not surprising in light of the absence of reaction center in these preparations. A 1.0 ns component is observed which exhibits small features at 680 nm and 730 nm and contributes 10% to the overall amplitude. A 3.3 ns component has a distinct maximum at 680 nm, yet adds less than 5% to the amplitude. We also resolve a 6.5 ns component. This component appears to peak at 680 nm where its relative amplitude is less than 1%. We attribute this longest lived component to non-functioning Chl released during the isolation process. The 3.3 ns component, despite its small amplitude, comprises approximately 40% of the total
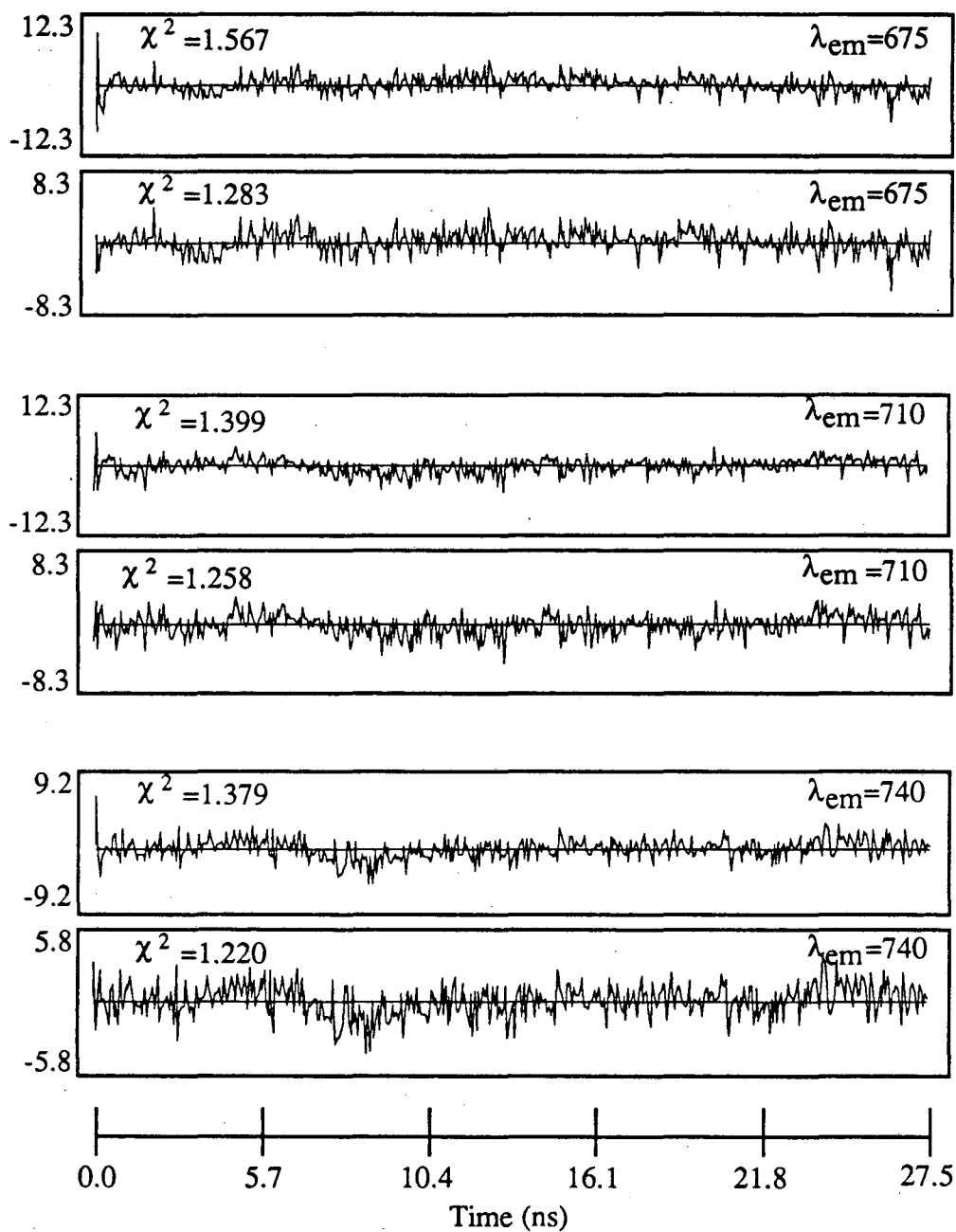
Figure 5.9: Comparison of residuals from 4 and 5 component global analysis. Representative weighted residuals from global analysis of emission decays using either a 4- or a 5-exponential model. Residuals from analyses using a 4-exponential model are displayed above residuals from the 5-exponential model at the same emission wavelength. Excitation was done at either 670 nm or 650 nm.

TABLE 5.1

Lifetimes and amplitude maxima
obtained from global analysis of fluorescence kinetics of LHC-1

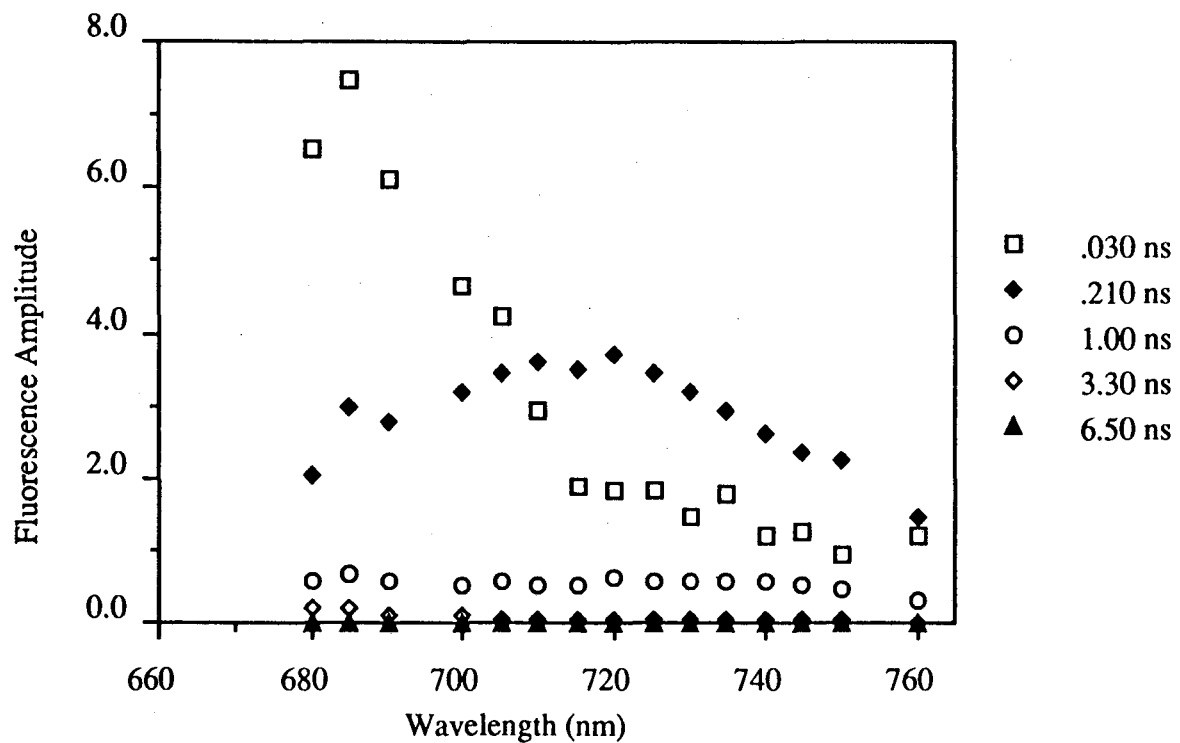| decay components	1	2	3	4	5
T=295K lifetimes (ns)	0.029 ±0.017	0.210 ±0.060	1.00 ±0.21	3.30 ±0.60	6.50 ±1.20
amplitude maximum (nm)	680-685	710-720	685-690 720-725	680	680-690
T=77K lifetimes (ns)	0.040 ±0.010	.200 ±0.060	1.10 ±0.10	3.60 ±0.25	6.70 ±0.50
positive amplitude maximum (nm)	680	685	715-720	730	680-685 735
negative amplitude maximum (nm)	725-735	735	745-750	---	---

Figure 5.10: Decay-associated spectra of LHC-I. Excitation wavelength at 670 nm. Data taken at 295K. Decays were fit to a sum of 5 exponentials using the global analysis method. Amplitudes are plotted as a function of emission wavelength. Samples were diluted with 0.05M Tricine, pH=7.8 to give a [Chl]=0.01 mg/ml.

yield owing to its long lifetime. It is possible that some of the free Chl present in the preparation is reflected in this component rather than in the 6.4 ns component.

Figure 5.11 depicts the decay component amplitudes plotted as a function of wavelength for λ_{ex} = 650 nm at 294K. It can be seen that the lifetimes and the wavelength dependence of the components are comparable to what is observed for λ_{ex} = 670 nm. We detect two major changes as a result of changing the excitation wavelength. The 0.21 ns component has significantly less amplitude and, hence, less yield when λ_{ex} =650 nm. Conversely, the increase in emission between 710-740 nm, as observed in the steady-state emission spectrum, appears to arise from an increase in amplitude of the 1.0 ns component. This component displays distinct maxima at 685 nm and 725 nm, in which the contribution to total amplitude is higher at 725 nm than at 685 nm. Thus, the enhancement of the yield of the 1.0 ns component upon excitation at the Chl b absorption maxima, reflects the coupling between Chl b and the long wavelength emitter. At 680 nm, the amplitude is still dominated by the relatively fast 0.03 ns component, although the amplitude of the 3.3 ns decay component has increased. Nevertheless, it is apparent that the enhanced emission observed at 710-720 nm as a result of excitation at Chl b arises mainly from the 1.0 ns decay component.

In figures 5.12 and 5.13 the decay associated spectra for λ_{ex} = 665 nm and λ_{ex} = 650 nm, respectively, taken at 77K are plotted as a function of wavelength. The choice of 665 nm as the excitation wavelength helps to eliminate contributions from scattering in the emission detected at 680 nm. It is observed that the lifetimes of the decay components have not changed significantly at the lower temperature; the decay component amplitudes, however, display a dramatic difference in wavelength dependence. These amplitude changes reflect the significant increase in F735 observed in the steady state fluorescence spectra when the temperature is lowered to 77K. The fastest decay component is slightly longer, reflecting reduced transfer rate constants at 77K, possibly due to decreased donor-acceptor spectral overlap. The 0.04 ns component peaks at 680 nm, contributing approximately 40% of the amplitude, similar to what was observed at RT. This component crosses over to a negative amplitude (rise component) at 695-700 nm and then exhibits a broad negative amplitude between 725-735 nm. (see table 5.1) A negative amplitude or rise, as opposed to decay, is indicative of fluorescence induction. Generally, a rise component is thought to be direct evidence for energy transfer within these complex antenna systems. The 0.20 ns component exhibits a maximum at 685 nm, in contrast to its wavelength behavior at 295 K, where the maximum was detected at 715-720 nm. At 685 nm this component
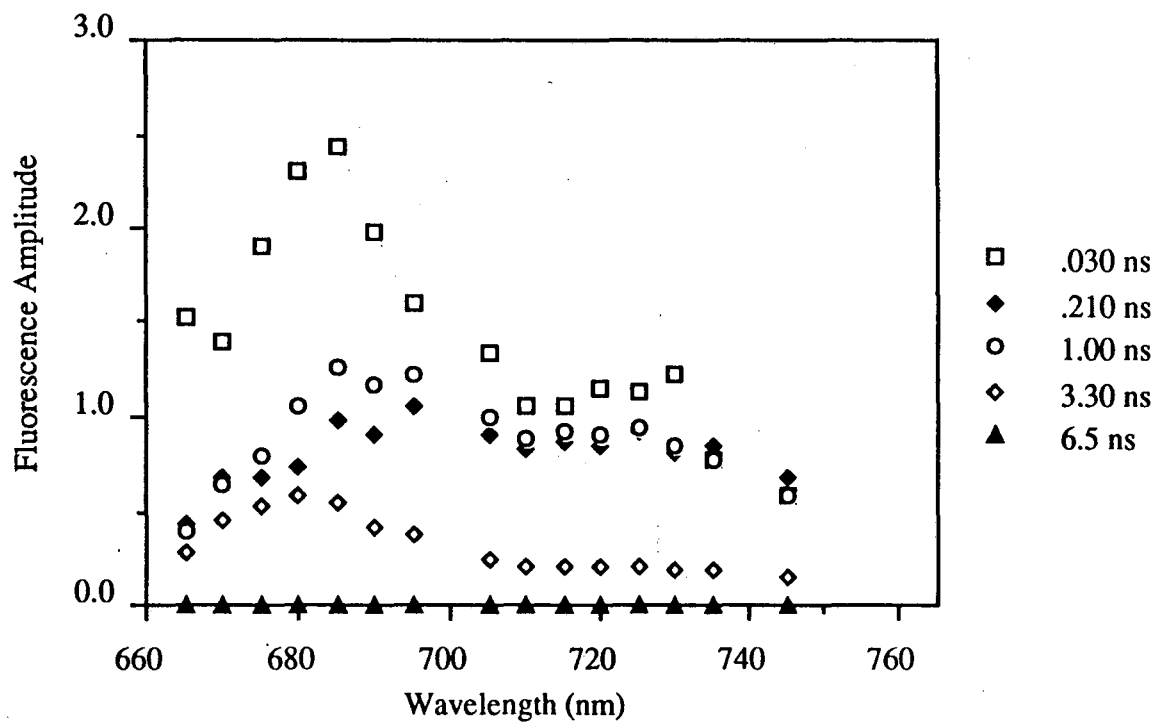
Figure 5.11: Decay associated spectrum of LHC-1. Excitation done at 650 nm. Decays were fit to a sum of five exponentials using the global analysis method. Data were taken at 295K. Amplitudes are plotted as a function of emission wavelength. Sample preparation as in figure 5.10.

Figure 5.12: Decay-associated spectrum of LHC-I. Excitation was done at 665 nm. Data were taken at 77K. Data analysis as in figures 5.10 and 5.11. Samples were diluted to <0.1 absorbance at 675 nm and were frozen to a cracked glass in 60% glycerol, 40% 0.05 M Tricine, pH=7.8.
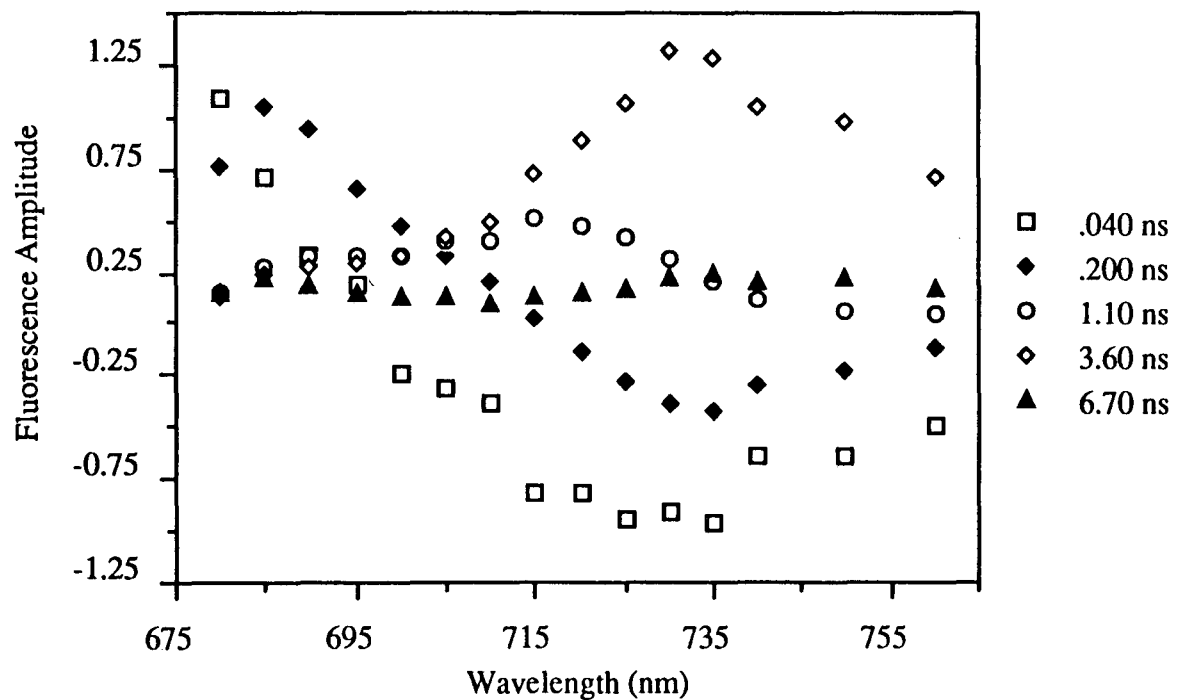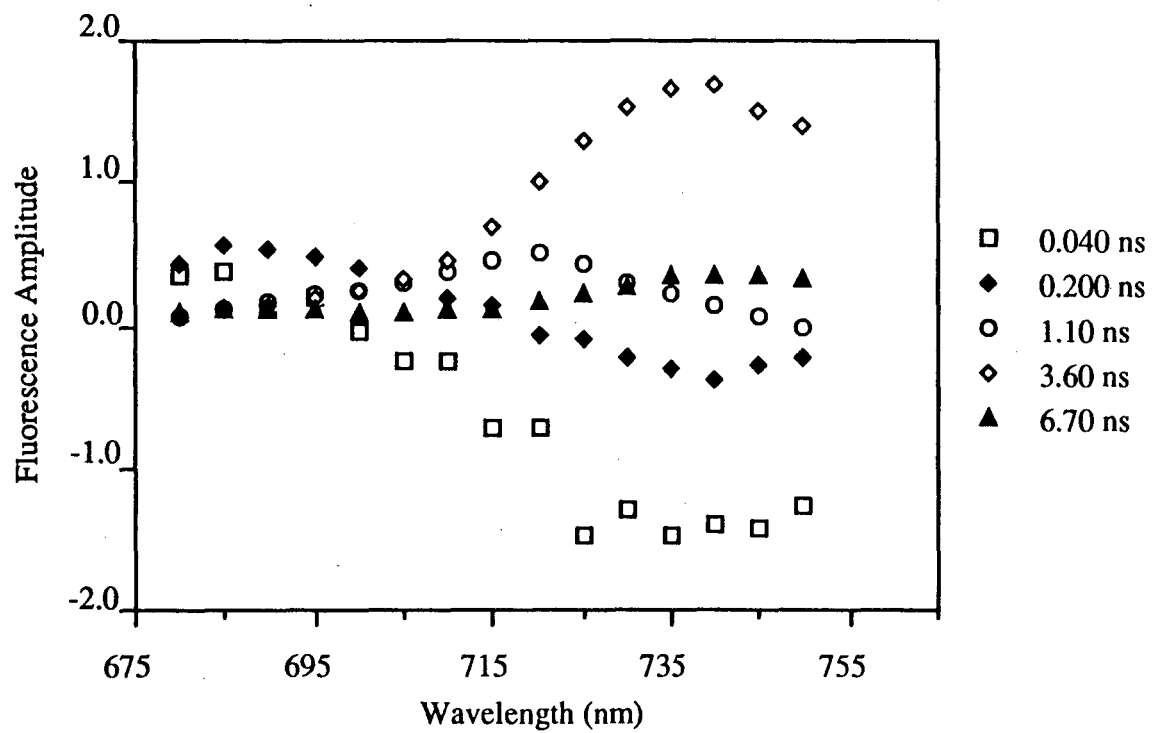
Figure 5.13: Decay-associated Spectrum of LHC-I. Excitation was done at 650nm. Data were taken at 77K. Data analysis as described in figures 5.10 and 5.11. Sample preparation as in figure 5.12.

accounts for approximately 40% of the total amplitude. It also converts to a rise component, crossing over to a negative amplitude between 715-720 nm and then exhibits a negative maximum at 735 nm. Because of the negative amplitude in the red-edge of the emission it is difficult to assess the wavelength dependence of the amplitude at 77K. Both relatively fast components in this system display rise behavior at 77K. The wavelength dependence of the two rise components are distinctly different from each other, with different cross-over points and negative maxima, indicating that we are successfully deconvolving two rise components in this system. The amplitude of the 1.0 ns component at 77K exhibits a distinct maximum at 720 nm. Slight rise behavior at longer wavelengths is also detected for this component. After peaking at 720 nm the amplitude crosses over to negative values between 730-735 nm and reaches a negative maximum between 745-750 nm. The presence of three rise components in the decay kinetics is suggestive of a very efficient trap for excitation energy at longer wavelengths. We observe that the 3.6 ns component completely dominates both the yield and the amplitude at longer wavelengths, reaching a maximum at 730 nm. The wavelength dependence of the amplitude at 77K of the 3.6 ns component reflects the efficient quenching of energy transfer within the antenna system. It is interesting to note that the 6.5 ns component displays an amplitude maximum at 685 nm and at 735 nm. This wavelength dependence is suggestive of this component containing contributions from both functional and non-functional Chl of the antenna system. From the wavelength dependence of the 6.5 ns component it appears that even at 77K the two longer lived components are not completely resolved.

The wavelength dependence of the amplitudes at 77K for λ_{ex} = 650 nm is similar to that observed for λ_{ex} = 665 nm. The enhanced emission ratio $\Phi730/\Phi685$ is the primary difference observed. In the time-resolved data it appears that this enhanced ratio is the result of several factors. In particular, the amplitude of the 0.04 ns component is decreased at 685 nm. We attribute the decrease in amplitude of the 0.04 ns component at 685 nm to the decreased absorption cross-section of the system at 650 nm. The amplitudes at short and long wavelengths are not correlated; the negative amplitude of this component in the longer wavelength regions increases. This point will be addressed in the discussion. Additionally, the amplitude of the 3.6 ns component at 730 nm is increased. Thus, our kinetic data support what was previously detected in the steady state fluorescence excitation spectra, namely that Chl b sensitizes emission at longer wavelengths. For both RT and 77K data the summation of the yields of each decay component results in a calculated spectrum that

should be identical to the steady state emission spectrum. (figure 5.14)

We observe that the lifetimes reported (table 5.1) have a large percent error associated with them. This percentage of error is higher than what is normally observed in a single photon counting experiment. Typically, lifetimes measured in this manner have an error of 10% associated with them. The lifetimes are averaged from several measurements on different preparations. As indicated earlier the LHC-I complex contains some non-functional Chl; the amount varies from preparation to preparation. This amount of free Chl has a significant effect on the recovered lifetimes, especially with respect to the longest lived components. We have discerned that for multiple measurements made on a given preparation, the variation in lifetime is approximately one-half to one-third less than the error reported for all the data sets. Thus, it is clear that a significant portion of the uncertainty in lifetime results from some non-reproducibility in the preparations, which we associate with the changing concentration of free Chl. This argument is supported by the fact that at 77K, where the contribution of dissociated Chl to the overall yield is less, the percent error in lifetime is also correspondingly less. Additionally, the fastest lifetime (0.03-0.04 ns) has a high degree of error associated with it. Partly, this is because the component is approaching the time resolution of the instrument. This error is then compounded because only 10,000 counts in the peak channel were collected. Unfortunately, data collection times became prohibitively long for collecting more counts in the peak channel; therefore, the maximum number of counts was limited to maintain integrity of the pigment-protein complex.

For the time-resolved emission spectra the main observations are: 1) Five decay components are required to satisfy the data at RT and 77K. We attribute the longest lived component to non-functional Chl. 2) Chl b excitation enhances the amplitude of the 1.0 and 3.3 ns decay components. Additionally, at 77K Chl b excitation increases the negative amplitude of the 0.04 ns component. 3) At 77K excitation is efficiently transferred to the 3.6 ns component as evidenced by the 3 risetimes observed in the far-red region of the emission spectrum.

Temperature dependent time-resolved fluorescence measurements

The kinetics of the fluorescence decay were monitored as a function of temperature over a small temperature range. Measurements were taken at approximately 5° intervals between 298K and 268K. Decays were measured at 690 nm and 735 nm, with excitation either at 650 nm or 670 nm. Emission was collected
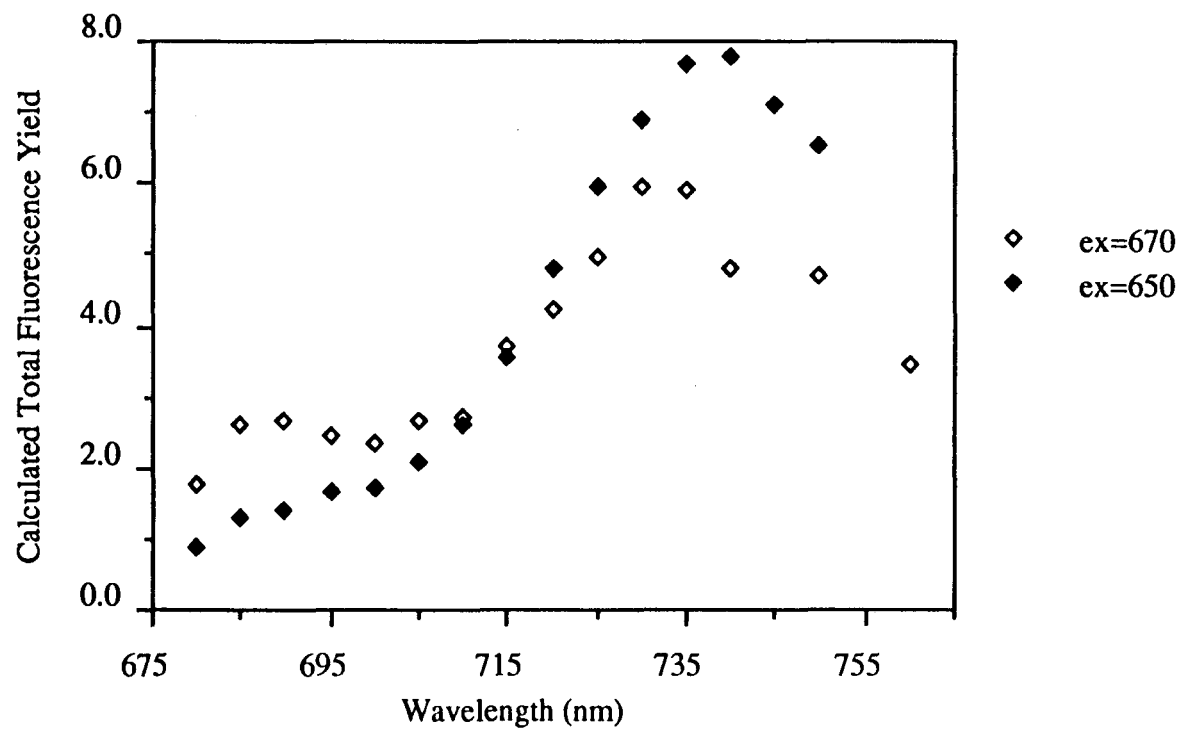
Figure 5.14: Calculated Total Fluorescence Yield of LHC-I. Data were taken at 77K. Excitation was done at either 650 nm or 665 nm. The yield of each component was calculated and then yields were summed together for total yield.

at 690 nm to insure that scattering from the excitation would not interfere with the fluorescence and also to minimize the contribution of non-functional Chl. Data were analyzed first using single temperature analysis. It was determined that the lifetimes of the decay components did not change appreciably as a function of temperature, therefore, the global analysis method was applied. Global analysis was used for sets of data collected at different temperatures, but at the same excitation and emission wavelengths. In these measurements it was difficult to resolve the two distinct long-lived components, 3.3 ns and 6.5 ns, detected in the time-resolved emission spectra. This lack of resolution possibly results from the relatively small amplitude of these components and the smaller number of data sets used for the analysis. Typically, analysis was done on 5-6 decays as compared with the 15 decays used for analysis of the entire emission band. Consequently, the lifetimes reported for these experiments are slightly longer than those reported for room temperature time-resolved emission spectra.

The complex energy transfer processes occurring within LHC-I (see discussion) and the amount of error associated with the data preclude a true quantitative treatment of the temperature dependence of each emitting species. Thus, we limit our discussion of results to the changes in amplitude and yield observed for each decay component. The lifetimes of each of the decay components remain relatively constant over the temperature range measured. It is possible that within the error of our measurement small changes in lifetime were not detected. Ten percent changes in lifetime would not be resolved by single photon counting. Time-resolved data taken at 77 K are also suggestive of decay constants, which ar independent of temperature. It would be necessary, however, to monitor the fluorescence kinetics over the entire temperature range from 298 K to 77 K, to specifically address this behavior. Larger changes in decay component amplitude rather than in lifetime as a function of lower temperature are consistent with data obtained on PSI-200 at high and low temperature. (chapter 4)

The amplitudes and hence, the yield of each of the decay components are temperature dependent. Comparable changes in amplitude are observed for excitation at either 670 nm or 650 nm. (table 5.2) Some differences could exist between the two excitation wavelengths, which are not resolved in our experiment. General trends of the decay components indicate that the amplitudes of the 0.04 ns and 0.24 ns components decrease approximately 10-35% from 298K to 273K for λ_{em} = 690 nm. (figure 5.15) Conversely, the longer lived components (0.95 ns and 3.9 ns) show

TABLE 5.2

Changes in decay component amplitude
of LHC-I as a function of temperature

lifetime (ns)	$\alpha_{298} / \alpha_{273}$[a]	percent change[b]
λ_{em}=690 nm		
0.040 ± 0.012	1.3 ± 0.2	$-25 \pm 15\ \%$
0.24 ± 0.03	1.3 ± 0.2	$-25 \pm 15\ \%$
0.95 ± 0.21	0.7 ± 0.1	$+30 \pm 10\ \%$
3.9 ± 0.8	0.8 ± 0.1	$+20 \pm 10\ \%$
λ_{em}=735 nm		
0.040 ± 0.012	1.4 ± 0.1	$-30 \pm 5\ \%$
0.34 ± 0.03	0.8 ± 0.1	$+20 \pm 10\ \%$
1.1 ± 0.1	0.5 ± 0.2	$+50 \pm 20\ \%$
5.2 ± 1.2	0.7 ± 0.1	$+30 \pm 10\ \%$

[a] $\alpha_{298} / \alpha_{273}$ = decay component amplitude measured at 298K relative to amplitude measured at 273K.

[b] Relative percent change in amplitude from 298K to 273K. Negative sign indicates a decrease in amplitude at 273K relative to 298K.
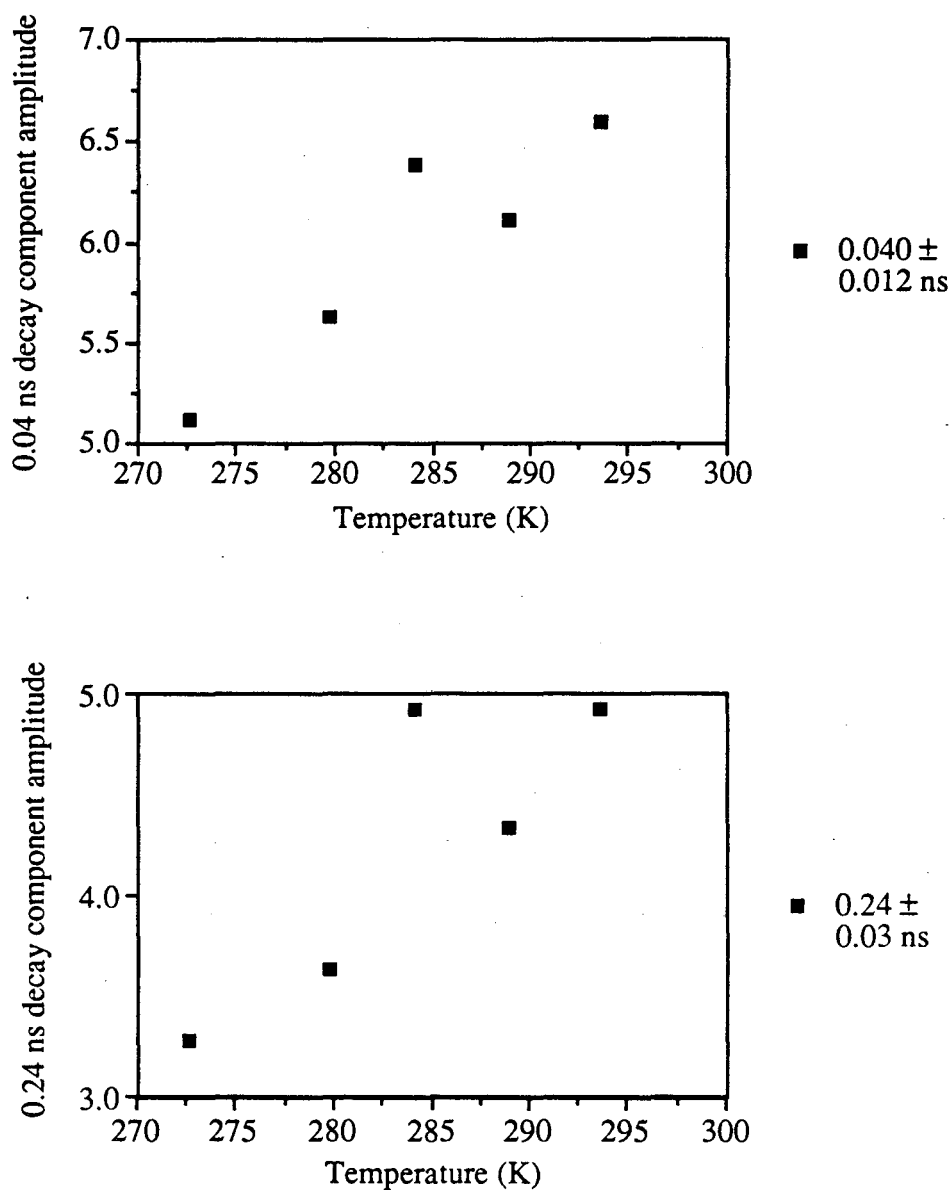
Figure 5.15: Amplitudes of 0.04ns and 0.24 ns decay components as a function of temperature. Data were analyzed globally using a 4-exponential model. Excitation at 670 nm and emission at 690 nm. Samples were diluted to [Chl]=0.01 mg/ml in 60% glycerol and 40% 0.05 M Tricine, pH=7.8.

increases in amplitude as the temperature is decreased. (figure 5.16) For the 0.95 ns component an increase in amplitude between 20 and 40% is observed. The 3.9 ns component shows a 10-30% increase in amplitude from RT to 273K.

Temperature dependent changes were also monitored at 735 nm. We observe that the relative changes in amplitude are larger for λ_{em} = 735 nm than for λ_{em} = 690 nm. We suggest that these larger differences arise because the postulated non-radiative fluorescence quenching mechanism in the antenna is more directly associated with longer wavelength emitting species. The temperature dependence of the steady state fluorescence in which F730 increases at a greater rate than F690 supports this premise. Similar to behavior observed at 690 nm the amplitude of the 0.04 ns component decreases approximately 25% as the temperature is lowered. At lower temperatures the amplitude of the 0.34 ns component increases approximately 15% compared to its room temperature value. (figure 5.17) The amplitude behavior for this component is not the same for the two different emission wavelengths. This contradictory temperature-dependent amplitude behavior and the longer lifetime observed at 735 nm are suggestive of two different emitting species with similar time constants. The amplitude of the 1.1 ns component increases approximately 50% as the temperature is lowered to 273K. 20-40% changes are observed for the amplitude of the 5.2 ns component between RT and 273K. (figure 5.18) These relative changes in amplitudes will be discussed in the context of a model for transfer energetics within LHC-I. (see discussion)

In summary, temperature dependent effects are: 1) At all excitation and emission wavelengths monitored we observe no large changes in lifetime. This effect implies that the total decay rate constants of the emitting species are remaining relatively constant over the temperature range observed. 2) For λ_{em} = 690 nm the shorter lived components (0.04 ns and 0.24 ns) decrease in amplitude, while the longer lived components (1.0 ns and 3.9 ns) increase in amplitude as a function of lower temperature. 3) For λ_{em} = 735 nm only the 0.04 ns component exhibits decreased amplitudes at lower temperature all other decay components show an increase in amplitude. 4) At both emission wavelengths the largest change in amplitude as a function of decreasing temperature is observed for the 1.0 ns component. Temperature dependent changes in decay component amplitude are larger for emission at 735 nm relative to emission at 690 nm.

Figure 5.16: Amplitudes of 0.95 ns and 3.9 ns decay components as a function of temperature. Data were analyzed globally using a 4-exponential model. Excitation at 670 nm and emission at 690 nm. Samples preparation as in figure 5.15.

Figure 5.17: Amplitudes of 0.04ns and 0.34 ns decay components as a
function of temperature. Data were analyzed globally using a
4-exponential model. Excitation at 650 nm and emission at 735 nm.
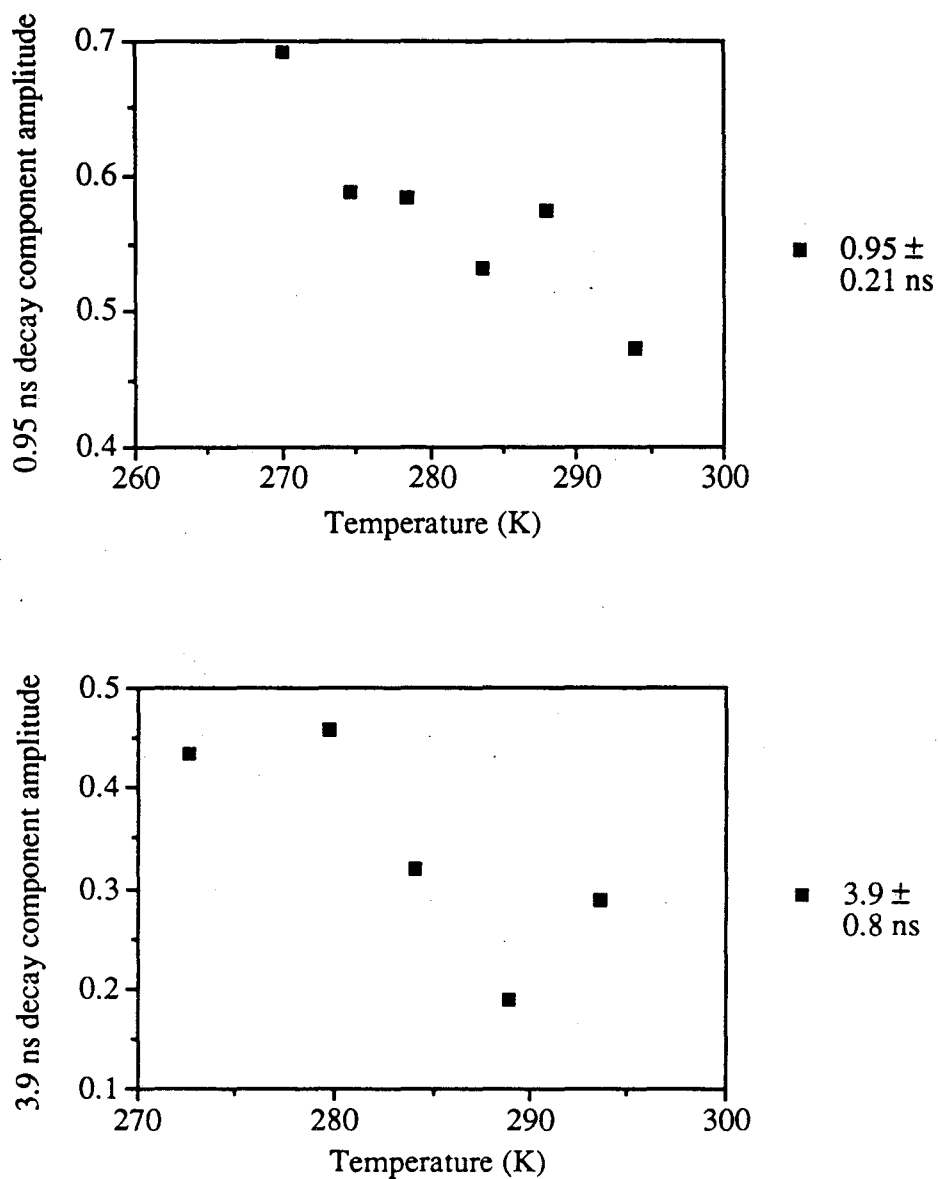Samples were diluted to [Chl]=0.01 mg/ml in 60% glycerol and 40%
0.05 M Tricine, pH=7.8.

Figure 5.18: Amplitudes of 1.1 ns and 5.2 ns decay components as a function of temperature. Data were analyzed globally using a 4-exponential model. Excitation at 650 nm and emission at 735 nm. Samples preparation as in figure 5.17.
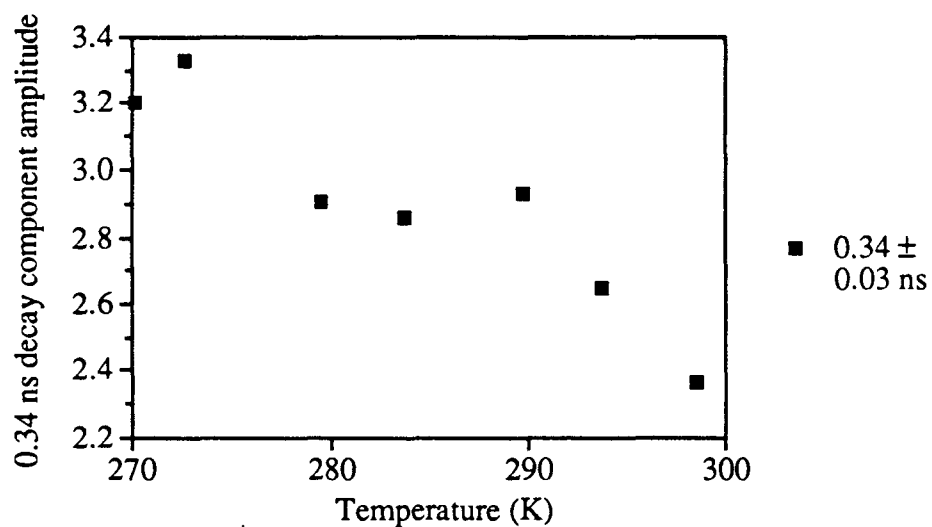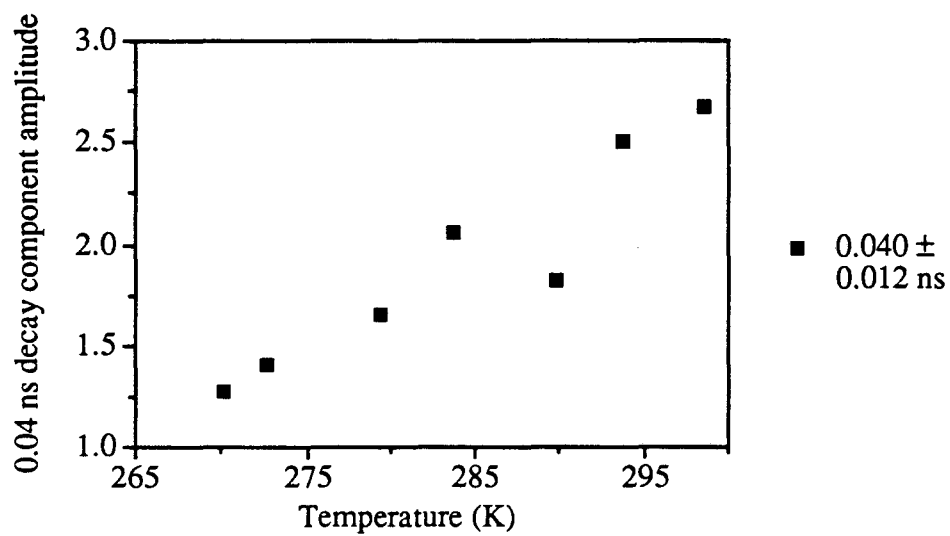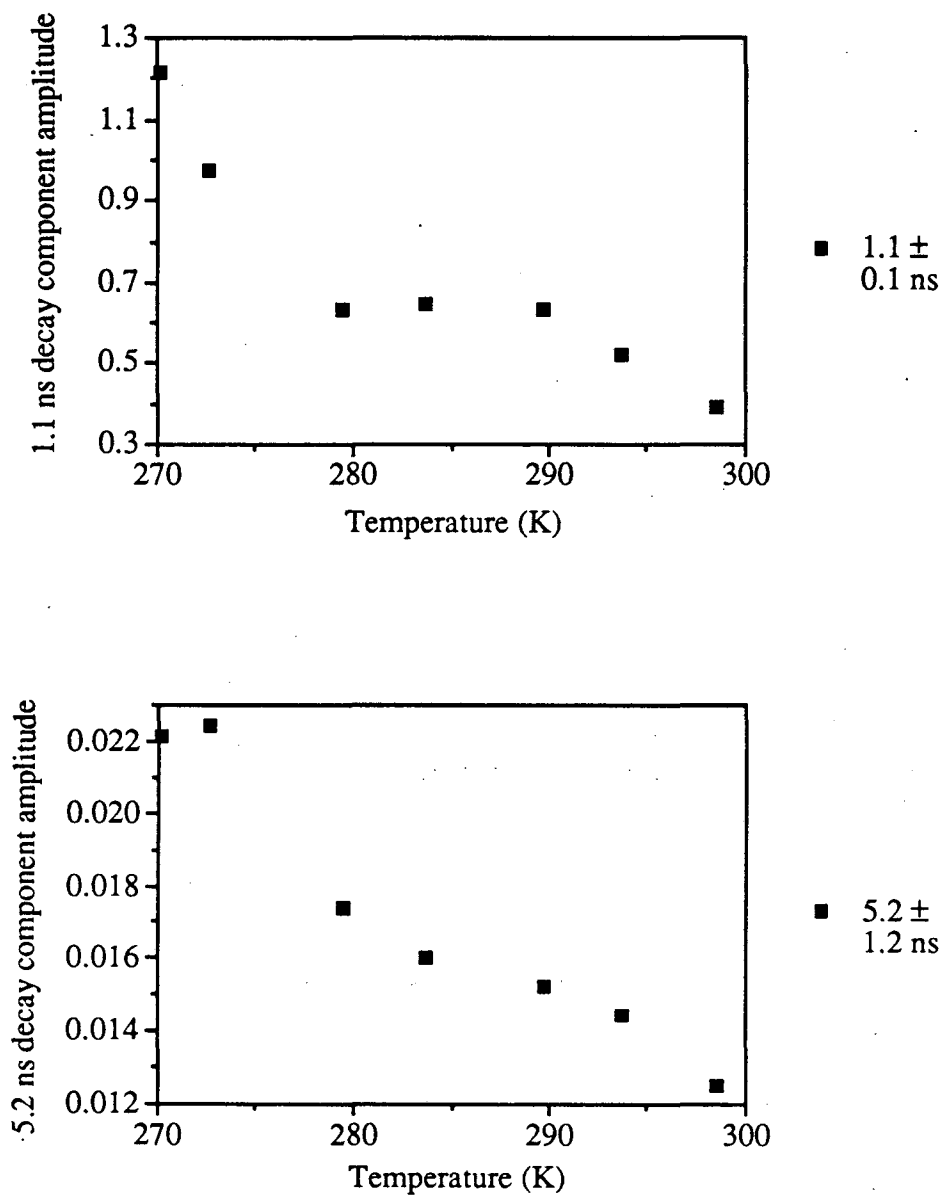
3. *Discussion*

Steady state fluorescence measurements

Excitation spectra of LHC-I demonstrate that Chl b is intimately connected with the origin of long wavelength emission. This effect was previously observed in the holocomplex, PSI-200 (chapter 3). Additionally, these spectra indicate the presence of a component or components, which stimulate F735 and lie at lower energy than the absorption maximum of the reaction center. The interaction between this component and Chl b is unclear; conservative CD features indicative of excitonic coupling are not observed in the 705-735 nm region of the spectrum. [5] Excitation polarization spectra show high values in the 705-725 nm range when monitoring F735 emission. These polarization values imply that F735 arises from a species that absorbs at long wavelengths. Therefore, the steady state excitation and excitation polarization spectra both associate long wavelength absorbing pigments with the peripheral light harvesting antenna of PSI and identify them as the origin of fluorescence at longest wavelengths. The wavelength dependence of the polarization was similar for PSI-200 and LHC-I, although, the maximum polarization value for PSI-200 was much lower. It appears that in LHC-I either the absorption and emission chromophores have a higher degree of relative alignment in comparison to the holocomplex or that there are less energy transfer processes occurring prior to emission. Our results agree with linear dichroism and polarized fluorescence emission measurements performed on similar particles. [24] In those experiments on LHC-I isolated from pea and oriented in a polyacrylamide gel, maximum dichroic ratio was observed in the 705-725 nm region. Chromophores are oriented in the matrix by uniaxial squeezing. The axis of squeezing is thought to be perpendicular to the membrane plane. The orientation of the chromophores will be discussed with respect to the membrane plane. From linear dichroism measurements it was observed that the Q_y transition of Chl b in the antenna complex is oriented at less than 35° to the membrane plane. Additionally, it has been determined that F735 has an angle of less than 23.5° with respect to the membrane plane. [25] These results are consistent with the premise that F735 originates from pigments, which absorb in the 705-725 nm region of the spectrum. It is also of interest that Chl b and C705 have approximately the same orientation within the complex, possibly facilitating energy transfer between the two components.

We have also tested the validity of the Stepanov relation, which predicts a linear correlation between absorption and emission, for LHC-I. The complex does follow the relation in the region of maximum overlap, however, the calculated

temperature is significantly elevated from ambient. In previous studies with LHC-II, the Kennard-Stepanov temperature, T_{ks}, was found to be equal to ambient temperature. It was proposed that LHC-II behaves as a single large molecule and equilibration was occurring among the vibrational states of the electronic excited state. Thus, in the case of LHC-II the system reaches an excited state thermal equilibrium prior to fluorescing and behaves more like a homogenous emitting species. [20] The T_{ks} obtained for isolated LHC-I resembles that of PSI-200 more closely than LHC-II. LHC-I like PSI-200 has a heterogeneous antenna pool, caused by the presence of the long wave emitters. As discussed in chapter 3 elevated Kennard-Stepanov temperatures can be attributed to inhomogeneous broadening of the emission band. Thus, we attribute the elevated T_{ks} observed to the heterogeneous emission of LHC-I. Similar T_{ks} are obtained for both LHC-I and PSI-200. An elevated T_{ks} has been observed in phycobilisomes; the increased temperature was attributed to a failure in reaching configurational equilibrium with the surrounding matrix prior to fluorescing. [21] In addition to the heterogeneity of the emission it is possible that configurational equilibrium is not being attained in LHC-I.

The steady state temperature-dependent fluorescence spectra show an increase in intensity as the temperature is decreased implicating a high temperature quenching mechanism for the excited state. The quenching efficiency of this process decreases with decreasing temperature. This process must operate independently of the reaction center and its chemical state, because reaction centers are not present in this preparation. We propose that the increase of F730 relative to F685 as the quenching efficiency lessens results in part from more of the excitation reaching the long wavelength energy "sink." Temperature dependence of both F685 and F730 show Arrhenius behavior. F730 has an activation energy of 1700 cm^{-1}. F685 is believed to consist of temperature independent and temperature dependent portions. We suggest that approximately 20% of F685 is temperature independent. If F685 is corrected for this amount of temperature independent fluorescence it has the same activation energy as F730, 1700 cm^{-1}. From our quantum yield measurements, the fluorescence yield is approximately 10 fold higher in the antenna complex relative to PSI-200. In a comparison of the room temperature steady state emission it is apparent that the entire emission band, F685 and F730, of LHC-I is quenched when the RC is present. We suggest that this excitation energy is quenched by the RC in the holocomplex.

Time-resolved emission spectra

The kinetic data that we have obtained on LHC-I shows good agreement with the data on the PSI-200 complex at 77K. The lifetimes reported in chapter 4 correspond well with those observed at both RT and 77K in the isolated antenna system. The wavelength dependent amplitude behavior of these components is different in the holocomplex when compared with the antenna complex. More rise behavior is observed in the antenna complex; it is possible that in the absence of the reaction center these components are more easily detected or that the quenching efficiency of far red pigments is enhanced. An alternate possibility is that fluorescence quenching by the reaction center is much faster and therefore not observed in our measurements. The correlation of lifetimes implies that at 77K in PSI-200 the energy transfer dynamics are completely dominated by the light harvesting complex. It is of interest that in both cases the increase in fluorescence yield at 735 nm mainly arises from increases in decay amplitude rather than longer lifetime. At RT the 80-100 ps component observed in PSI-200 is not present in the kinetics of LHC-I. This absence confirms our previous assignment of this component to lower energy emitting pigments (F720). Biochemical fractionation results indicate that the majority of this pigment pool is located on the reaction center-containing polypeptides. [14] Recently, in a PSI-100 preparation, rise behavior in the shorter wavelength region has been observed for this decay component. [26] Previously, we had observed that the amplitude of this component increases with Chl b excitation, suggesting that it was associated with LHC-I. We speculate that transfer from LHC-I to the F720 emitting species was not detected in the earlier experiment.

We propose that the 0.03 ns (0.04 ns at 77K) decay component corresponds to the majority of the Chl in the antenna. The very fast decay reflects the rapid redistribution of energy to other spectral forms within the antenna complex. This decay component is similar to fast decay components observed in PSI particles isolated from spinach and cyanobacteria. [27,28] Steady state fluorescence emission spectra support the postulate that energy absorbed at 672 nm is rapidly distributed to longer wavelength pigments. In the PSI-200 steady state emission spectrum, the shoulder from 710-740 nm has almost the same intensity as the main peak at 690 nm. In the LHC-I complex this shoulder is approximately two-thirds the height of the main peak. Possibly, dissociated Chl fluorescence contributes to the intensity at 685 nm. Nevertheless, a substantial amount of the excitation is reaching the low energy emitters at RT. It is disturbing that a rise time is not detected at longer wavelengths. In part

this results from the lower signal to noise ratio caused by collecting only 10,000 counts in the peak channel. Also this component nears the edge of our time resolution and the measurement could be instrumentally limited. Experiments by Holzwarth et al. in which a very fast risetime was observed were conducted at 5°C. [27,28] At that temperature the amplitude of the rise component is larger and therefore more easily detected in the single photon counting method.

All components faster than 3 ns have negative amplitudes in the long wavelength region at 77K. The wavelength dependence of these components is suggestive of all energy being transferred to C705 or other far red pigments, which are acting as very efficient sinks for excitation. Each of the rise components exhibits progressively red-shifted negative maxima, indicating a downhill flow of energy to the sink. The 1.1 ns component peaks at 720 nm prior to its conversion to a rise. From this behavior we postulate the presence of an intermediate pigment pool between F685 and F735, similar to the one(s) present in the reaction center antenna. The emission at 735 nm is dominated by the 3.6 ns component, correlating this decay with the longest wavelength emitter.

Time-resolved temperature-dependent fluorescence

In the time-resolved temperature dependent data, all the decay components exhibited temperature dependent behavior. Resolution of the 3.3 ns and the 6.0 ns decay components was not possible. Changes in temperature resulted in changes of decay component amplitude only. At 690 nm the two faster components (0.04 ns and 0.24 ns) demonstrated a decrease in amplitude, while the longer lived components (1.0 ns and 3.9 ns) displayed a distinct increase in amplitude at lower temperatures. At 735 nm only the amplitude of the 0.04 ns component decreased with decreasing temperature. The lifetimes were essentially invariant over the temperature range examined. This behavior implies that the rate constant of a non-radiative process is temperature dependent, resulting in the changing amplitudes observed. We suggest, as in PSI-200, that non-radiative fluorescence quenching is a primary mechanism of de-activation of the excited state near RT. The decrease in quenching at lower temperatures is reflected in the increased amplitudes of the longer-lived emitting species suggestive of an association between the quenching mechanism and low energy emitters.

Transfer energetics within LHC-I

Based upon time-resolved emission data taken at 77 K and 298 K, we propose a tentative scheme for excitation transfer within LHC-I. Although, we have resolved five kinetic components within this system, it is evident from analysis of the data that other components may exist, which we are not resolving within our current experimental limitations. We have neglected the 6.5 ns component in our transfer scheme, since we believe this component reflects primarily emission from dissociated or non-functional Chl molecules.

<u>77K.</u> The relatively distinct spectral characteristics of each kinetic component at this temperature are suggestive of at least four emitting species. (figures 5.12 and 5.13) Stepanov temperatures and excitation polarization spectra support the existence of heterogeneous antenna pools in LHC-I. The four antenna pools, A, B, C and D, each have a distinct emission wavelength dependence. In addition three rise terms (0.04, 0.20 and 1.0) are detected in the data. These rise times are indicative of energy transfer processes occurring within the system. To determine the correlation between the different proposed emitting species, we have ratioed the positive and negative amplitudes of the decay components. In a simple scheme where A transfers energy to B, this ratio equals one. In this system we interpret a constant relation between the decay amplitudes to signify energy transfer between the respective components. In the long wavelength region constant ratios are observed for the 0.04 ns, the 0.20 ns and the 1.0 ns components with respect to the 3.6 ns component. (figure 5.19) This method of analysis is suggestive of energy transfer between the 685 nm emitting species, A to the 720 nm emitting species, C. D has a fluorescence maximum at 735 nm and receives energy from both C and B (695 nm). We also suggest that energy flows from A to B, although, the data do not provide direct evidence for this transfer step.

The amplitude of the 0.04 ns decay component as a function of wavelength is not the same for the two excitation wavelengths, 650 and 670 nm. For excitation at 650 nm the positive amplitude is decreased relative to excitation at 670 nm. This decrease is commensurate with the decrease in absorption cross-section at 650 nm. At longer wavelengths where a negative amplitude is observed, excitation at 650 nm results in a relative increase in amplitude. (figure 5.11 and 5.13) Typically, increases in positive and negative amplitudes are consistent for one emitting species. We suggest that the different amplitude behavior of the 0.04 ns decay component reflects the presence of two distinct emitting species with comparable lifetimes. The larger
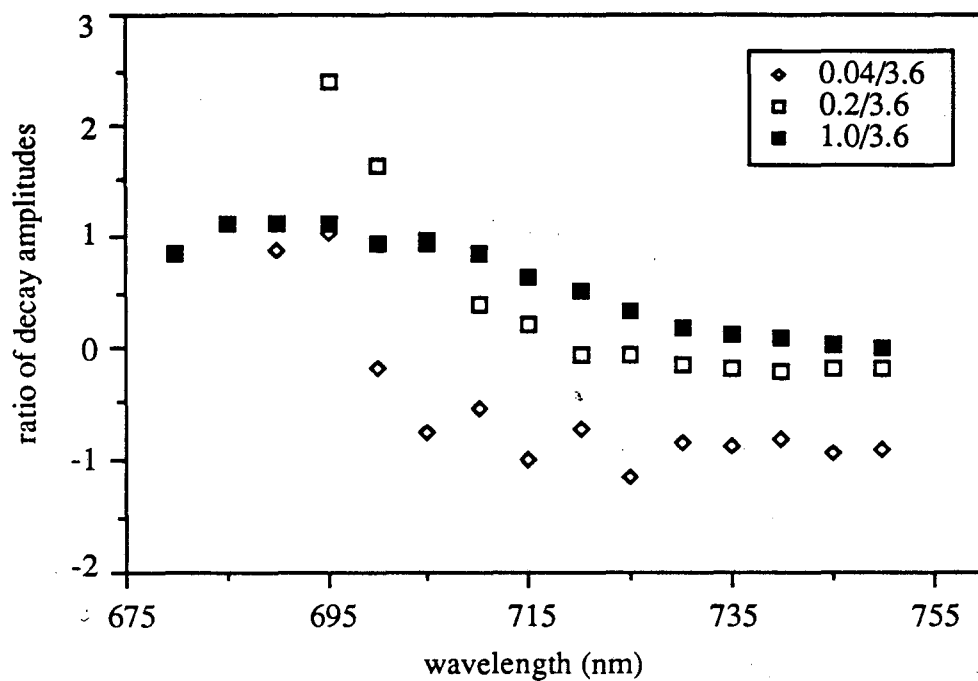
Figure 5.19: Ratio of decay component amplitudes. Original data depicted in figure 5.13. Data were taken at 77K; excitation was done at 650 nm. The relatively constant relation obtained in the far-red region between the decay component amplitudes is suggestive of energy transfer between the components. For the 0.04 ns component constancy is observed from 700-750 nm, for the 0.20 ns component from 720 to 750 nm and for the 1.0 ns component from 735 to 750 nm, in all cases implying energy transfer to the 3.6 ns component.

species A, has an emission maximum at 680 nm and contains only Chl a. We speculate that the other species E, consists of both Chl a and Chl b and fluoresces maximally at higher energy. Both A and E transfer excitation to C. The increase in negative amplitude, caused by direct excitation of the E pool, is reflected in an increase in positive amplitude of the 3.6 ns component. We interpret the correlated behavior of the rise and decay amplitudes to indicate energy transfer from E to D. This transfer pathway agrees well with steady state fluorescence results, which are indicative that Chl b is specifically associated with the longest wavelength emitter. For excitation at 650 nm an increase in positive amplitude at wavelengths less than 680 nm is expected from E . Current data begin at 680 nm therefore, the proposed wavelength dependent behavior of E cannot be addressed. Selective excitation of Chl a at 625 nm compared with results obtained with 650 nm excitation should resolve this question.

298K. For the modelling of excitation transfer within LHC-I at RT we employ essentially the same framework as at 77K, but back transfer reactions are larger relative to the corresponding forward transfer reactions. An increase in back transfer from the 735 nm emitting species, D to the 680 nm emitting species, A is reflected in the increased amplitude of the 3.3 ns component at 680 nm. Similarly, the increased amplitude of the 1.0 ns component at 680 nm is evidence for back transfer from C to A. At present we cannot rule out the possibility that the amplitude of the 3.3 ns component at RT also reflects emission from dissociated Chl, which emits at 680 nm. Nevertheless, we suggest that the increased amplitude of the 1.0 ns and the 3.3 ns decay components at 690 nm represents back transfer from the longer wavelength emitting species, C and D, to the shorter wavelength emitters, A and E.

To explain our steady state fluorescence data obtained on PSI-200 and LHC-I we have invoked the presence of a temperature-dependent fluorescence quencher. Our data are indicative of efficient quenching at RT, which decreases at lower temperatures. Additionally, analysis of temperature-dependent steady state emission of LHC-I suggests the presence of only one temperature-dependent fluorescence quencher. We speculate that this quencher is specifically associated with D, the 735 nm emitting species.

Modelling of decay kinetics of LHC-I

We have attempted to model the kinetics of LHC-I, using the proposed transfer steps and a non-radiative temperature-dependent fluorescence quencher. For modelling, we have assumed the presence of five emitting species, A, B, C, D and E.

(figure 5.20) We can express the time-dependent population and depopulation of each emitting state using the following rate equations:

$$\frac{d[A]}{dt} = -(k_{AB}+k_{AC}+k_{fa})[A]+k_{BA}[B]+k_{CA}[C]$$

$$\frac{d[B]}{dt} = -(k_{BA}+k_{BD}+k_{fb})[B]+k_{AB}[A]+k_{DB}[D]$$

$$\frac{d[C]}{dt} = -(k_{CA}+k_{CD}+k_{CE}+k_{fc})[C]+k_{AC}[C]+k_{DC}[D]+k_{EC}[E]$$

$$\frac{d[D]}{dt} = -(k_{DB}+k_{DC}+k_{DE}+k_{Q}+k_{fd})[D]+k_{BD}[B]+k_{CD}[C]+k_{ED}[E]$$

$$\frac{d[E]}{dt} = -(k_{EC}+k_{ED}+k_{fe})[E]+k_{CE}[C]+k_{DE}[D]$$

In these equations the subscripts of the rate constant indicate the direction of energy transfer, for example k_{AB} designates the rate constant of energy transfer from A to B. Fluorescence decay rate constants are represented as k_f.

The following constraints have been imposed upon the model:

1) The different emitting species are distinct and are not in rapid equilibrium. Consequently, the total decay rate constant of a species is larger than the rate constant of transfer from that state to another state. Additionally, the sum of all depopulating rate constants for a given species is equal to the experimentally observed lifetime for that state. For example $(k_{AB}+k_{AC}+k_{fa}) = k_{TOT} = (0.04 \text{ ns})^{-1}$.

2) The fluorescence rate constant for each species was assumed to be temperature independent.

3) The presence of only one temperature-dependent fluorescence quencher was assumed.

4) The total decay rate constant of each species was constrained to be relatively constant when simulating kinetic data at 298 and 273K.

To estimate the values of the rate constants, we have examined the decay-associated spectra at RT and 77K. The ratio of decay component amplitudes at the emission maximum of a given emitter provided a guideline for determining the ratio of forward and back transfer constants. These values were then adjusted to conform to the experimental data.

It is difficult to solve this problem analytically; therefore, we have employed an alternative approach. Numerical methods were used to obtain a solution. A numerical
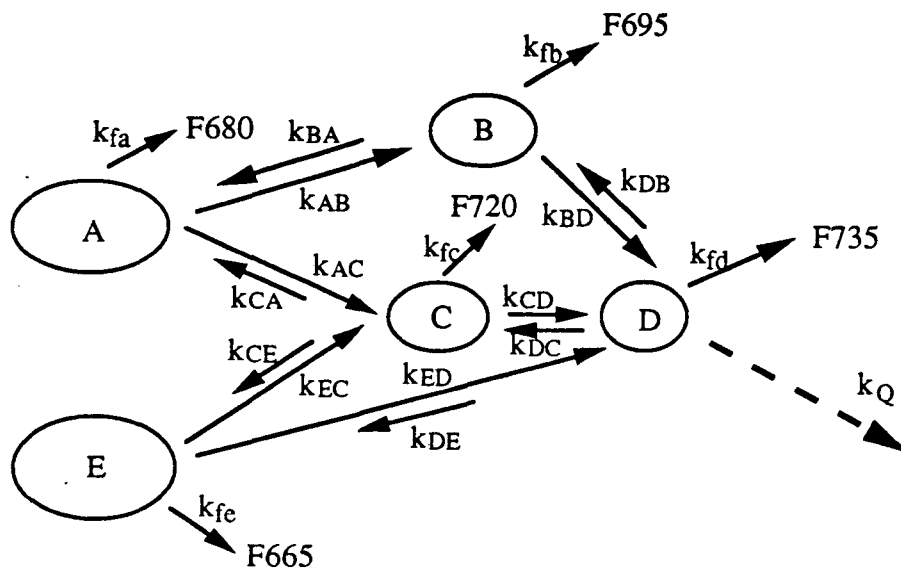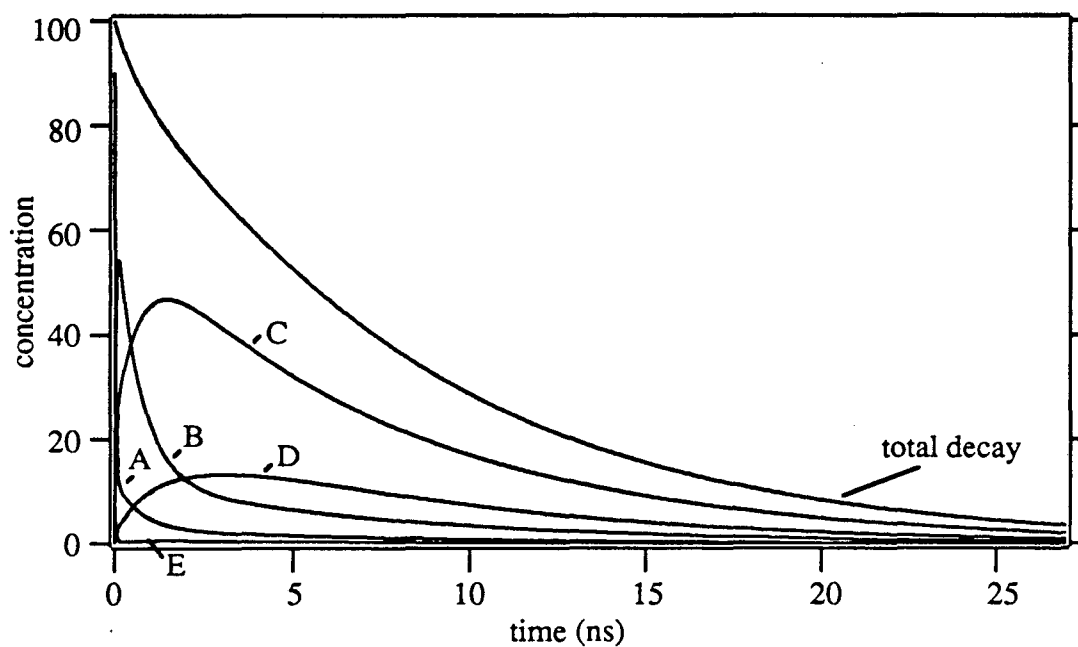
Figure 5.20: Proposed model of transfer energetics within LHC-I. Model consists of five emitting species, emission maxima as shown. Non-radiative temperature-dependent fluorescence quenching occurs at the D pool, depicted with dashed arrow.

solution, however, is only an approximation to the analytical solution. To minimize deviations from the analytical solution the time interval for each calculation was very small (1-100ps). Simulations using the model indicate that the temperature-dependent fluorescence quencher is specifically associated with the longest wavelength emitter, as opposed to the C pool. Additionally, we observe that simulations of the temperature-dependent changes observed experimentally require temperature-dependent changes in the rate constants of fluorescence quenching and energy transfer.
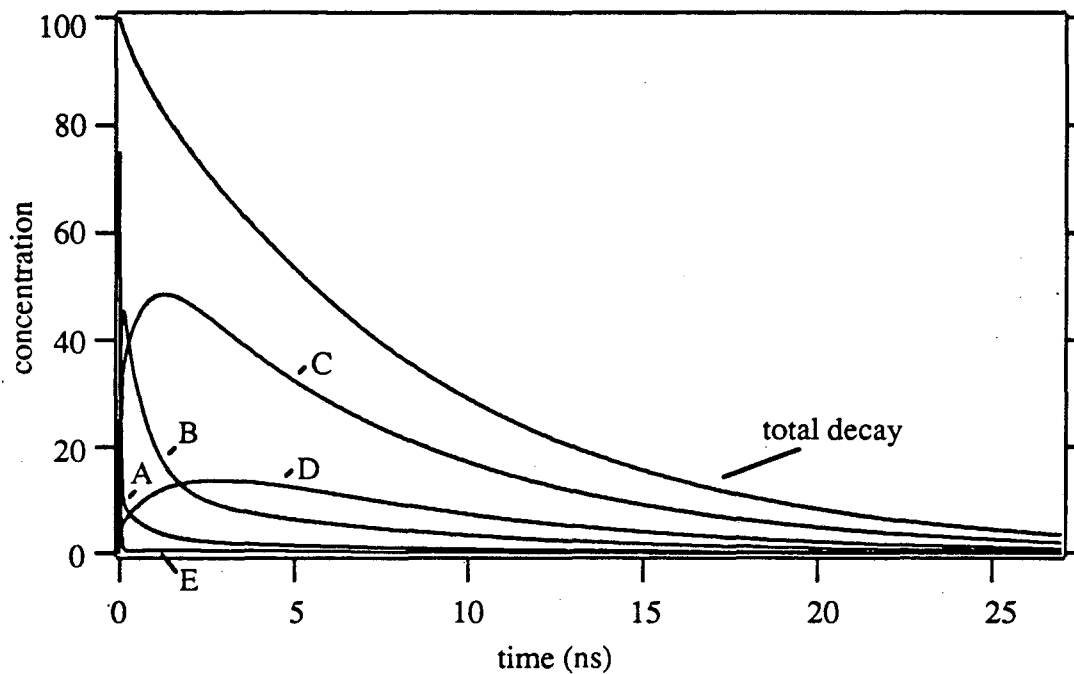
We have successfully modelled certain features of our time-resolved kinetic data. Figure 5.21 depicts a simulation of a fluorescence decay using the rate equations expressed above, in which excitation is done at 670 nm. We are able to simulate the effects of excitation at this wavelength by assuming that 90% of the excitation is initially absorbed by the A pool and the remaining 10% is absorbed by the E pool. Similarly excitation at 650 nm is represented by an increased initial excited state population of the E pool (25%) and a decrease in the initial excited state population of the A pool (75%) as shown in figure 5.22. The initial population of all other pools is assumed to be 0. Both the C and D pools have a larger relative excited state population in simulations with Chl b excitation. The increase in decay component amplitude observed experimentally of the 1.0 ns and 3.3 ns components corresponds to the increase in relative population of the excited state.

Using this method we have attempted to simulate the effects of decreasing temperature on the system. In this scheme we observed that the experimental results are best modelled by decreasing the rate constant for non-radiative fluorescence quenching, occurring at the D pool. (figure 5.23) Our data are indicative of temperature-dependent increases in amplitude of the 1.0 ns and 3.3 ns decay components at 690 nm. These changes can be simulated in our model by increasing the back transfer rate constants from the D pool to the B, C and E pools. These increases in back transfer rate constants are consistent with the experimental observation that the decay lifetime of the D pool remains relatively independent of temperature. If the transfer rate constants remain unchanged then the largest changes in population occur for the D pool, while the populations of the A and the B pool remain relatively constant. This result does not concur with our experimental data. It is possible that small temperature-dependent shifts in absorption and emission maxima result in increased transfer constants. These changes in rate constants cause an increase in the population of A and B at longer times as a result of excitation transfer from C and D. (figure 5.24) The simulations also show an increase in population of

rate constant	value (ns)$^{-1}$	rate constant	value (ns)$^{-1}$
k_{AB}	20	k_{BA}	4.5
k_{AC}	5	k_{CA}	0.3
k_{BD}	0.2	k_{DB}	0.07
k_{CD}	0.03	k_{DC}	0.025
k_{EC}	20	k_{CE}	0.3
k_{ED}	5	k_{DE}	0.05
k_{fa}	0.3	k_{fb}	0.3
k_{fc}	0.3	k_{fd}	0.05
k_{fe}	0.3	k_Q	0.25

Figure 5.21: Simulation of room temperature kinetic decay with excitation at 670 nm. Initial excited state population of A is 90 and of E is 10; initial excited state population of all other pools is 0. Rate constants refer to figure 5.20.

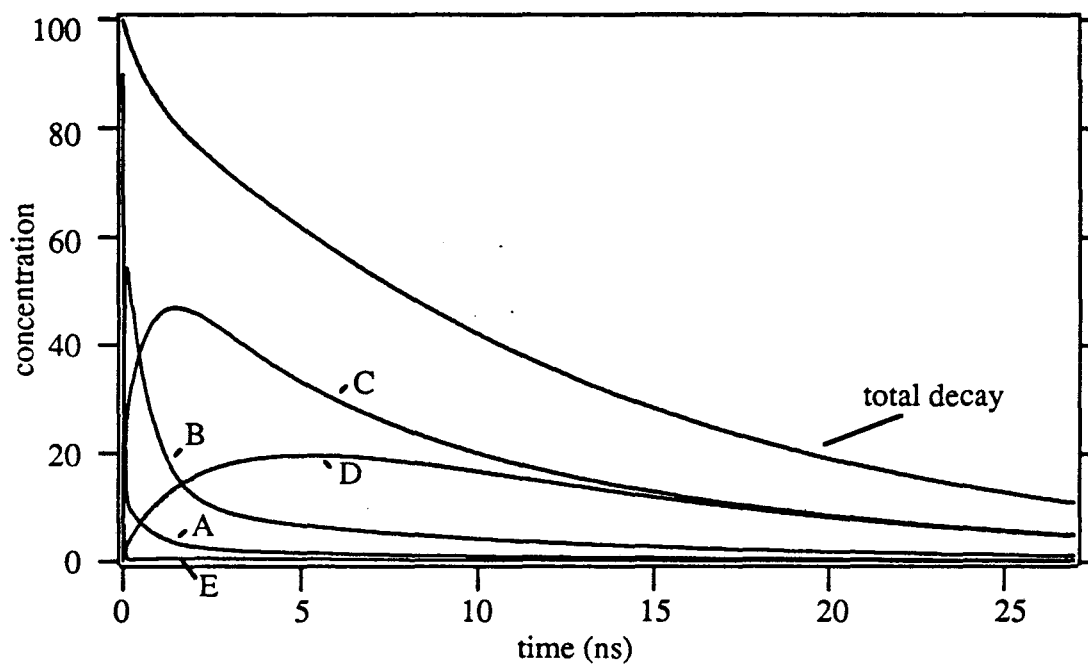| rate constant	value (ns)$^{-1}$	rate constant	value (ns)$^{-1}$
k_{AB}	20	k_{BA}	4.5
k_{AC}	5	k_{CA}	0.3
k_{BD}	0.2	k_{DB}	0.07
k_{CD}	0.03	k_{DC}	0.025
k_{EC}	20	k_{CE}	0.3
k_{ED}	5	k_{DE}	0.05
k_{fa}	0.3	k_{fb}	0.3
k_{fc}	0.3	k_{fd}	0.05
k_{fe}	0.3	k_Q	0.25

Figure 5.22: Simulation of room temperature kinetic decay with excitation at 650 nm. Initial excited state population of A is 75 and of E is 25; initial excited state population of all other pools is 0. Rate constants refer to figure 5.20.

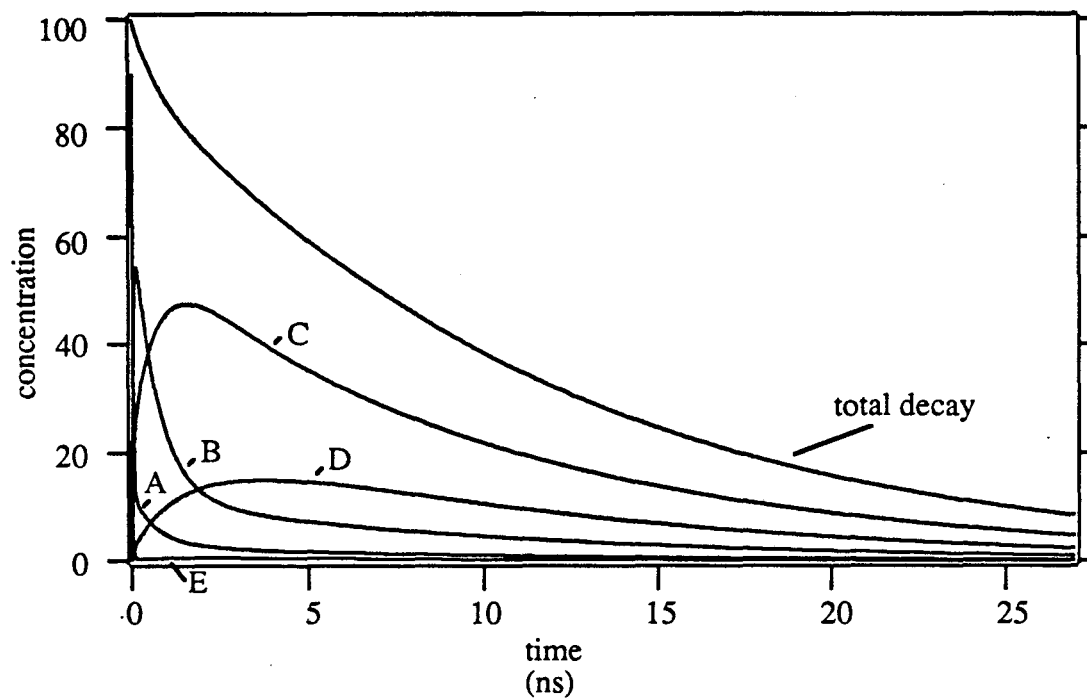| rate constant	value (ns)$^{-1}$	rate constant	value (ns)$^{-1}$
k_{AB}	20	k_{BA}	4.5
k_{AC}	5	k_{CA}	0.3
k_{BD}	0.2	k_{DB}	0.07
k_{CD}	0.03	k_{DC}	0.025
k_{EC}	20	k_{CE}	0.3
k_{ED}	5	k_{DE}	0.05
k_{fa}	0.3	k_{fb}	0.3
k_{fc}	0.3	k_{fd}	0.05
k_{fe}	0.3	k_Q	0.05

Figure 5.23: Simulation of kinetic data at lower temperatures. In this simulation the initial excited state population of A is 90 and of E is 10. Only the quenching rate constant has been changed to simulate changes induced by lower temperatures. Largest changes in population are observed for the D pool.

the longer wavelength emitting species, commensurate with the increases in decay component amplitude detected at 735 nm for the 1.0 ns and 3.3 ns components.

The increased back transfer from the longer wavelength emitting species results in a slower decay of the population of A. We suggest that as the relative amount of back transfer increases the decay of A becomes slower, resulting in an increase in the population of A relative to RT data. This mechanism implies that the decay of the initial population of A is temperature independent, which is consistent with steady state temperature-dependent fluorescence. For those data, it was suggested that the emission at 690 nm is composed of both temperature dependent and temperature independent portions. Our kinetic modelling is indicative of the temperature dependence of F690 arising from the 1.0 ns and 3.3 ns decay components. These results agree with our initial premise that in LHC-I only one temperature-dependent non-radiative fluorescence quencher exists.

77K data (figure 5.25) were simulated by completely removing any temperature dependent fluorescence quenching in the system and increasing the relative ratios of forward to back transfer. We suggest that the decreases in back transfer rate constants result because of decreased overlap between donors and acceptors. Using the theory of energy transfer formulated by Förster the rate constant for energy transfer is proportional to the overlap of the emission spectrum of the donor and the absorption spectrum of the acceptor molecules. As the temperature is lowered these bands narrow, resulting in a decreased overlap integral leading to a smaller transfer rate constant. The distinct spectral characteristics observed in the 77K kinetic data support this hypothesis. In the situation of uphill energy transfer, even at RT the amount of overlap between F735 and A675 is small. Thus, we expect changes in temperature to affect uphill energy transfer rate constants more so than downhill transfer.

Certain aspects of the data are not predicted by the preceding model. The model predicts the presence of rise times in the high temperature kinetic data, which are not observed experimentally. We speculate that at higher temperatures significant overlap of absorption and emission bands of the proposed species prevents the detection of rise components. At lower temperature the problem of band overlap is alleviated because of narrowing of the bands. An additional contradiction between the simulated data and the experimentally observed data lies in the temperature-dependent behavior of the 0.2 ns component. At 735 nm the amplitude of this decay component increases (15%) with decreasing temperature, while at 690 nm the amplitude decreases (10-30%). We speculate that two species are present which have different emission

rate constant	value (ns)$^{-1}$	rate constant	value (ns)$^{-1}$
k_{AB}	20	k_{BA}	4.5
k_{AC}	5	k_{CA}	0.3
k_{BD}	0.2	k_{DB}	0.09
k_{CD}	0.03	k_{DC}	0.03
k_{EC}	20	k_{CE}	0.3
k_{ED}	5	k_{DE}	0.1
k_{fa}	0.3	k_{fb}	0.3
k_{fc}	0.3	k_{fd}	0.05
k_{fe}	0.3	k_Q	0.1

Figure 5.24: Simulation of kinetic decay at 273K with excitation at 670 nm. Initial excited state population of A is 90 and of E is 10; initial excited state population of all other pools is 0. Rate constants refer to figure 5.20.
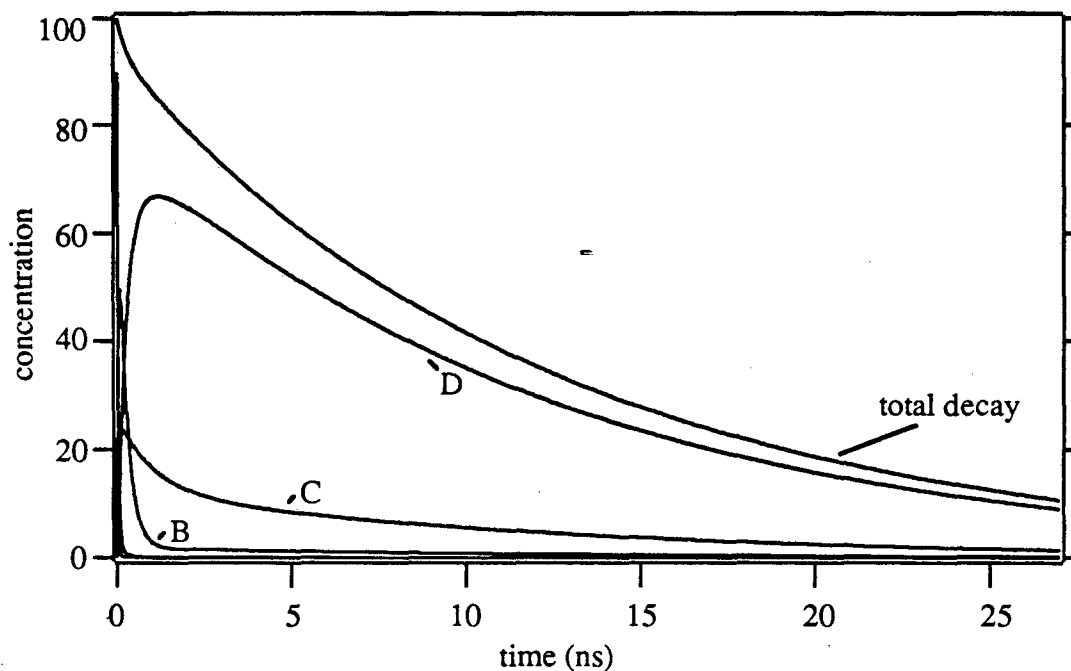
rate constant	value (ns)$^{-1}$	rate constant	value (ns)$^{-1}$
k_{AB}	20	k_{BA}	0.5
k_{AC}	5	k_{CA}	0.07
k_{BD}	3.75	k_{DB}	0.09
k_{CD}	0.55	k_{DC}	0.08
k_{EC}	20	k_{CE}	0.07
k_{ED}	5	k_{DE}	0.05
k_{fa}	0.3	k_{fb}	0.3
k_{fc}	0.3	k_{fd}	0.05
k_{fe}	0.3	k_Q	0.0

Figure 5.25: Simulation of kinetic decay at 77K with excitation at 670 nm. Initial excited state population of A is 90 and of E is 10; initial excited state population of all other pools is 0. Rate constants refer to figure 5.20.

wavelength dependence, but comparable lifetimes. One species would emit at 695 nm and the other at longer wavelengths. In temperature-dependent time-resolved data (figure 5.17) slightly longer lifetimes are observed for this component at longer wavelength. The observed longer lifetime could also result from a lack of resolution in this data, which only deconvolved to 4 kinetic components rather than 5. It is also possible that this lack of resolution causes the amplitude of the 0.2 ns component to be influenced by the longer lived components, which could account for the apparent increase in amplitude at longer wavelengths.

The transfer scheme presented is merely a plausible model for the energetics occurring in LHC-I. Since it does not successfully predict all aspects of the experimental data it is clear that further refinement and experimentation is necessary to completely simulate the transfer kinetics. Nevertheless, the experimentally observed dominant changes in decay component amplitude as a function of temperature, are predicted by this model and as such signify that the basic transfer reactions proposed are essentially correct. Furthermore, since the temperature-dependent behavior of the system is best simulated by changes in both transfer rate constants and a fluorescence quenching rate constant, the activation energy calculated from the steady state fluorescence data represents a composite of temperature dependent reactions. We suggest that the Arrhenius behavior of the system is somewhat fortuitous and cannot be ascribed to one particular process.

Comparison of LHC-I results with other systems

Each of the emitting pools discussed in this model could actually represent clusters of pigment. Recent hole-burning studies by Gillie et al. [29] demonstrate the existence of clusters of Chl a in PSI. Within these clusters, excitation is rapidly equilibrated. Pump-probe transient absorption experiments, in which a polarized absorption is detected indicate that excitations are equilibrated spectrally within 1 ps. [30] Struve [31] proposes that clusters of antenna pigments containing 5-7 chromophores experience sub-picosecond exciton equilibration. This ultrafast equilibration time is supported by recent fluorescence upconversion experiments in which energy transfer from Chl b to Chl a in LHC-II was measured to occur in 0.5 ps ± 0.2 ps. [32] This equilibration time is not detected in our experiments because of the time resolution. Recent results by Holzwarth et al. [27] from single photon counting experiments have a fast decay of 22 ps for spinach PSI particles. Based upon other measurements on PS II, Holzwarth et al. states that antenna equilibration occurs

in most Chl proteins complexes in a time less than 25 ps. [28]

There are several questions with respect to LHC-I, which remain unanswered. Specifically, the function of the long wavelength emitting pigments within an antenna array is perplexing. Recent results obtained on purple bacteria, indicate that excitation is concentrated on lower energy chromophores prior to transfer either between different antenna or from the antenna to the RC. [33,34] The long wavelength pigment B896 in *Rb. sphaeroides* has many spectral characteristics similar to those of C705. Both pigments are significantly red-shifted compared to the main antenna pool, and their absorption and emission properties are highly anisotropic. Our kinetic data are indicative that in LHC-I this species is efficient at quenching excitation.

Using non-denaturing gel electrophoresis Peter et al. [35] have isolated a RC complex which consists of LHCI Chl b-containing polypeptides only in addition to the reaction center core polypeptides. Bassi and Simpson [8] using similar techniques on PSI particles from barley have isolated a particle which contained two polypeptides of LHC-I, 21.5 kDa and 24 kDa, and the RC containing polypeptides. Fluorescence from this complex occurred at 730 nm, indicating the presence of C705. Based on their results Bassi and Simpson [8] propose a model in which energy is transferred from LHCI-680 through LHCI-730 to the PSI core antenna. We infer from these results that the polypeptides which contain C705 are coupled very tightly to the RC polypeptides. Recent electron microscopy studies of the structure of PSI [36] indicate that the LHC-I forms a shell around the core polypeptides of PSI. Boekema et al. suggest that this shell is comprised of 8 polypeptides resulting from double copies of each LHC-I polypeptide. This would imply that each LHC-I polypeptides binds approximately 12 Chl molecules. We speculate that as a result of this protein configuration, some of the the light harvesting pigments are located closer than others to the RC, and these chromophores are the low energy emitters. Transfer from these long wavelength pigments to the RC, however, is not resolved in our data on PSI-200. Our kinetic data are indicative that these low energy emitters have relatively long-lived excited states. It is possible that the long-lived excited states act to store energy within an antenna array prior to trapping by the RC. Time-resolved experiments performed on complexes which contain LHCI-730 and the RC could address this question.

Additionally the nature and function of the temperature-dependent fluorescence quenching mechanism is unclear. At RT or temperatures close to RT, we invoke a quenching process for the excited state which is highly temperature dependent. This process is very efficient at 295K, yet it is difficult to define the exact nature of this

process. It is a radiationless de-activation process and potentially could be a form of internal conversion back to the ground state, or it could be a triplet quenching mechanism which is inefficient at lower temperature. Alternately, as Schuster et al. [11] suggest, some of the light harvesting proteins may serve as control elements in energy transfer to the reaction center but do not contain pigment. In this case temperature-dependent changes in protein conformation could be giving rise to the behavior observed. Changes in protein conformation could also result in unfavorable orientations of transition dipoles, effectively blocking the flow of energy transfer.

If the quenching mechanism represents conversion to a triplet state, it would be possible to investigate this either by EPR measurements or by monitoring absorbance changes at longer wavelength. To address the unresolved questions regarding excitation transfer from C705 to the RC, picosecond pump-probe anisotropy measurements could be employed. These experiments directly probe the kinetics of re-population of the ground state and could be used to monitor the temperature dependence of the quenching of C705. We speculate that the quenching is extremely efficient; thus, we would expect the ground state recovery of C705 to be faster at RT and decrease at lower temperatures. This quencher could have one of two possible functions: either it facilitates energy transfer to the RC, or it is an alternate method for dissipating energy. By detecting both the rate of photochemistry and the rate of quenching when far-red illumination is used, it might be possible to address the function of the putative quencher in this antenna system. Time-resolved fluorescence measurements could also be used to address the nature of fluorescence quenching in this system. Excitation of the system with wavelengths greater than 710 nm should excite only the long wavelength absorbing pigments, simplifying the observed kinetics. A study of the system under these conditions would provide more direct information regarding the relation between the long wavelength absorbing pigments and the quenching mechanism. Temperature dependent kinetic measurements using far-red illumination would provide more quantitative information with respect to fluorescence quenching within this system.

Additionally, the existence of the E emitting pool needs to be verified. LHC-I can be separated into smaller complexes, one of which emits at 730 nm only. Time-resolved measurements on a further fractionated LHC-I complex should resolve the kinetics of the E pool separately from the A pool. Time-resolved anisotropy and picosecond pump-probe anisotropy measurements might also be able to distinguish between the two species, since excitation polarization spectra are indicative of different

relative orientations for the two species.

4. *Summary*

1. Excitation and excitation polarization measurements demonstrate the existence of long wavelength emitting chromophores, first observed in PSI-200. The quantum yield of LHC-I is 0.27 ± 0.06, ten folder higher than PSI-200. In PSI-200 quenching of LHC-I fluorescence appears to be uniform across the emission band. The Stepanov relation applied to LHC-I yields an elevated temperature, 363 ± 5K. A heterogeneous antenna pool that is unrelaxed prior to emission possibly results in the elevated T_{ks} observed.

2. Excitation of Chl b stimulates emission at 735 nm. In kinetic measurements this enhanced emission is reflected in the increased amplitudes of the 1.0 and 3.6 ns decay components.

3. Steady state fluorescence emission is highly temperature dependent. The two emission bands F730 and F685 conform to the Arrhenius relation. We suggest that F685 contains both temperature-dependent and temperature-independent fluorescence. Taking the temperature independent fluorescence of F685 into account, it is shown that F685 has the same temperature dependence as F730. An activation energy of 1700 cm^{-1} is obtained. Simulations of kinetic data are indicative of more than one temperature-dependent process giving rise to the observed fluorescence behavior.

4. Temperature dependent steady-state and time-resolved measurements are suggestive of a non-radiative quencher in the system. Kinetic measurements demonstrate that the largest change in yield are associated with long wavelength emitting species. We suggest that the fluorescence quencher is associated with the longest wavelength emitter.

5. We propose a model for transfer energetics within LHC-I, that incorporates 5 emitting species. We attribute the temperature dependent fluorescence behavior observed to reduced fluorescence quenching and back transfer reactions at lower temperatures. Simulations of kinetic data support this premise.

5. References for Chapter V

1. Mullet, J.E., Burke, J.J. and Arntzen, C.J. (1980) *Plant Physiol.*, **65**, 817-822.

2. Wollman, F.A. and Bennoun, P. (1982) *Biochim. Biophys. Acta*, **680**, 352-360.

3. Haworth, P., Watson, J.L. and Arntzen, C.J. (1983) *Biochim. Biophys. Acta*, **724**, 151-158.

4. Lam, E., Ortiz, W., Mayfield, S. and Malkin, R. (1984) *Plant Physiol.*, **74**, 650-655.

5. Lam, E., Ortiz, W. and Malkin, R. (1984) *FEBS Lett.*, **168**, 10-14.

6. Bassi, R., Machold, O. and Simpson, D. (1985) *Carlsberg Res. Commun.*, **50**, 145-162.

7. Garnier, J., Maroc, J. and Guyon, D. (1986) *Biochim. Biophys. Acta*, **851**, 395-406.

8. Bassi, R. and Simpson, D. (1987) *Eur. J. Biochem.*, **163**, 221-230.

9. Nechushtai, R., Peterson, C.C., Peter, G.F. and Thornber, J.P. (1987) *Eur. J. Biochem.*, **164**, 345-350.

10. Vainstein, A., Peterson, C.C. and Thornber, J.P. (1989) *J. Biol. Chem.*, **264**, 4058-4063.

11. Schuster, G., Nechushtai, R., Ferreira, P.C.G., Thornber, J.P. and Ohad, I. (1988) *Eur. J. Biochem.*, **177**, 411-416.

12. Maroc, J., Garnier, J. and Guyon, D. (1989) *J. Photochem. Photobiol. B.*, **4**, 97-109.

13. Anandan, S., Vainstein, A. and Thornber, J.P. (1989) *FEBS Lett.*, **256**, 150-154.

14. Mullet, J.E., Burke, J.J. and Arntzen, C.J. (1980) *Plant Physiol.*, **65**, 823-827.

15. Arnon, D.I. (1949) *Plant Physiol.*, **24**, 1-15.

16. Sieferman-Harms, D. (1985) *Biochim. Biophys. Acta*, **811**, 325-355.

17. Acker, S., Brown, J.S. and Duranton, J. (1986) *Photosynthetica*, **20**, 274-280.

18. Stepanov, B.I. (1957) *Soviet Physics-Doklady*, **2**, 81-84.

19. Van Metter, R.L. and Knox, R.S. (1976) *Chem. Phys.*, **12**, 333-340.

20. Knox, R.S. and Van Metter, R.L. (1979) in <u>Chlorophyll Organization and Energy Transfer in Photosynthesis</u> Ciba Foundation Symposium 61 (new series) Amsterdam: Medica Excerpta, 177-190.

21. Björn, L.O. and Björn, G.S. (1986) *Photochem. Photobiol.*, **44**, 535-542.

22. Butler, W.L. (1961) *Arch. Biochem. Biophys.*, **93**, 413-422.

23. Lakowicz, J.R. (1983) <u>Principles of Fluorescence Spectroscopy</u>, New York: Plenum Press.

24. Tapie, P., Choquet, Y., Breton, J., Delepelaire, P. and Wollman, F.A. (1984) *Biochim. Biophys. Acta*, **767**, 57-69.

25. Kramer, H.J. and Amesz, J. (1982) *Biochim. Biophys. Acta*, **682**, 201-207.

26. M.F.J. Talbot, personal communication.

27. Holzwarth, A.R., Haehnel, W., Ratajczak, R., Bittersmann, E. and Schatz, G.H. (1990) in <u>Current Research in Photosynthesis</u> (M. Baltscheffsky, ed), Vol. II, The Netherlands: Kluwer Academic Publishers, 611-614.

28. Holzwarth, A.R. (1990) in <u>Current Research in Photosynthesis</u> (M. Baltscheffsky, ed.), Vol. II, The Netherlands: Kluwer Academic Publishers, 223-230.

29. Gillie, J.K., Small, G.J. and Golbeck, J.H. (1989) *J. Phys. Chem.*, **93**, 1620-1627.

30. Causgrove, T.C., Yang, S. and Struve, W.S. (1989) *J. Phys. Chem.*, **93**, 6844-6850.

31. Struve, W.S. (1990) *J. Opt. Soc. Am. B.*, **7**, 1586-1593.

32. Eads, D.D., Castner, E.W., Jr., Alberte, R.S., Mets, L. and Fleming, G.R. (1989) *J. Phys. Chem.*, **93**, 8271-8275.

33. van Dorssen, R.J., Hunter, C.N., van Grondelle, R., Korenhof, A.H. and Amesz, J. (1988) *Biochim. Biophys. Acta*, **932**, 179-188.

34. van Grondelle, R., Bergström, H., Sundström, V. and Gillbro, T. (1987) *Biochim. Biophys. Acta*, **894**, 313-326.

35. Peter, G.F., Machold, O. and Thornber, J.P. (1988) in <u>Plant Membranes: Structure, Assembly and Function</u> (J.L. Harwood and T.J. Walton, eds.) London: Biochemical Society, 17-31.

36. Boekema, E.J., Wynn, R.M. and Malkin, R. (1990) *Biochim. Biophys. Acta*, **1017**, 49-56.

Chapter 6: Conclusions and Future Directions

In this study we have attempted to clarify the energetics within PSI using two different approaches. We have used fluorescence spectroscopy as a powerful probe of the dynamics of energy transfer. Additionally, measurements were performed on a holocomplex, PSI-200 and a subdivision of that complex, LHC-I. The study of energy transfer dynamics within Photosystem I represents a challenging problem. The antenna complement possesses certain characteristics which are not common to more extensively studied light harvesting systems, such as the phycobilisomes. At room temperatures PSI has a significant amount of emission at lower energy than the absorption maximum of the reaction center and this emission increases dramatically at lower temperatures. These spectroscopic features are suggestive of alternate mechanisms of energy transfer within this antenna system. Temperature dependent fluorescence behavior has been observed in both green and purple bacteria, while the occurrence of uphill energy transfer to the reaction center has been mainly detected in purple bacteria. In the PSI antenna of cyanobacteria, emission occurs at higher wavelengths than what is currently observed for the full antenna complement of PSI of higher plants. It appears that PSI has evolved into a system with an additional antenna, LHC-I which contains chromophores that emit at even longer wavelengths than their cyanobacterial counterpart. Data obtained on PSI-100* isolated from *Synechococcus*, sp. and PSI-200, isolated from spinach, demonstrate that increased emission at longer wavelengths confers an additional degree of thermal stability to the system. Measurements on isolated LHC-I show that this antenna complex contains the longest wavelength emitting chromophores of PSI and also retains the temperature dependence of the entire complex despite the absence of the reaction center.

From low temperature kinetic fluorescence measurements on LHC-I certain spectral characteristics of the low energy emitters can be identified. The relatively fast decay detected at shorter wavelengths, coupled with a rise in fluorescence at longer wavelengths are suggestive of low energy pigments receiving excitation from shorter wavelength absorbing pigments within 40 ps. In steady state measurements the high intensity of the 710-740 nm shoulder at room temperature supports the premise that a substantial amount of excitation is reaching the long wavelength emitters, in spite of their relatively small absorption cross-section. Kinetic measurements on LHC-I argue for a relatively long-lived excited state (1.0-3.0 ns) for these low energy pigments. It is possible that these chromophores act to store energy prior to transfer to the reaction

center. Time-resolved measurements on the holocomplex indicate that the excited state is not as long-lived in the presence of the reaction center. We speculate that in LHC-I energy is transferred to the RC antenna through F685. An alternate pathway for excitation transfer might exist from the long wavelength emitting species to the reaction center through an intermediate non-radiative quencher. Quantum yield measurements of photochemistry demonstrate that far-red excitation is efficient at oxidizing the reaction center. From our measurements it is not clear if this excitation is transferred through the main antenna pool or directly from long wavelength absorbing pigments. In purple bacteria recent evidence is suggestive that excitation is focussed at a long wavelength pigment prior to transfer to the reaction center. [1,2]

Although, simplification was the initial premise for subdividing the complex, we observe that the isolated antenna retains the same degree of complexity as the holocomplex. Nevertheless, our fluorescence studies on PSI-200 and LHC-I allow us to draw a few conclusions regarding the system:

1) Excitation of Chl b enhances emission at longer wavelengths (F735).

2) The intensity of F735 is highly temperature dependent, increasing dramatically with decreasing temperature. In reaction center-containing systems, emission at shorter wavelengths (F690) is relatively temperature independent.

3) Measurements on the isolated antenna complex, LHC-I, demonstrate that the increase in fluorescence intensity is independent of the reaction center, suggestive of an alternate fluorescence quenching mechanism which is highly temperature dependent.

4) Kinetic studies on LHC-I indicate that the temperature dependence arises from fluorescence quenching mechanisms and also changes in energy transfer dynamics amongst the emitting species within the antenna.

5) Fluorescence quenching appears to be directly associated with long wavelength emitting pigments.

Several aspects of this system remain undetermined. In particular some fundamental questions which remain are: 1) What is the nature of the fluorescence quenching mechanism? 2) Does this mechanism facilitate energy transfer to the RC? We propose certain experiments which could be useful in unravelling the energetics within PSI. If fluorescence quenching is occurring because of generation of a triplet state, then it should be possible to detect evidence for the triplet either in EPR measurements or by monitoring absorbance changes at longer wavelength as a function of temperature. Alternately, the fluorescence quenching could be more coupled to the protein matrix, in which case experiments on smaller systems could provide more

direct evidence regarding the nature of quenching. If the changes in conformation were large enough, it might be possible to detect them by monitoring changes in infra-red spectroscopy bands as a function of temperature.

Picosecond spectroscopy is a fundamental tool for detecting the ultrafast early events in photosynthesis. We have extensively used single photon counting measurements to monitor energy transfer pathways between different chromophores. Using this technique, however, it is not possible to probe energy transfer events between like chromophores. Antenna systems, such as PSI, are largely composed of pigments with similar absorption and emission spectra. Thus, an important tool for discerning interactions between like chromophores and possibly excitonic interactions is time-resolved fluorescence anisotropy measurements. In PSI this technique could potentially detect energy transfer between putative chromophore clusters. An additional technique for probing these types of interactions is picosecond transient absorption spectroscopy, which monitors repletion of the ground state. In PSI detection of far-red absorbance changes specifically related to the long wavelength emitters and the reaction center would be quite fruitful for determining energy transfer dynamics between the two species. Potentially, this technique could be used to monitor changes in fluorescence quenching of LHC-I or PSI-200.

Biochemical isolation techniques enable us to perform spectroscopic measurements on a potentially simpler system. In this instance the isolation of LHC-I demonstrated that the energetics within the isolated antenna are just as complex as those in the holocomplex. Of course, it is always important to consider the effects of isolation and separation on the subsequent results. We chose to work on a simpler system to improve our ability to interpret results and also to improve our theoretical modelling of the system. Since isolation of LHC-I did not simplify the system enough, we suggest that further fractionation of the LHC-I complex could provide important information regarding the nature of fluorescence quenching within the system. Time-resolved measurements performed on isolated LHC-I constituents containing only Chl b would confirm certain aspects of the model proposed in chapter 5. Also, experiments done on complexes containing LHCI-730 and the reaction center could provide direct evidence for fluorescence quenching within the antenna and also would address the pathway of excitation transfer to the reaction center.

An exciting method for looking at simpler systems lies in the generation of mutants which lack functional parts of the light harvesting apparatus. *Chlamydomonas reinhardtii* has an antenna complex, CP0 which is very similar in spectroscopic

properties to LHC-I. Steady state fluorescence measurements on a mutant lacking the antenna component, CP0a indicates that it is an important link between CP0 and the reaction center. [3,4] We suggest that time-resolved measurements on mutants of *Chlamydomonas reinhardtii*, which lack specific constituents of the antenna complex would provide important information regarding energy transfer from peripheral antenna complexes to the RC. Additionally, the use of mutants could alleviate the problems of biochemical isolation often encountered in these types of spectroscopic measurements. The generation of mutants, however, has the potential of disrupting the system and introducing non-native configurations. Care should be exercised in relating results to the native system. In any case time-resolved fluorescence measurements performed on simpler antenna systems provides an important means for understanding the nature of energy transfer dynamics within a light harvesting array.

References for Chapter 6

1. Hunter, C.N., van Grondelle, R. and van Dorssen, R.J. (1989) *Biochim. Biophys.Acta*, **973**, 383-389.

2. Hunter, C.N., van Grondelle, R. and Olsen, J.D. (1989) *Trends in Biochem. Sci.*, **14**, 72-76.

3. Garnier, J., Maroc, J. and Guyon, D. (1986) *Biochim. Biophys. Acta*, **851**, 395-406.

4. Maroc, J., Garnier, J. and Guyon, D. (1989) *J. Photochem. Photobiol. B*, **4**, 97-109.

LAWRENCE BERKELEY LABORATORY
TECHNICAL INFORMATION DEPARTMENT
1 CYCLOTRON ROAD
BERKELEY, CALIFORNIA 94720